Statistics of
large contact forces
in granular matter

Statistics of large contact forces
in granular matter

————————

Statistiek van grote contactkrachten in granulair materiaal

(met een samenvatting in het Nederlands)

Proefschrift

ter verkrijging van de graad van doctor aan de Universiteit Utrecht op gezag van de rector magnificus, prof. dr. J.C. Stoof, ingevolge het besluit van het college voor promoties in het openbaar te verdedigen op maandag 20 oktober 2008 des middags te 2.30 uur

door

Adrianne Rudolfine Titia van Eerd

geboren op 27 november 1979 te Heesch.

Promotor   Prof. dr. J.P.J.M. van der Eerden
Co-promotor   Dr. ir. T.J.H. Vlugt

"... en dan denk ik aan Brabant, want daar brandt nog licht."

Guus Meeuwis, Brabant

Contents

1

Introduction

1.1   Granular materials and jamming

Granular materials are systems consisting of a large number of interacting macroscopic particles, such as sand, rice or apples, in which the range of the interaction is short compared to the particle size. These materials play an important role in everyday life. A good understanding of the physics of granular materials is desired, for example, to predict and control landslides and avalanches [1, 2], to design efficient transport and handling of coal or chemicals [3, 4] and to make high quality tablets (medicine), i.e. the correct amounts of active and inert ingredients [5, 6]. Unfortunately, there still remains a poor understanding of the behavior of granular matter [7–9].

As the particles of granular materials (the grains) are larger than roughly 10 microns, the thermal energy of the grains is small compared to the gravitational and elastic energy. Depending on the conditions, these athermal systems may behave like a solid, liquid or gas. For example, sand behaves like a solid when standing on it, sand behaves like a fluid in an hourglass and sand behaves like a gas when it is shaken. The different states are in this case determined by the density and the applied stress. Below a certain stress the system is jammed (stuck in a certain configuration) and above this stress the system is unjammed [10].

Jamming is not limited to granular materials; colloidal suspensions of small particles jam as the packing density is raised and supercooled molecular liquids jam as the temperature is lowered. Liu and Nagel have proposed that stress, packing fraction and temperature are important parameters that control jamming for all systems, and that the state of the system can be represented by a "jamming phase diagram" [10]. For the athermal granular materials, the temperature is not included in the jamming phase diagram.

A collection of grains remains easily trapped in one of the configurations that have a local energy minimum (metastable configurations). In this thesis, we focus on the behavior of static granular materials, for which grains are packed in one of the many possible metastable configurations. In particular, we are interested in the forces between the grains. It is generally believed that forces between grains on the microscopic scale are responsible for material properties at the macroscopic scale, and therefore they are worth studying. In principle there can be attractive forces between grains (e.g. caused by liquid bridges), but in this study we restrict ourselves to electrically neutral, non-magnetic grains in vacuum or air. This implies that there are
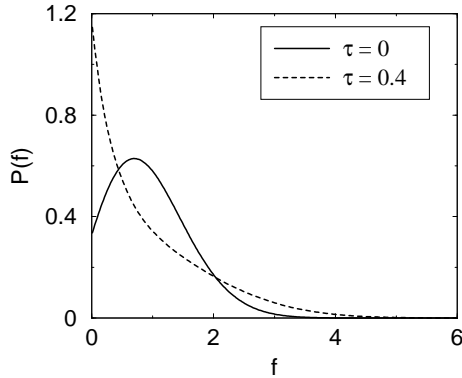
Figure 1.1: Probability distribution $P(f)$ of the magnitude of the contact force f for 2D systems of $N = 500$ frictionless particles that have an average coordination number $z = 5.5$. All forces are normalized such that the average force $\langle f \rangle = 1$. If no shear stress is applied on the system ($\tau = 0$), $P(f)$ shows a peak close to the average force $\langle f \rangle$. The system with $\tau = 0.4$ shows a monotonously decreasing $P(f)$. This suggests unjamming by shear stress [11].

no forces between the grains unless they are in contact. Such forces are called *contact forces*. Various experimental and theoretical approaches have been used to study contact forces in granular matter. In this thesis, computer simulations are performed to study the contact forces.

The collection of all contact forces in a system, as considered above, is called a *force network*. The central quantity to characterize force networks is the probability distribution $P(f)$ of the magnitude of the contact force f. A general feature of the force distribution of a jammed system is the peak close to the average force $\langle f \rangle$, while an unjammed system shows a monotonously decreasing probability distribution [10, 12–14]. In Fig. 1.1 force distributions are shown for two-dimensional (2D) systems without shear stress ($\tau = 0$) and with shear stress $\tau = \sigma_{xy}/\sigma_{xx} = \sigma_{xy}/\sigma_{yy} = 0.4$, $\sigma_{\alpha\beta}$ being the elements of the stress tensor. These systems show the characteristic features of jammed and unjammed systems, respectively. For each system, typical force networks are shown in Fig. 1.2. The magnitude of the force is isotropically distributed in the unsheared system ($\tau = 0$). However, in a system in which τ is close to its yield stress the force network clearly becomes anisotropic. This force network shows that the large forces have the tendency to align and to form so-called *force chains* [15].

Large contact forces, $f > 5\langle f \rangle$, occur very infrequently. The decreasing proba-
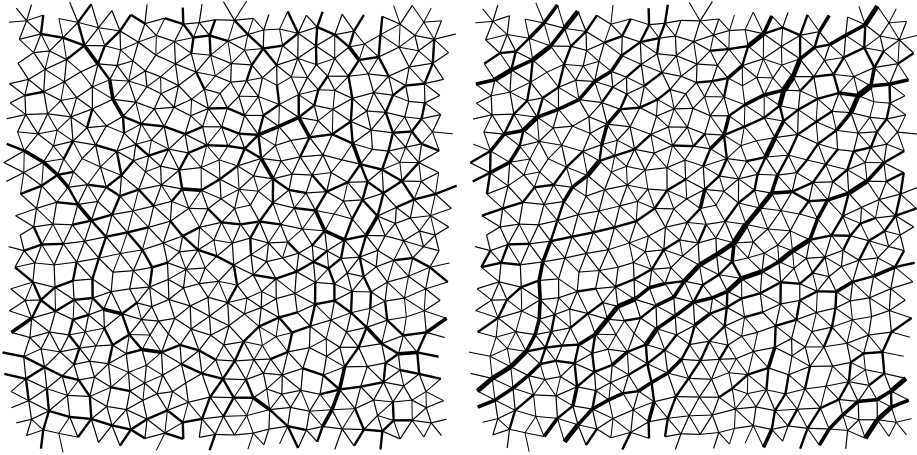
Figure 1.2: Force networks of the systems in Fig. 1.1. The thicknesses of the lines represent the magnitude of the force. The magnitude of forces is isotropically distributed if no shear stress is applied (left). If the system is under shear stress, the force network becomes anisotropic and contains chains of large forces (right). Note that the positions of the grains are identical in both figures.

bility of these large forces forms the *tail* of the contact force distribution $P(f)$. Contradicting findings about the exact shape of the tail give still rise to much debate in literature: has the contact force distribution an exponential tail $P(f) = a\exp[-bf]$ or a Gaussian tail $P(f) = a\exp[-bf^2]$? [8] In the next section, a summary of several studies of the force statistics of granular materials is presented.

So far, we only considered contact forces in the direction perpendicular to the contact surface (normal forces). However, contacting grains often experience also tangential forces. The tangential forces can act in any direction perpendicular to the normal force, but their magnitude is always limited. If the tangential forces get too large, the two contacting surfaces will slip relative to each other. The Coulomb friction law states that when two grains are pressed together with a normal force, the contact can support any tangential friction force with

$$|f_t| \leq \mu f_n, \tag{1.1}$$

where μ is the static friction coefficient, f_t is the tangential force and f_n is the normal force. The friction coefficient μ is a dimensionless variable which depends on the material. Typical values for μ are in the range of 0.05–4.00 [16, 17]. In order to
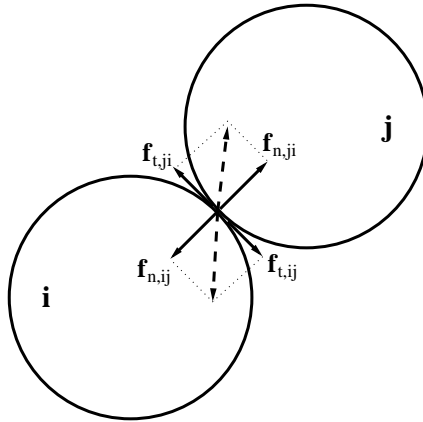
Figure 1.3: Representation of normal and tangential contact forces ($\mathbf{f}_{n,ij}$ and $\mathbf{f}_{t,ij}$ respectively) between two particles i and j.

investigate the role of friction in the system, we study systems of frictionless ($\mu = 0$) and frictional ($\mu > 0$) particles. In Fig. 1.3, a schematic representation of the normal and tangential contact forces is shown. According to Newton's third law, forces acting on particle i are of the same magnitude but in the opposite direction as the force acting on particle j: $\mathbf{f}_{n,ij} = -\mathbf{f}_{n,ji}$ and $\mathbf{f}_{t,ij} = -\mathbf{f}_{t,ji}$.

1.2 Studying force statistics

In recent years, the behavior of granular matter has been studied by many physicists [18, 19]. The contact force distribution is found to be a structural signature that distinguishes the jammed granular state from its flowing counterpart [20]. The contact force distribution $P(f)$ of normal forces above the average force $\langle f \rangle$ decays quickly and in the jammed state $P(f)$ has a plateau or small peak at force magnitudes around or below $\langle f \rangle$. However, the exact shape of the distribution is still under discussion. In this thesis we focus on the statistics of large contact forces, especially the tail of the contact force distribution. We will summarize some experimental studies, simulations and theories on this subject.

1.2.1   Experiments: boundary forces

The first experiments to study contact forces in granular materials used the carbon-paper technique [15, 21–23]. The experimental setup usually contains a cylinder with close-fitting pistons at the top and bottom surfaces. The piston at the bottom is covered with white and carbon paper. When grains are confined in the cylinder, all bottom grains press the carbon paper into the white paper. The size and the intensity of the mark left on the white paper depend on the magnitude of the normal force on the corresponding grain. Using image analysis software and calibration curves, the contact forces at the surface can be extracted. Note that only boundary forces are extracted and not the forces in the bulk of the system. In these studies, the obtained contact force distribution $P(f)$ displays an exponential decay for large forces. Little or no dependence on crystallinity, friction or deformation is observed.

Løvoll *et al.* [24] used an electronic balance to measure normal forces on individual grains at the bottom of a granular system without applying any external load. With this method it is possible to investigate systems which are under gravity like regular silo systems or sand piles. The resulting $P(f)$ also shows an exponential decay.

Corwin *et al.* [20] measured $P(f)$ with a photoelastic (birefringent under strain) plate at the bottom surface of a three-dimensional (3D) cylindrical pack. This plate rotates the polarization of light in proportion to the applied local pressure. The position and magnitude of the local pressure is detected by a video camera that views the transducer through an analyzer oriented to block any unrotated light. A roughened piston that applies a fixed normal load to the top surface, was rotated at a constant rate. In this way, the local pressures on the bottom surface vary with time. The boundary forces show a slower than exponential distribution for short packs (height < 20 beads) and an exponential contact force distribution for taller packs (height $\geq$ 20 beads). The shape of this distribution does not change when a shear stress below the yield stress is applied. However, at the outer edge of the pack, within the shear band $P(f)$ exhibits markedly different behavior: the slope on a triple-log plot (see Section 1.7) is $\frac{5}{3}$ suggesting that for large f, $P(f) \sim \exp[-cf^{5/3}]$.

1.2.2   Experiments: bulk forces

Majmudar *et al.* [25] measured the normal and tangential forces inside a 2D system of $N = 2500$ bidisperse photoelastic disks that were subjected to pure shear and

isotropic compression. The experimental setup contains a biaxial cell with walls that can be moved by motorized linear slides. The cell rests horizontally on a sheet of Plexiglas and is placed between crossed circular polarizers. From below the system was illuminated and from above digital images of the internal stresses were made with a high-resolution camera. The frictional disks ($\mu = 0.8$) are either 0.8 cm or 0.9 cm in diameter with a number ratio 4:1. The sheared states were created by compressing in one direction and expanding by an equal amount in the other direction. Isotropically compressed states were created by compressing in both directions. Both systems shows a tangential force distribution $P(f_t)$ with an exponential tail. In contrast, the normal force distribution $P(f_n)$ shows a nearly exponential tail for the sheared system and a Gaussian tail for the isotropically compressed system.

Brujić *et al.* [26] presented a method for measuring the contact force distribution within the bulk of a 3D compressed emulsion system using confocal microscopy. The dispersed oil phase of the emulsion was fluorescently labeled and consisted of 450 droplets. The emulsion droplets were compressed by an external pressure through centrifugation, resulting in a system which is close to the jamming transition. The degree of deformation, extracted from image analysis, was used to calculate the interdroplet normal force

$$f = \frac{\sigma A}{R}, \tag{1.2}$$

where A is the area of the deformation, σ is the interfacial tension of the droplets and R is the geometric mean of the radii of curvature of the undeformed droplets. The large forces show an exponential force distribution, which is consistent with results of many previous experimental and simulation data on granular matter, foams and glasses [12, 22, 27, 28]. However, at large pressures, the probability distribution shows a crossover to a Gaussian-like distribution.

Zhou *et al.* [29] measured the interparticle contact forces inside 3D piles of frictionless liquid droplets with no Brownian motion. Three different systems were studied: *(1)* a monodisperse pile, *(2)* a polydisperse pile subjected to its own weight, and *(3)* a polydisperse pile with a Teflon disk immersed in fluid on top. The droplet surfaces were labeled with a monolayer of fluorescent nanoparticles to obtain 3D images with confocal fluorescence microscopy. The systems contain on the order of 10^7 droplets; ca.10^3 droplets near the bottom of the piles were imaged. The contact forces were calculated with Eq. (1.2) and its probability distribution approximates a Gaussian decay.

1.2.3   Simulations

Granular dynamics simulations were performed by Makse *et al.* [27]. The authors used the discrete element method which was developed by Cundall and Strack [30]. The simulated system with periodic boundary conditions contains deformable elastic grains ($N = 10000$) which interact via normal and tangential Hertz-Mindlin forces plus viscous dissipative forces [31]. Packings were created by compressing the initial configuration of non-overlapping spheres. At low stress, the contact force distribution is exponential, however, a gradual transition to a Gaussian contact force distribution is found when the system is compressed further. A similar transition is observed in simulations involving frictionless grains under isotropic compression.

Radjai *et al.* [28] used the contact dynamics (CD) approach to study the dynamics of perfectly rigid particles ($N = 4025$). In CD the contact forces are calculated by virtue of their effect, which is to fulfill constraints such as the volume exclusion of the particles or the absence of sliding due to static friction [32]. The systems of Radjai are in static equilibrium as the kinetic energy of the system is fully dissipated in friction and collisions. The contact force distribution $P(f)$ shows an exponential decay for larger forces and is quite robust with respect to changes in the grain-grain friction coefficient.

O'Hern *et al.* [12] performed molecular dynamics simulations of binary 50%/50% mixtures in 2D with $N = 1024$ particles at constant temperature, using the Gaussian constraint thermostat and leapfrog algorithm [33]. The effect of different interparticle pair potentials was studied. The contact forces followed directly from the particle positions. The simulations on purely repulsive potentials were carried out at constant reduced density $\rho = N/V = 0.747$; the simulations of attractive pair potentials were carried out at zero average pressure. All particles have the same mass but different diameters ($\sigma_2/\sigma_1 = 1.4$) which prevents the system from crystallization [34]. The particles were confined to a square box with periodic boundary conditions. This model system was studied in and out of equilibrium. Systems out of equilibrium were created by thermal quenches from high temperature to a temperature below the glass transition temperature T_g. Systems in equilibrium were created by a simulation at $T > T_g$ followed by an equilibration. At all temperatures, an exponential tail of $P(f)$ was observed. However, when shear stress was applied to the system out of equilibrium, the tail of the force distribution bends down on a logarithmic plot, suggesting a faster than exponential decay. In a follow-up study by the same authors [35], also exponential behavior of $P(f)$ at large f is found for systems at $T = 0$ close to density

at which the system starts to unjam.

Tkachenko *et al.* [36] used adaptive network simulations to study a 2D packing $N = 500$ of variable-sized discs (polydispersity = 10%) and periodic boundary conditions in one direction. In the simulation procedure, individual contacts between adjacent beads are sequentially removed and added, while the bead positions are not modified. Finally, a stable configuration without tensile contact forces is found. The contact force distribution $P(f)$ does not show a convincing exponential decay; it clearly decays faster than exponentially.

Silbert *et al.* [37] performed 3D molecular dynamics simulations of unloaded frictional granular packings. The $N = 12800$ monodisperse and cohesionless spheres interact only via a Hooke spring ($f = k\delta$ in which k is the elastic constant and δ is the deformation from equilibrium) or a Hertz contact law ($f = k\delta^{3/2}$) and static friction. The packings were generated from a dilute system under gravity. Particles settled onto a bottom wall that was either a planar base or a frozen template of a close-packed random particle configuration until the kinetic energy of the system was much smaller than the potential energy. The packings are spatially periodic in the horizontal plane to ignore the effects of sidewalls. In this case, the system can be compared to free-standing sand piles. The system can also be compared with experimental packings poured into a cylindrical container with a wall that has the same properties as the particles, but then the average force need to be normalized by the average contact force at a depth z in the packing. The distribution of the particle-particle and particle-wall normal and tangential contact forces were computed. The distribution of normal forces $P(f_n)$ shows an exponential-like decay at large forces for both the Hookean and the Hertzian contact force law in both systems (spatially periodic and cylindrical) with $\mu = 0.5$. The distribution of tangential forces $P(f_t)$ decays more slowly than $P(f_n)$.

1.2.4   Theoretical studies

The q-model [15, 38] provides a quantitative way to study granular matter and to understand the experimentally observed exponential tail of the force distribution $P(f)$, but at the cost of a significant simplification. This scalar model only takes the normal component of the force (i.e. weight) into account. The grains of mass unity are assumed to be positioned on a regular lattice. A fraction q_{ij} of the total weight supported by a grain i in a certain layer is transmitted to grain j in the layer underneath it. The fractions are generated randomly, satisfying the constraint $\sum_i q_{ij} = 1$, which

assures mechanical equilibrium in the vertical direction. At large depths, the weight distribution $P(q)$ yields an exponential tail. In principle, this tail depends on details of the stochastic rules for force transmission and need not to be exponential [39, 40]. Note that the q-model does not ensure balance on the horizontal forces.

Edwards had proposed a theory for powders, which is based on analogies with statistical mechanics [41]. In Edwards' ensemble, besides the force distribution also thermodynamic quantities can be computed by averaging over force and positional configurations of grains. Valid configurations are all possible static packings with no overlap between grains. Edwards assumes that all valid configurations are equally probable, like in the microcanonical ensemble. The large number of degrees of freedom, i.e. positions and forces, makes it difficult to calculate averages. Recently, Snoeijer *et al*. presented an approach [42, 43] inspired by Edwards' ensemble, the so-called *force network ensemble*. The allowed configurations are also sampled with equal probability, but the ensemble of Snoeijer is limited to a *single* packing. Limiting Edward's ensemble to a single configuration of particles has also been suggested by Bouchaud in a different context [44]. A detailed description of the force network ensemble is presented in Section 1.5.

Rottler and Robbins studied a coarse-grained model for polymers that shows jamming behavior [45]. Each linear polymer was modeled by N beads of mass m. Van der Waals interactions were described with a standard Lennard-Jones potential and a simple analytic potential was used for covalent bonds between adjacent beads along the chain. Jamming behavior is shown under tension in which the covalent bonds carry most of the stress. The distribution of forces between any pair of particles shows an exponential tail. The authors make an analogy with the Boltzmann distribution, because in jammed systems the total force is conserved and one may imagine that the number of microstates is maximized. We will come back to this analogy in Chapter 2.

Kruyt and Rothenburg developed a theory for the distribution of contact forces for cohesionless, frictional granular materials, which is based on a maximum information entropy principle [46]. In their study, entropy is maximized under the constraints of a prescribed stress and the requirements that the normal component of the contact forces is compressive and that the tangential component of the contact force is limited by Coulomb friction. The distribution of both the normal and tangential contact forces exhibit an exponential decay for large forces. The crossover to a Gaussian decay is not observed when the stress increases, which may be caused by the absence

of kinetics that are important for elastic effects.

In a series of papers [47–49], Metzger presents a very elegant model to describe contact force statistics of force balanced grains in the isostatic limit, based on entropy maximization of the Edwards ensemble. Although an exponential tail is explicitly mentioned in Ref. [47], a closer inspection reveals that the contact force distribution decays faster than exponential [50].

1.3 Molecular Simulation techniques

Real-life situations and experiments can often be simulated with computer models. Models used in molecular simulations contain a detailed description of the system at microscopic level (e.g. the atomic or molecular positions and momenta). Statistical mechanics relates the microscopic properties to the macroscopic properties of materials, such as temperature, pressure, energy and heat capacity. Computer simulations can be used to actually compute these properties from the microscopic interactions.

Simulations are often relatively easy and cheap compared to experiments, especially under extreme circumstances. Therefore, simulations can be used to study phenomena that are not yet fully understood, such as avalanches, crystal growth or protein folding. Although, computers are becoming faster every year, a typical simulation may still run for several days, weeks or even months depending on the system size, complexity, etc. Note that simulations have a fixed duration, meaning that only a finite number of the total number of microstates, i.e. specific microscopic configurations of a system, can be generated. Therefore, molecular simulations nearly always provide an *estimate* of a certain property.

The collection of all microstates which correspond to an identical macroscopic state is called an ensemble. Different macroscopic environmental constraints lead to different types of ensembles. The following are the most important: the canonical ensemble (constant number of particles N, volume V and temperature T), microcanonical (constant N, V, and energy E) [51], grand-canonical (i.e., constant chemical potential μ, V, T), isobaric-isothermal, constant-stress-isothermal, and the Gibbs ensemble [52].

Molecular simulation methods can roughly be divided in two categories: Monte Carlo (MC) methods and Molecular Dynamics (MD) methods. In Molecular Dynamics, the time evolution of a system is followed by integrating the equations of motion. From the resulting trajectory, one can not only compute configurational or

thermodynamic averages, but also transport properties like the diffusivity, heat conductivity etc. In Monte Carlo simulations, we compute averages over a representative part of all possible configurations. The ergodicity hypothesis states that in principle time averages should be identical to configurational averages [33, 52]. For a more in-depth discussion of molecular simulation techniques we also refer the reader to Refs. [33, 53–57].

In computer simulations an interaction model is used to describe a system at microscopic level. A pair of charge neutral atoms or molecules is subject to two types of forces: an attractive force at large distances and a repulsive force at short distances. The Lennard-Jones potential [58] is a simple and very popular model that mimics this behavior:

$$u_{\text{LJ}}(r_{ij}) = 4\varepsilon \left[\left(\frac{\sigma}{r_{ij}} \right)^{12} - \left(\frac{\sigma}{r_{ij}} \right)^{6} \right], \tag{1.3}$$

in which $r_{ij} = |\mathbf{r}_{ij}| = |\mathbf{r}_i - \mathbf{r}_j|$ is the distance between the particle, ε is the depth of the potential well and σ is the (finite) distance at which the interparticle potential is zero. $u_{\text{LJ}}(r)$ has a minimum at $r^* = 2^{1/6}\sigma$ and $u_{\text{LJ}}(r^*) = -\varepsilon$. Usually, interactions beyond a certain distance r_{cut} are not taken into account.

If one wants to simulate a bulk system without a surface present, a set of *periodic boundary conditions* can be used [52]. This means that a simulation box is surrounded by copies of itself. When a particle leaves the central box on one side, it enters the central box on the other side. Particle i in the central box only interacts with the nearest image of particle j, which may be located in the central box or in one of the images. This is called the *nearest image convention*. The nearest image convention is automatically satisfied if the cut-off radius r_{cut} is smaller than half the box size.

1.3.1 Molecular Dynamics

Molecular Dynamics (MD) simulations were first introduced by Alder and Wainwright in the late 1950's [59, 60] to investigate the phase diagram of a hard sphere system, and in particular the solid and liquid regions. In a hard sphere system, particles interact via instantaneous collisions, and travel as free particles between collisions.

MD simulations are very similar to real experiments. The system is "prepared" by selecting a model system consisting of N particles and after equilibration some

quantities can be measured at different time steps, such as the instantaneous temperature. To measure an observable quantity in a MD simulation, the trajectory of the particles in the system is needed. For instance, the instantaneous temperature $T(t)$ can be calculated using the following relation

$$T(t) = \sum_{i=1}^{N} \frac{m_i \mathbf{v}_i^2(t)}{k_B N_f}, \tag{1.4}$$

in which $N_f = dN - d$ is the number of degrees of freedom for a d-dimensional system of N particles with fixed total momentum, m_i is the mass and $\mathbf{v}_i$ is velocity of particle i. This relation follows from equating the kinetic energy of the system $\sum_{i=1}^{N} \frac{1}{2} m_i \mathbf{v}_i^2(t)$ to the average kinetic energy $\frac{1}{2} N_f k_B T$. The temperature T is calculated by averaging the instantaneous temperature over many time steps: $T = \langle T(t) \rangle$.

The velocities need to be solved numerically by integrating Newton's equations of motion. First, the forces on all particles need to be computed. Forces between the particles are given by an interaction potential $u(r_{ij})$. From the positions of the particles, the net force $\mathbf{F}_i$ on each particle i can be calculated

$$\mathbf{F}_i = \sum_{j} \mathbf{f}_{ij}, \tag{1.5}$$

$$\mathbf{f}_{ij} = -\frac{\mathbf{r}_{ij}}{|\mathbf{r}_{ij}|} \frac{du(r_{ij})}{dr_{ij}}, \tag{1.6}$$

in which $|\mathbf{r}_{ij}|$ is the distance between particle i and j. Given this force and using Newton's second law $\mathbf{F}_i = m_i \mathbf{a}_i$, the acceleration $\mathbf{a}_i$ of each particle with mass m_i can be calculated. Numerous numerical algorithms have been developed for integrating the equations of motion. The Verlet algorithm uses positions and accelerations at time t and the positions at time $t - \Delta t$ to calculate new positions at time $t + \Delta t$

$$\mathbf{r}_i(t + \Delta t) = 2\mathbf{r}_i(t) - \mathbf{r}_i(t - \Delta t) + \frac{\mathbf{F}_i(t)}{m_i} \Delta t^2. \tag{1.7}$$

The velocity can be derived from the trajectory, using

$$\mathbf{v}_i(t) = \frac{\mathbf{r}_i(t + \Delta t) - \mathbf{r}_i(t - \Delta t)}{2\Delta t}. \tag{1.8}$$

Alternatives to the Verlet algorithm are the Euler algorithm [52], the Leap Frog algorithm [61], the Velocity Verlet algorithm [62] and the Beeman algorithm [52].

For the case of particles with friction, Silbert *et al.* [63, 64] used MD simulations that account for both the normal and tangential forces. Particles in contact experience a relative normal compression $\delta = \left| |\mathbf{r}_{ij}| - d \right|$ (in which d is the particle diameter). The normal and tangential contact forces are given by

$$\mathbf{f}_{n,ij} = k_n \delta \frac{\mathbf{r}_{ij}}{r_{ij}} - \frac{m}{2} \gamma_n \mathbf{v}_n, \tag{1.9}$$

$$\mathbf{f}_{t,ij} = -k_t \mathbf{s}_t - \frac{m}{2} \gamma_t \mathbf{v}_t, \tag{1.10}$$

where $k_{n,t}$ and $\gamma_{n,t}$ are elastic and viscoelastic constants. $\mathbf{s}_t$ is the elastic tangential displacement between spheres. By integrating the velocities during elastic deformation of the contact $\mathbf{s}_t$ can be calculated

$$\frac{d\mathbf{s}_t}{dt} = \mathbf{v}_t - \frac{(\mathbf{s}_t \cdot \mathbf{v}) \mathbf{r}_{ij}}{r_{ij}^2}. \tag{1.11}$$

At the initiation of a contact $\mathbf{s}_t$ is set to zero. As necessary to satisfy a local Coulomb yield criterion, the magnitude of $\mathbf{s}_t$ is truncated. From Eqs. 1.9, 1.10, 1.11 it becomes clear that the preparation history of the contacts will have a strong influence on the final contact force distribution at mechanical equilibrium.

1.3.2 Monte Carlo

The physicists Stanislaw Ulam, Enrico Fermi, John von Neumann, and Nicholas Metropolis proposed a method to study differential equations with a statistical approach [65]. More than fifty years ago, the first Monte Carlo simulations were performed in the Los Alamos National Laboratory for early work relating to the development of the hydrogen bomb. Monte Carlo simulations were named after the famous casino in Monte Carlo. This emphasized the importance of randomness or probability.

Monte Carlo simulation methods are especially useful in studying systems with a large number of degrees of freedom $\mathbf{c}$, such as the coordinates of particle, spin states and in our case contact forces. The instantaneous value of an observable quantity $A(\mathbf{c})$ depends only on the degrees of freedom $\mathbf{c}$. Not every state is equally probable; the probability of finding the system in state $\mathbf{c}$ is proportional to the probability density

$\rho(\mathbf{c})$. Therefore, the average of an observable A follows from

$$\langle A \rangle = \frac{\int d\mathbf{c}\,\rho(\mathbf{c})A(\mathbf{c})}{\int d\mathbf{c}\,\rho(\mathbf{c})}. \tag{1.12}$$

For almost all physically relevant systems, it is not possible to solve these integrals analytically or numerically using conventional numerical integration techniques, because of the high dimensional phase space of these systems. A possible way to compute averages is to generate a sufficiently large number K of random states k. Equation (1.12) can be approximated using

$$\langle A \rangle = \frac{\lim\limits_{K\to\infty} \sum\limits_{k=1}^{K} \rho(\mathbf{c}_k)A(\mathbf{c}_k)}{\lim\limits_{K\to\infty} \sum\limits_{k=1}^{K} \rho(\mathbf{c}_k)}. \tag{1.13}$$

However, *random sampling* is a very inefficient approach, because almost all states have a very low probability density $\rho(\mathbf{c})$ and will not contribute much to the numerator and denominator of Eq.1.13. *Importance sampling* solves this problem by generating states with a probability proportional to $\rho(\mathbf{c})$. In this case, the statistical weight is already taken into account in the generation of the state and therefore ensemble averages can be calculated as unweighted averages

$$\langle A \rangle = \lim\limits_{K\to\infty} \frac{\sum\limits_{k=1}^{K} A(\mathbf{c}_k)}{K}. \tag{1.14}$$

This sampling scheme should not change the equilibrium distribution of the system. This is guaranteed by imposing *detailed balance*, which means that in equilibrium the average number of accepted moves from the old state o to any other new state n is exactly canceled by the number of accepted reverse moves. Note that imposing strict detailed balance is often convenient but not necessary, see Refs. [66, 67]. Metropolis developed a scheme with an acceptance rule that obeys detailed balance [68]:

1. Generate an initial configuration $\mathbf{c}_o$ and calculate $\rho(\mathbf{c}_o)$.

2. Generate a new state $\mathbf{c}_n$ by adding a random displacement to $\mathbf{c}_o$ and calculate $\rho(\mathbf{c}_n)$

3. Accept the trial move with the following acceptance rule

$$P_{\text{acc}}(o \to n) = \min\left(1, \frac{\rho(\mathbf{c}_n)}{\rho(\mathbf{c}_o)}\right). \tag{1.15}$$

The function $\min(a,b)$ returns the smaller of its arguments. If rejected, the old configuration $\mathbf{c}_o$ is kept. According to Eq. (1.15), new states with a larger ρ are always accepted, and new states with a smaller ρ are accepted with a certain probability.

4. Update ensemble averages, also after a rejected move.

5. Consider the actual configuration as old configuration and repeat from step 2.

It has already been mentioned that averages can be calculated in different ensembles. For systems consisting of interacting particles, the most conventional one is the canonical ensemble, in which the number of particles N, volume V and temperature T are constant. The system can exchange energy with a much larger system that act as a heat bath at a fixed temperature. The heat bath is sufficiently large that it is not significantly affected by the smaller system. The ensemble average $\langle A \rangle$ is calculated with Eq. (1.14). Here, the degrees of freedom $\mathbf{c}$ are the coordinates $\mathbf{r}^N$ of all N particles, and $\rho(\mathbf{r}^N) \sim \exp[-\beta U(\mathbf{r}^N)]$ in which $U(\mathbf{r}^N)$ is the total energy of the system and $\beta = 1/(k_B T)$, k_B being the Boltzmann constant. The acceptation rule is therefore as follows

$$P_{\text{acc}}(o \to n) = \min(1, \exp[-\beta(U(\mathbf{r}_n^N) - U(\mathbf{r}_o^N))]) = \min(1, \exp[-\beta \Delta U]). \tag{1.16}$$

Experiments at constant N, V and E are rare, but simulations under these conditions (the microcanonical ensemble) are comparable to the force network ensemble, which will be explained in Section 1.5.

1.3.3   Umbrella sampling

Umbrella sampling is a simulation technique designed to enhance the sampling of rare but important regions of configuration space in a Monte Carlo simulation. This technique was originally invented by Torrie and Valleau in 1977 [69], but it has been re-invented many times under different names [33, 52]. In a Monte Carlo simulation, ensemble averages are computed by sampling configurations with a probability proportional to the probability density $\rho(\mathbf{c})$. However, one can perform the simulation in

a different ensemble (here denoted by π), in which configurations are sampled with a probability

$$\rho'(\mathbf{c}) = \rho(\mathbf{c})\exp[W(\mathbf{c})], \tag{1.17}$$

In this equation, $W(\mathbf{c})$ is an arbitrary function that only depends on $\mathbf{c}$. The ensemble average $\langle A \rangle_\pi$ in ensemble π is defined as

$$\langle A \rangle_\pi = \frac{\int d\mathbf{c}\, A(\mathbf{c})\rho'(\mathbf{c})}{\int d\mathbf{c}\, \rho'(\mathbf{c})}. \tag{1.18}$$

It is important to note that $\langle A \rangle \neq \langle A \rangle_\pi$. In the ensemble π some regions of the configuration space are oversampled compared to the original ensemble, but when calculating the averages this oversampling can be corrected *exactly*

$$
\begin{aligned}
\langle A \rangle &= \frac{\int d\mathbf{c}\, A(\mathbf{c})\rho(\mathbf{c})}{\int d\mathbf{c}\, \rho(\mathbf{c})} \\[2ex]
&= \frac{\int d\mathbf{c}\, A(\mathbf{c})\exp[-W(\mathbf{c})]\rho'(\mathbf{c})}{\int d\mathbf{c}\, \exp[-W(\mathbf{c})]\rho'(\mathbf{c})} \\[2ex]
&= \frac{\dfrac{\int d\mathbf{c}\, A(\mathbf{c})\exp[-W(\mathbf{c})]\rho'(\mathbf{c})}{\int d\mathbf{c}\, \rho'(\mathbf{c})}}{\dfrac{\int d\mathbf{c}\, \exp[-W(\mathbf{c})]\rho'(\mathbf{c})}{\int d\mathbf{c}\, \rho'(\mathbf{c})}} \\[2ex]
&= \frac{\langle A(\mathbf{c})\exp[-W(\mathbf{c})]\rangle_\pi}{\langle \exp[-W(\mathbf{c})]\rangle_\pi}. \tag{1.19}
\end{aligned}
$$

In this thesis we will apply umbrella sampling to enhance the sampling of networks with large contact forces. A natural order parameter to characterize force networks with large forces is the maximum force $f_{\max}$ of a force network $\mathbf{f}$, and therefore we choose $W(\mathbf{c}) = W(f_{\max}(\mathbf{f}))$. In the ideal case, the weight function is chosen $W(f_{\max}) = -\ln P(f_{\max})$ such that all values $f_{\max}$ will be sampled with equal probability in the ensemble π. However, to construct such a weight function, already a good estimate of $P(f_{\max})$ is needed. Therefore, several simulations are performed
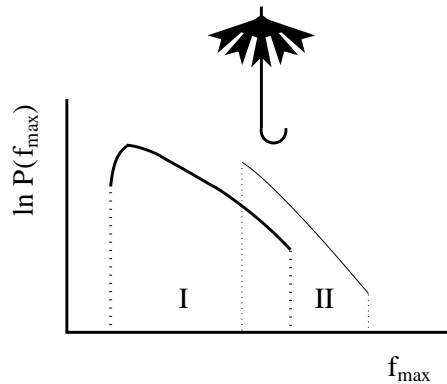
Figure 1.4: Schematic representation of the probability distribution of the order parameter $P(f_{max})$ in two different windows I and II that have a small overlap. The order parameter distribution in both windows are related by $\ln P_I(f_{max}) = \ln P_{II}(f_{max}) + C$ in which C is a constant.

starting with $W(f_{max}) = 0$. After each simulation, an improved weight function can be calculated. This iterative process is stopped when $P(f_{max})$ is approximately flat. See Section 1.6 for a more detailed explanation of umbrella sampling applied to the force network ensemble. In Chapter 3, we will investigate the distribution of *local pressure p* of a grain. To sample large local pressures, it turns out that it is convenient to perform umbrella sampling using a weight function $W(p_{max}(\mathbf{f}))$ in which p_{max} is the largest local pressure in the system.

The weight function can also be used to force the system to stay in some particular regions (windows) of the phase space. When the whole range of the order parameter is divided into overlapping windows, for each window a separate simulation with a unique weight function can be performed. In this way, for each window an order parameter distribution can be computed (see Fig. 1.4). By matching these order parameter probabilities where the windows overlap one finally obtains the distribution over the whole order parameter range. This overlapping property is responsible for the name *umbrella sampling*.

1.4 Generation of disordered packings

All numerical results presented in this thesis concern the statistics of contact forces in static granular matter. We will investigate both positionally ordered (triangular, square, fcc and hcp lattices) and positionally disordered systems.

To generate a disordered packing of N particles in 2D, first an initial particle configuration is made by placing the particles randomly in the box. Following O'Hern *et al.* [12], we simulate a bidisperse 50%/50% binary system with a size ratio of 1.4. This size ratio prevents the system from crystallization [34]. The particles interact via the Weeks-Chandler-Anderson (WCA) potential [70]

$$u_{\text{WCA}}(r_{ij}) = \begin{cases} u_{\text{LJ}}(r_{ij}) + \varepsilon, & r_{ij} \leq 2^{1/6}\sigma_{ij} \\ 0, & r_{ij} > 2^{1/6}\sigma_{ij}, \end{cases} \tag{1.20}$$

The WCA potential has the same shape as the Lennard-Jones (LJ) potential, but it is truncated (at the minimum of $u_{\text{LJ}}(r_{ij})$) and shifted. The attractive dispersion tail of the LJ interaction is not included: the WCA potential is purely repulsive. Simulations to generate a force balanced packing start from randomly positioned particles in a square box with periodic boundaries. To prepare the initial particle configuration, the energy is minimized using a combination of the steepest descent algorithm [71] and the algorithm of Snyman [72–74]. The latter algorithm is very efficient in generating configurations with very small energy gradients. Finding a local energy minimum or saddle point in a high-dimensional space is not trivial, see for example Refs. [75, 76].

We use two methods to generate the final particle configuration from the initial configuration: quenching [12] and compressing [77]. In practice, quenching is only applicable for preparing systems with a high coordination number. In this method, first, a molecular dynamics simulation at constant volume V is performed at a temperature T above the glass transition temperature T_g. After equilibration, we set $T < T_g$ and continue the MD simulation at constant T, V. Finally, the potential energy is minimized. From the final configuration, we determine all contacts in the system. As the interaction potential is short-ranged and vanishes for distances larger than the size of the particle, it is natural to define the presence of a contact between particles i and j if $r_{ij} < r_{\text{cut}} = 2^{1/6}\sigma_{ij}$. Note that for systems with long-range interactions (e.g. the full Lennard-Jones potential truncated at $r_{\text{cut}} \geq 2.5\sigma_{ij}$) it is less trivial to define contact and the average contact number [78]. The final packing (positions of all particles and a list of all pair contacts) can be used as input for simulations using the

force network ensemble. The coordination number z of the packing can be tuned by varying the initial density of the system.

In the compressing method, we start with a configuration in which all particles are randomly placed in a very large volume V in such a way that none of the particles overlap (i.e. $r_{ij} > 2^{1/6}\sigma_{ij}$ for all i and j). The system is slowly compressed. If an overlap between particles is detected, we perform an energy minimization at constant volume. This procedure is continued until the required coordination number is reached. Particles with two or less neighbors are removed from the final packing, because these particles can never have force balance unless their contact forces are zero. The final packing (positions of all particles and a list of all contacts) can be used as input for simulations using the force network ensemble.

1.5   Force network ensemble

In Section 1.2 we have seen that many different model systems are used to study the statistics of contact forces in granular matter, which makes it difficult to compare different studies. In particular, parameters like particle rigidity, crystallinity, construction history, friction, pressure and shear stress may or may not strongly influence the tail of the contact force distribution. In this thesis, we will study the influence of various parameters like the system size, the dimensionality, the structure of the packing, the average contact number, the applied shear stress and the presence of friction in the so-called *force network ensemble*.

The force network ensemble is a recently introduced statistical formulation to study the statistics of contact forces in granular media [43]. The crucial assumption is that for fixed particle positions, all force configurations of non-cohesive forces that result in force balance on all particles are equally likely. This approach can be regarded as a restricted version of the Edwards ensemble [41]. For several regular and disordered packings the contact force distribution $P(f)$ was calculated, which had all the features that are typically observed in experiments and numerics, and subsequently the force network ensemble has received a lot of attention [79–84].

Actual forces in a physical realization of particles that interact via a short-ranged pair potential depend on the distance r_{ij} between the particles. However, for compressed systems that are in mechanical equilibrium, a tiny change in $\mathbf{r}_{ij}$ has a strong effect on the corresponding contact forces. In the force network ensemble it is assumed that a separation of length scales between the forces and the positions occurs.

Therefore, one can treat the forces as independent from the positions [41]. In this way, one can construct an ensemble in which the positions of all particles are fixed, and the non-cohesive contact forces are the degrees of freedom that have to satisfy force balance on each particle. For a fixed packing geometry, the net force $\mathbf{F}_i$ on each particle i is zero

$$\mathbf{F}_i = \sum_j \mathbf{f}_{ij} = \mathbf{0}, \tag{1.21}$$

in which j runs over the particles in contact with particle i. For a frictionless system, this reduces to

$$\mathbf{F}_i = \sum_j \mathbf{f}_{ij} = \sum_j f_{ij} \frac{\mathbf{r}_{ij}}{|\mathbf{r}_{ij}|} = \mathbf{0}, \tag{1.22}$$

in which $\mathbf{r}_{ij} = \mathbf{r}_i - \mathbf{r}_j$. Consider a d dimensional system with N particles and periodic boundary conditions. To describe mechanical equilibrium in d directions, $dN - d$ linear constraints are needed. If frictional particles are considered, then N (for 2D) or $3N$ (for 3D) additional constraints are needed to obtain torque balance on each particle.

In addition to the force balance constraints, it is necessary to constrain the applied stress on the system. The applied stress on a system is defined by the stress tensor

$$\sigma = \begin{pmatrix} \sigma_{xx} & \sigma_{xy} \\ \sigma_{yx} & \sigma_{yy} \end{pmatrix} \quad \text{in 2D, and} \quad \sigma = \begin{pmatrix} \sigma_{xx} & \sigma_{xy} & \sigma_{xz} \\ \sigma_{yx} & \sigma_{yy} & \sigma_{yz} \\ \sigma_{zx} & \sigma_{zy} & \sigma_{zz} \end{pmatrix} \quad \text{in 3D} \tag{1.23}$$

in which

$$\sigma_{\alpha\beta} \sim \frac{1}{V} \sum_{ij} f_{ij,\alpha} r_{ij,\beta}. \tag{1.24}$$

However, in the Force Network Ensemble it is more convenient to use a slightly different normalization:

$$\sigma_{\alpha\beta} = \frac{1}{N_b} \sum_{ij} f_{ij,\alpha} r_{ij,\beta}. \tag{1.25}$$

In this equation $N_b = zN/2$ equals the total number of contacts. In 2D, the contact force in the direction α, $f_{ij,\alpha}$ can be written as

$$f_{ij,x} = f_{n,ij} \frac{r_{ij,x}}{|\mathbf{r}_{ij}|} + f_{t,ij} \frac{r_{ij,y}}{|\mathbf{r}_{ij}|}, \tag{1.26}$$

$$f_{ij,y} = f_{n,ij} \frac{r_{ij,y}}{|\mathbf{r}_{ij}|} - f_{t,ij} \frac{r_{ij,x}}{|\mathbf{r}_{ij}|}. \tag{1.27}$$

Table 1.1: The number of constraints (force and torque balance on each particle, and a fixed stress tensor σ) and the number of elements of **f** for systems with periodic boundary conditions, N particles and an average coordination number z. The terms -2 and -3 originate from Newtont's third law applied to the whole system.

dimension d	friction	# constraints	# elements of **f**
2	no	$2N-2+3$	$zN/2$
2	yes	$2N-2+3+N$	zN
3	no	$3N-3+6$	$zN/2$
3	yes	$3N-3+6+3N$	zN

in which $f_{n,ij}$ and $f_{t,ij}$ are the normal and tangential components of the force respectively. The dimensionless shear stress is defined as $\tau = \sigma_{\alpha\beta}/\sigma_{\alpha\alpha}$ and the pressure on a system is proportional to $\sum_\alpha \sigma_{\alpha\alpha}$. An isotropic pressure corresponds to $\sigma_{xx} = \sigma_{yy} (= \sigma_{zz})$. By imposing $\langle f \rangle = 1$ a scale for the forces is introduced. Substituting Eqs. (1.26) and (1.27) into Eq. (1.25) we find $\sigma_{\alpha\alpha} = 1/d$ in the case that $|\mathbf{r}_{ij}| = 1$ (regular packings). However, in the case that $|\mathbf{r}_{ij}| \neq 1$, we will find $\sigma_{\alpha\alpha} \neq 1/d$ and $\langle f \rangle \neq 1$.

The contact forces $f_{ij,\alpha}$ in a force network are the elements of the vector **f**. The elements of this vector **f** are subject to the constraint that all particles have force and torque balance, and that the constraints on the stress tensor are satisfied. In Table 1.1, the number of constraints and the number of elements of **f** are summarized. For packings with $z > z_c$ ($z_c = 4$ for frictionless and $z_c = 3$ for frictional 2D packings [43]), the number of elements of **f** exceeds the number of constraints, which means that there is a high-dimensional force space of solutions. Note that in dry granular media all forces are repulsive, which is incorporated by demanding all normal forces f_n to be positive,

$$f_{n,ij} \geq 0. \qquad (1.28)$$

Snoeijer *et al.* assumed that all allowed solutions of this force space are equally likely, like in the microcanonical ensemble and the Edwards ensemble [41]. The corresponding ensemble is therefore called the force network ensemble. Using the force network ensemble with this flat measure, realistic $P(f)$ have been obtained, both on triangular lattices and on disordered packings [43].

In Ref. [85], analytical solutions for $P(f)$ in the force network ensemble for various small systems were obtained: "snooker" packings [42] of 3 and 6 particles, peri-

odic triangular lattices of 2×2 and 3×3, and a periodic fcc unit cell (8 particles). In Ref. [80] analytical expressions are derived for both isotropic and anisotropic force distributions in the 3×3 triangular lattice. Unfortunately, these analytical approaches are not suited for larger systems so we have to rely on computer simulations. To compute a *single* solution of the force space of a disordered system, a simulated annealing procedure can be applied [71]. For arbitrary forces, a penalty function $U(\mathbf{f})$ is defined that describes the deviation from the required constraints. For a 2D frictionless system with $|r_{ij}| = 1$, this penalty function is defined as

$$U(\mathbf{f}) = |\sigma_{xy}(\mathbf{f}) - \sigma_{xy}^{\mathrm{req}}| + |\sigma_{xx}(\mathbf{f}) - \tfrac{1}{2}| + |\sigma_{yy}(\mathbf{f}) - \tfrac{1}{2}|$$
$$+ \sum_{i=1}^{N} |F_{i,x}(\mathbf{f})| + \sum_{i=1}^{N} |F_{i,y}(\mathbf{f})|. \qquad (1.29)$$

in which $\sigma_{xy}^{\mathrm{req}}$ is the required (imposed) shear stress of the system. The following Monte Carlo procedure can be used to generate a *single* force network $\mathbf{f}$ that obeys the required constraints

1. Start with a configuration $\mathbf{f}_{\mathrm{old}}$ in which all forces are taken from an arbitrary distribution with $\langle f \rangle = 1$ and $f_{ij} \geq 0$. Set the control parameter $\beta = 1$ (equivalent to the temperature) and calculate the penalty function $U(\mathbf{f}_{\mathrm{old}})$.

2. Select two elements (contact forces) of $\mathbf{f}$ at random.

3. Add a randomly selected Δf to one contact force and $-\Delta f$ to the other contact force, so that $\langle f \rangle$ still equals 1. If any of these forces becomes smaller than 0, the move is rejected and we return to step 2.

4. Calculate the penalty function $U(\mathbf{f}_{\mathrm{new}})$.

5. Accept the trial move with the acceptance rule Eq. (1.16). If rejected, the old configuration is kept.

6. Increase β by multiplying with a factor $h > 1$ (i.e. annealing).

7. Return to step 2 until the penalty function is very small (typically 10^{-12}). The resulting $\mathbf{f}$ is considered as a particular solution of the force network ensemble.

It is trivial to extend this scheme for frictional packings and packings with $|\mathbf{r}_{ij}| \neq 1$. In previous studies [11, 43, 85, 86], the solution space of the force network ensemble

was sampled by generating many particular solutions obtained using this simulated annealing scheme. This scheme reproduces analytic results for small regular packings very well [85] and it was verified that the results do not depend on the initial configurations and details of the annealing scheme. Unfortunately, this simulated annealing procedure is computationally expensive and it cannot be guaranteed that force networks are indeed generated with equal *a priori* probability. Moreover, accurate statistics for large contact forces can not be obtained directly.

At this point it is important to note that the force network ensemble can be formulated as an inhomogeneous matrix equation

$$\mathscr{A}\mathbf{f} = \mathbf{b}, \tag{1.30}$$

in which static force (and torque) balance on each particle as well as a conserved stress tensor are incorporated [43]. The elements of the fixed matrix $\mathscr{A}$ are determined by the geometry of the packing. The vector $\mathbf{b}$ reflects the force and torque balance on each grain, as well as the fixed stress tensor. For a 2D system, $\mathbf{b} = (0, 0, \cdots, 0, \sigma_{xx}, \sigma_{yy}, \sigma_{xy})$. All possible solutions of Eq. (1.30) can be written as

$$\mathbf{f} = \mathbf{f}_0 + \sum_k a_k \mathbf{v}_k, \tag{1.31}$$

where $\mathbf{f}_0$ is a *particular* solution and the vectors $\mathbf{v}_k$ span the null-space of matrix $\mathscr{A}$, i.e.,

$$\mathscr{A}\mathbf{v}_k = \mathbf{0}. \tag{1.32}$$

The number of independent null vectors follows directly from Table 1.1. The coefficients a_k are restricted by the condition that all elements of $\mathbf{f}$ corresponding to *normal* forces need to be positive. For disordered packings, we used the simulated annealing procedure described earlier to obtain both a particular solution $\mathbf{f}_0$ and the null vectors $\mathbf{v}_k$. Note that in order to compute a null-vector, the penalty function has to be modified slightly and one needs to realize that the elements of $\mathbf{v}_k$ can be positive as well as negative. All vectors of the null-space are orthogonalized for efficiency reasons of our sampling scheme, although in principle this is not needed for the correctness of our scheme.

The force network ensemble is sampled by the usual Metropolis Monte Carlo technique (see Section 1.3.2) in which the coefficients a_k are the degrees of freedom. The Monte Carlo scheme is started with $a_k = 0$ and a particular solution $\mathbf{f}_0$. In a trial move, a coefficient a_k is chosen at random and its value is changed randomly.
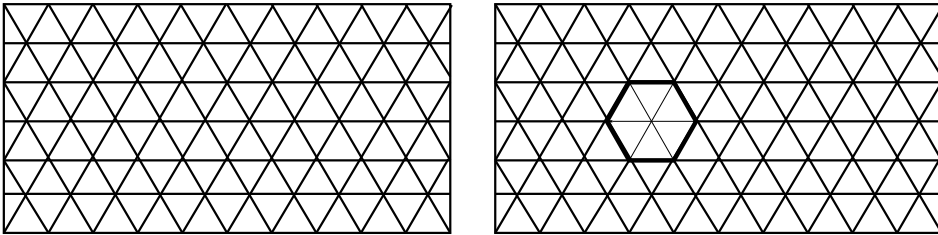
Figure 1.5: Sampling force networks of a frictionless triangular lattice [80]. The thickness of the lines represent the magnitude of the (normal) force. In the starting configuration (left) all normal contact forces are equal to 1. After a wheel move, 6 normal forces (the "rim") get displacement of $+\Delta$ and six other forces (the "spokes") get a displacement of $-\Delta$. This new configuration (right) still satisfies force balance on each particle and the stress tensor does not change. If any of the contact forces will become smaller than zero, the wheel move is rejected.

A trial move is accepted when all normal forces $f_{ij} \geq 0$. For frictional systems, one has to take into account the Coulomb criterium Eq. 1.1 in the acceptance rule. In this scheme, it is guaranteed that all allowed force networks are sampled with equal probability.

For the triangular, square, and fcc lattice, it is convenient to choose $\mathbf{f}_0$ such that all elements $\mathbf{f}_0$ are all equal to 1. The null-space $\mathbf{v}_k$ can be expressed by the so-called "wheel moves" developed by Tighe *et al*. [80]. For a frictionless triangular lattice, a wheel move is centered around a single particle. As can be seen in Fig. 1.5, only 12 forces are involved in a wheel move: 6 contact forces of the central particle ("spokes") and six forces that form the "rim" of the central particle. Therefore, all elements of $\mathbf{v}_k$ are equal to zero except these 12 forces. In the MC procedure described above, the forces of the rim get a displacement of $+\Delta$ and the spokes get a displacement of $-\Delta$. The obtained configuration still satisfies the required constraints. The advantage of a local wheel move is the low number of forces that are changed. This means that a larger maximum displacement Δ is allowed. B.P. Tighe has developed a set of (local) wheel moves for the frictionless triangular lattice, the frictionless fcc lattice, the frictional triangular lattice, and the frictional square lattice [87].

In previous simulations in the force network ensemble for *disordered systems* [11, 40, 43, 85, 86], the value of all bond lengths $|\mathbf{r}_{ij}|$ in Eqs. (1.26) and (1.27) was simply set to 1, even for contacts at a distance *not* equal to 1. Essentially, this
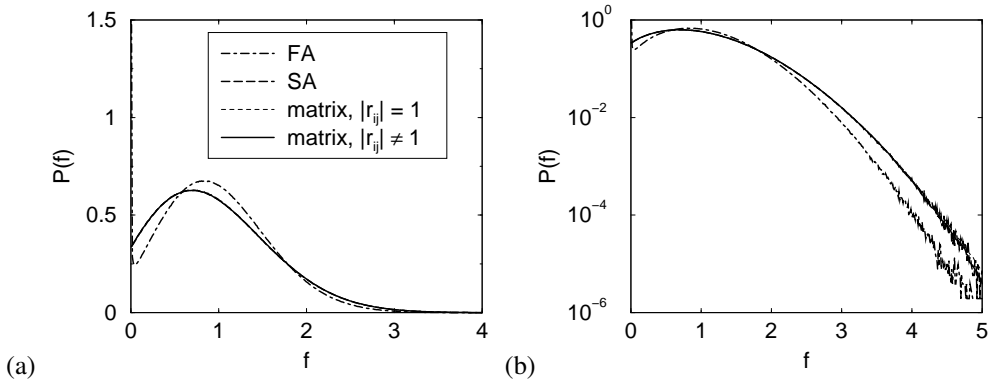
Figure 1.6: Contact force distribution $P(f)$ of frictionless particles in 2D ($N = 750$, $z = 5.5$) computed with a simulated annealing procedure (FA: fast annealing, SA: slow annealing) and the matrix method Eq. (1.31). Forces are normalized such that $\langle f \rangle = 1$. In the simulated annealing method, all bond lengths $\left| \mathbf{r}_{ij} \right|$ were normalized to 1. Clearly, setting all $\left| \mathbf{r}_{ij} \right| = 1$ does not alter the contact force statistics. The curves of SA and the matrix method lay exactly on top of each other. When the annealing is performed too quickly (FA, large value of h), incorrect contact force distributions are obtained.

means that it is assumed that the value of the contact force and the bond length are uncorrelated, which has been verified numerically [43]. The possible advantage of this approach is that this assumption directly results in normalization of forces: $\sigma_{xx} + \sigma_{yy} (+\sigma_{zz}) = \langle f \rangle = 1$ and at isotropic pressure $\sigma_{xx} = \sigma_{yy} (= \sigma_{zz}) = 1/d$. In later work, this assumption was *not* used, but instead we set $\sigma_{xx} = \sigma_{yy} (= \sigma_{zz})$. This means that in these simulations, the average force in the force network ensemble is not constant.

In Fig. 1.6, we have compared the various methods and assumptions to sample the force network ensemble for a disordered system in 2D. The simulated annealing method produces the same contact force distribution as the matrix method when the annealing rate h is sufficiently low, even though it is not guaranteed that simulated annealing samples force networks uniformly. If the annealing rate is too large, we observe an incorrect contact force distribution in which many forces are very small. This is not the case for slow annealing and the matrix method. The assumption that the distance between two particles and their contact force are uncorrelated is valid as was reported earlier [43].

1.6 Umbrella sampling applied to the force network ensemble

In Section 1.5, we have shown how to sample all solutions of the force network ensemble using a Monte Carlo scheme. The sampling is performed in the space spanned by the null-vectors of matrix $\mathscr{A}$ (see Eq. (1.31)). All force networks for which all elements of $\mathbf{f}$ are positive are in principle equally likely. However, the number of force networks in which at least one of the forces is much larger than the average force is low compared to force networks in which all forces are quite close to the average force. Therefore, standard Monte Carlo sampling results in poor statistics for the tail of the contact force distribution $P(f)$. As explained in Section 1.3.3, this can be improved using *umbrella sampling*. To improve the statistics for large contact forces, we use the largest force of a certain force network $f_{\max}(\mathbf{f})$ as an order parameter. The probability density in the modified ensemble then becomes

$$\rho'(\mathbf{f}) = \rho(\mathbf{f}) \exp[W(f_{\max}(\mathbf{f}))], \tag{1.33}$$

in which $\rho(\mathbf{f})$ is the statistical weight of the force network ensemble and $W(f_{\max}(\mathbf{f}))$ is a weight function. Ensemble averages in the force network ensemble can be computed using

$$\langle A \rangle = \frac{\langle A(\mathbf{f}) \exp[-W(f_{\max}(\mathbf{f}))]\rangle_\pi}{\langle \exp[-W(f_{\max}(\mathbf{f}))]\rangle_\pi}, \tag{1.34}$$

in which we used the shorthand $\langle \cdots \rangle_\pi$ to compute averages in the modified ensemble. For example, the probability distribution of the largest force in the system can be computed from

$$
\begin{aligned}
P(f_{\max}) &= \frac{\int d\mathbf{f}\,\rho(\mathbf{f})\,\delta(f_{\max} - f'_{\max}(\mathbf{f}))}{\int d\mathbf{f}\,\rho(\mathbf{f})} \\
&= \frac{P_\pi(f_{\max})\exp[-W(f_{\max})]}{\int df'_{\max}\,P_\pi(f'_{\max})\exp[-W(f'_{\max})]},
\end{aligned} \tag{1.35}
$$

in which $P_\pi(\cdots)$ denotes a probability distribution in the modified ensemble. Note that the probability distribution $P(f_{\max})$ will depend on the size of the system. Simi-

larly, we can write for the contact force distribution

$$P(f) = \lim_{a \to \infty} \frac{\int_0^a df_{\max} P(f|f_{\max}) P(f_{\max})}{\int_0^a df' \int_0^a df_{\max} P(f'|f_{\max}) P(f_{\max})}, \tag{1.36}$$

in which $P(f|f_{\max})$ is the conditional contact force distribution given that the maximum force in the force network equals $f_{\max}$. Of course, $P(f|f_{\max}) = 0$ if $f > f_{\max}$. The distribution $P(f|f_{\max})$ can be computed directly in a simulation in the modified ensemble.

To illustrate the umbrella sampling technique for the force network ensemble, in Fig. 1.7 we have plotted the probability distributions $P(f)$ and $P(f_{\max})$ computed with and without umbrella sampling. Clearly, without umbrella sampling large contact forces are hardly sampled. Umbrella sampling significantly improves the contact force statistics for large forces, while still the correct distributions are obtained after reweighting. Interestingly, for small forces, all $P(f)$'s in Fig. 1.7(c,d) are very close, suggesting that $P(f|f_{\max})$ does not strongly depend on the precise value of $f_{\max}$ as long as f is small. This means that the presence of a single large force does not influence the statistics of the small forces very much. Fig. 1.8 shows a typical configuration of a force network for a large value of $f_{\max}$. Clearly, a large force induced correlations over many contacts. When the size of these correlations are of the order of the system size, finite size effects can be expected. We will come back to this issue in Section 4.4.

In Fig. 1.9 we have plotted the contact force distribution computed using Eq. (1.36) for various values of the maximum allowed force a in the ensemble. The contact force distributions fall on top of each other, which means that force networks for which $f_{\max} > a$ have no influence on $P(f)$ for $f < a$. The reason for this is that $P(f_{\max})$ decays very quickly for large forces.
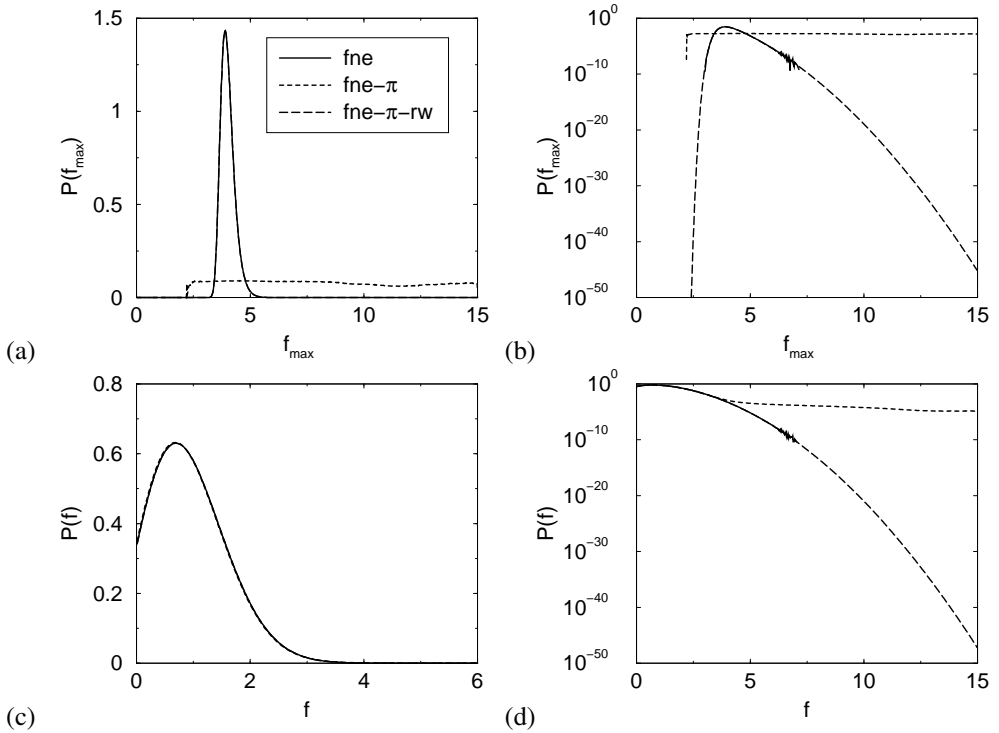
Figure 1.7: (a,b) Probability distributions of the maximum force f_{max} in a force network and (c,d) contact force distributions of a frictionless triangular lattice ($N = 1840$) in three different ensembles: *(1)* the force network ensemble without umbrella sampling (fne), *(2)* the ensemble π in which $W(f_{max})$ is chosen such that $P_\pi(f_{max})$ is approximately flat (fne-π), and *(3)* the ensemble π in which ensemble averages are reweighted to the force network ensemble using Eq. (1.34) (fne-π-rw). Forces are normalized such that $\langle f \rangle = 1$. Forces larger than $5 \langle f \rangle$ are hardly sampled in the force network ensemble unless umbrella sampling is applied.
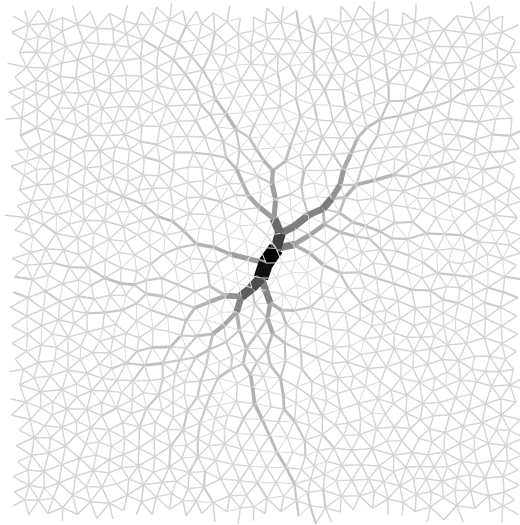
Figure 1.8: Typical snapshot of a force network with a large value of $f_{\max}$.
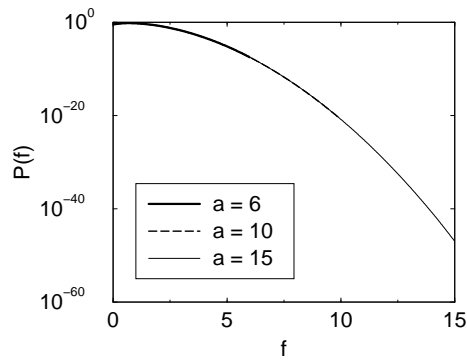

Figure 1.9: Contact force distribution computed using Eq. (1.36) as a function of the maximum allowed force a in the ensemble. Forces are normalized such that $\langle f \rangle = 1$.

1.7   Determination of the asymptotic behavior of $P(f)$

In Chapter 2 we will see that for very large contact forces, the asymptotic behavior (the "tail") of contact force distributions can be described by

$$P(f) \sim a \exp[-bf^{\alpha}]. \tag{1.37}$$

In particular, it is interesting to see whether this distribution is exponential ($\alpha = 1$), Gaussian ($\alpha = 2$), or something else. We considered two options to extract α:

1. The use of a triple-log plot, i.e. a plot of $\log_{10}(-\log_{10} P(f))$ versus $\log_{10} f$. In good approximation the slope of such a plot will equal α.

2. For $f \gg \langle f \rangle$, we perform linear regression to fit a and b in $\log_{10} P(f) = a - bf^{\alpha}$ for a wide range of α. The maximum in the regression coefficient R^2 is used to determine α.

In Fig. 1.10, we have used both methods to extract α from a *known* exponential and Gaussian distribution (note $f \geq 0$):

$$P_{\exp}(f) = \frac{1}{a} \exp[-f/a], \tag{1.38}$$

$$P_{\text{Gauss}}(f) = \frac{2}{\sqrt{2\pi}\sigma} \exp[-f^2/(2\sigma^2)], \tag{1.39}$$

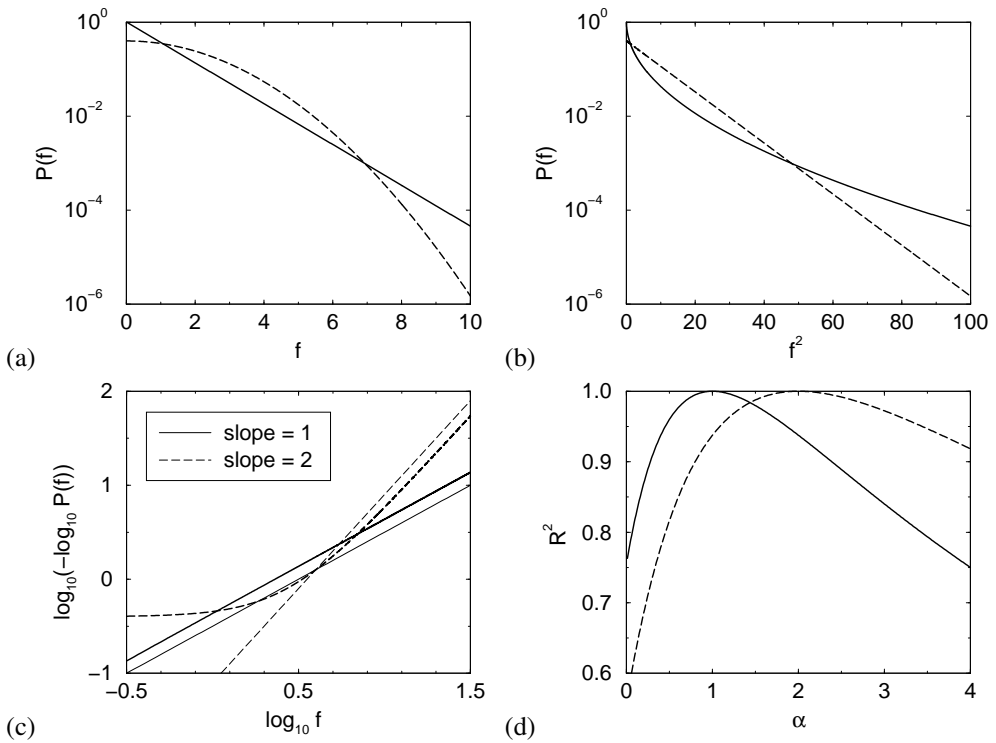with $a = 1$ and $\sigma = 2$. Clearly, both methods quickly recover the correct asymptotic behavior.

Figure 1.10: An exact exponential (solid, Eq. (1.38)) and Gaussian (dashed, Eq. (1.39)) distribution on a logarithmic scale plotted against (a) f and (b) f^2. (c) A triple-log plot of these distributions. The slope (i.e. α) for the exponential distribution equals 1 and for the Gaussian distribution the slope equals 2. (d) The regression coefficient R^2 as a function of α for fits to Eq. 1.37 of both distributions. The best fit for the exponential distribution is obtained with $\alpha = 1$ and for the Gaussian distribution with $\alpha = 2$.

1.8 Outline

This thesis focuses on the statistics of large forces in granular media by using the force network ensemble. One of the crucial questions is whether the tail of the contact force distribution $P(f)$ is exponential, Gaussian, or even some other form. We resort to umbrella sampling to unambiguously resolve the asymptotic decay of $P(f)$ for large f, and determine $P(f)$ down to values of order 10^{-45}.

In Chapter 2, we study the distribution $P(f)$ of contact forces between frictionless particles. We explore the effect of packing structure, dimensionality, system size, contact number and shear stress. We find that local force balance constraints determine the asymptotic behavior of $P(f)$ and that the dimensionality is the most important parameter that determines the tail of $P(f)$. In particular, we find that $P(f)$ decays as $a\exp[-bf^\alpha]$ with $\alpha = 2.0 \pm 0.1$ for 2D systems, $\alpha = 1.7 \pm 0.1$ for 3D systems and $\alpha = 1.4 \pm 0.1$ for 4D systems. Other factors like the coordination number and the structure of the packing are of less importance.

Chapter 3 presents simulations of the local pressure distribution for both frictionless and frictional packings. The numerically obtained pressure distributions are in excellent agreement with the pressure distributions obtained from an entropy maximization argument by B.P. Tighe *et al*. [88]. The latter follows from a previously not exploited conserved quantity in the force network ensemble: the total area of the so-called reciprocal tiling, which follows directly from force balance on each particle.

Finally, in Chapter 4 we present a detailed study on the force network ensemble for various packings/systems. In particular, we focus on dimensionality of the force space, the maximum possible force of a packing, the effect of boundary forces, and the angle-resolved contact force distribution. We also present a comparison of the contact force statistics between the force network ensemble and packings of particles that interact with a real pair potential.

2

Tail of the contact force distributions in static granular materials

We numerically study the distribution $P(f)$ of contact forces in frictionless bead packs, by averaging over the ensemble of all possible force network configurations. We resort to umbrella sampling to resolve the asymptotic decay of $P(f)$ for large f, and determine $P(f)$ down to values of order 10^{-45} for ordered and disordered systems in two (2D) and three dimensions (3D). Our findings unambiguously show that, in the ensemble approach, the force distributions decay much faster than exponentially: $P(f) \sim \exp(-cf^{\alpha})$, with $\alpha \approx 2.0$ for 2D systems, $\alpha \approx 1.7$ for 3D systems, and $\alpha \approx 1.4$ for 4D systems.

2.1 Introduction

The contact forces inside a static packing of grains are organized into highly het-erogeneous force networks, and can be characterized by the probability density of contact forces $P(f)$ [18]. Such force statistics were first studied in a series of exper-iments that measured forces through imprints on carbon paper at the boundaries of a granular assembly. Unexpectedly, the obtained $P(f)$ displayed an exponential rather than a Gaussian decay for large forces [15, 21–23]. After these initial findings, other experimental techniques have revealed similarly exponentially decaying distributions of the boundary forces [20, 24].

As it is difficult to experimentally access contact forces *inside* the packing, nu-merous direct numerical simulations of $P(f)$ have been undertaken [12, 27, 28, 36, 37]. While many of these studies claim to find an exponential tail as well, the evi-dence is less convincing than for the carbon paper experiments: apart from Ref. [27], nearly all numerical force probabilities bend down on a logarithmic plot, suggesting a faster than exponential decay [12, 28, 36, 37]. In addition, new experimental tech-niques using photoelastic particles [25] or emulsions [26, 29] have produced bulk measurements, and these also reveal a much faster than exponential decay for $P(f)$, consistent with a Gaussian tail.

Nevertheless, much theoretical effort has focused on explaining the exponential tail of $P(f)$, starting with the pioneering q model [38]. Here, scalar forces are bal-anced on a regular grid, but it was later realized that, in this model, the tail of $P(f)$ depends on details of the stochastic rules for the force transmission and need not be exponential [39]. Other explanations for the exponential tail hinge on "entropy max-imization" [46, 77], or closely related, on an analogy with the Boltzmann distribu-tion [45, 47]. The essence of the latter argument is that a uniform sampling of forces that *(1)* are all positive (corresponding to the repulsive nature of contact forces), and *(2)* add up to a constant value (set by the requirement that the overall pressure is con-stant) strongly resembles the microcanonical ensemble, in which configurations are flatly sampled under the constraint of fixed total energy.

In this chapter, we will probe the tail of $P(f)$ in the force network ensemble [11, 43, 79–81, 85]. This ensemble is obtained by flatly sampling all force config-urations for which forces are repulsive and add up to satisfy overall stresses, i.e., *(1)* and *(2)* as listed above, under the additional constraints of force balance on all grains. We numerically resolve the probability for large forces using the technique of

umbrella sampling [52], which yields accurate statistics for $P(f)$ for relative probabilities down to 10^{-45} and f up to $f = 15$ (throughout the rest of this thesis, all forces are normalized such that $\langle f \rangle = 1$). This high accuracy is crucial for excluding any crossover effects and allows us to unambiguously identify the behavior for $f \gg 1$. We study the force ensemble for frictionless systems in two and three dimensions, with both ordered and disordered contact networks, and also explore the effect of system size and contact number. We also studied a single contact network in 4D.

For all systems, we have found that the ensemble yields force distributions that decay much faster than exponentially. The dimensionality of the system is crucial, while other factors hardly affect the asymptotics: $P(f)$ decays as $\exp(-cf^{\alpha})$, with $\alpha = 2.0 \pm 0.1$ in two dimensions, while in three dimensions $\alpha = 1.7 \pm 0.1$ and in four dimensions $\alpha = 1.4 \pm 0.1$. It is important to note that similar exponents emerge for the potential energy of Hertzian contacts [20], which scale as f^2 (in 2D) and $f^{5/3}$ (in 3D). As the ensemble considers rigid particles without any contact law, this appears to be a coincidence.

2.2   Force network ensemble and umbrella sampling

The ensemble approach to force networks is inspired by the proposal of Edwards to assign an equal probability to all "blocked" states, *i.e.*, states that are at mechanical equilibrium [41]. By limiting the Edwards ensemble to a single packing of fixed contact geometry [44], where the contact forces are the remaining degrees of freedom and all allowed force configurations are sampled with equal weight, one obtains the force network ensemble. Here we restrict ourselves to spherical particles with frictionless contacts, so that every contact force f_i corresponds to one scalar degree of freedom. Furthermore, we require all $f_i \geq 0$ due to the repulsive nature of the contacts. As the equations of mechanical equilibrium are linear in the contact forces, one can cast the solutions $\mathbf{f} = (f_1, f_2, \dots)$ in the form $\mathbf{f} = \mathbf{f}_0 + \sum_k a_k \mathbf{v}_k$. The solution space is spanned by the vectors $\mathbf{v}_k$ and $\mathbf{f}_0$, and can be sampled through the coefficients a_k; for details we refer to Refs. [43, 80, 85] and Section 1.5. Ensemble averages using a uniform measure in this force space can be calculated using Monte Carlo simulations (Section 1.3.2). To obtain accurate statistics for large forces, we perform *umbrella sampling*. The idea is to bias the numerical sampling toward solutions with large forces, using a Monte Carlo technique with a modified measure and then correct for this bias when performing the averages, see Sections 1.3.3 and 1.6. Defin-

ing f_{max} as the largest force for a given **f**, we have used a measure chosen such that the probability of f_{max} in the modified ensemble is approximately flat in the range $1 < f_{max} < 15$. This procedure exactly reproduces $P(f)$ in the range accessible by the conventional unbiased sampling. However, forces of the order of 15 are now sampled only 10^4 times less frequently than forces around 1, even though their relative probability is about 10^{-45}, leading to the spectacular improvement in numerical accuracy. The asymptotic behavior of $P(f)$ is determined by the asymptotic behavior of both $P(f|f_{max})$ and $P(f_{max})$, see Eq. (1.36).

2.3 Triangular lattice

A well-studied geometry for which the force network ensemble yields nontrivial results is that when all particles are of equal size and form a triangular lattice [43, 80, 85]. The umbrella sampling allows us to access the statistics beyond $f = 5$. Fig. 2.1(a) shows that $P(f)$ decays much faster than exponentially, and that effects of the finite size of the system are weak. Figs. 2.1(b,c,d) illustrate that, for increasingly large systems, $P(f)$ rapidly converges to an asymptotic form which is characterized by a purely Gaussian decay. This can also be seen in Fig. 2.1(c), where we exploit the fact that we have access to $P(f)$ over more than 40 decades. Assuming that, for large f, $P(f) \sim \exp(-cf^{\alpha})$, one can infer the exponent α from the asymptotic slope of a triple-logarithmic plot in which $\log_{10}(-\log_{10}P)$ is plotted as function of $\log_{10}f$ [20]. Fig. 2.1(d) shows that $\alpha = 2.0 \pm 0.1$, confirming that the tail of $P(f)$ is well described by a Gaussian decay. Intriguingly, the force distribution is surprisingly well approximated at small f by $P(f) \simeq 1/3 + 3f/4$, which hints that a simple analytic expression may exist for the triangular lattice. A decent fit over the whole range of f is given by $P(f) = (a+bf)e^{-c(f-f_0)^2}$, where a,b are determined by the observed small-f behavior, and f_0,c are determined by $\langle f \rangle = 1$ and $\int P(f)df = 1$, but deviations from the numerical $P(f)$ can be observed in the tail.
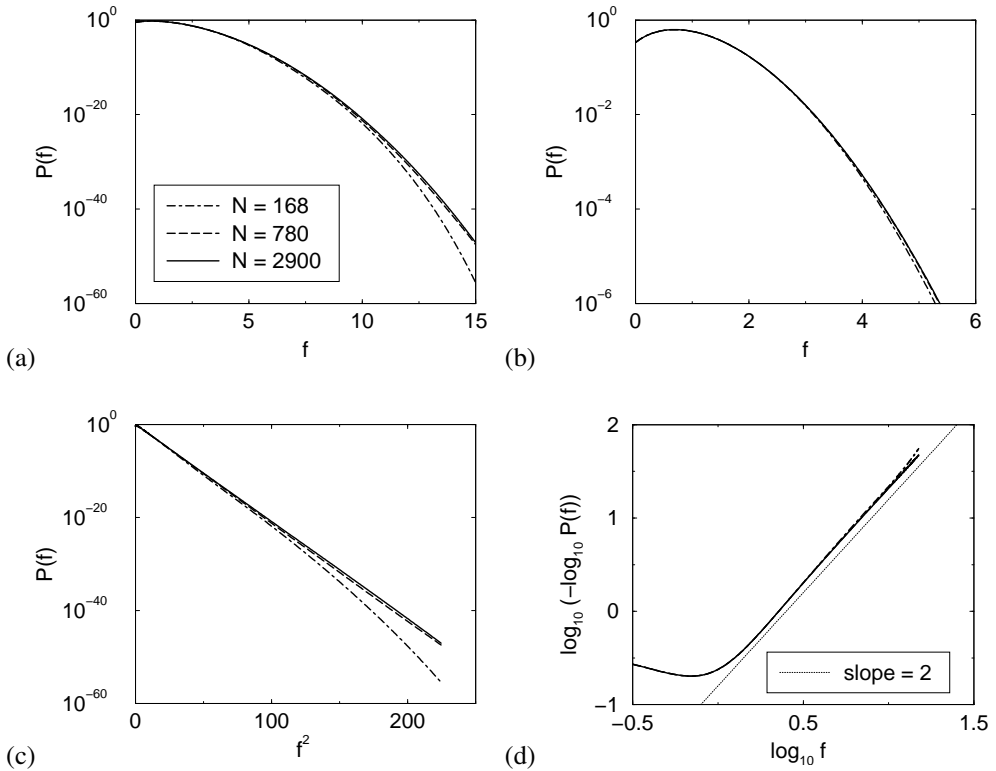
Figure 2.1: Force probabilities in two-dimensional triangular lattices of N particles with periodic boundary conditions. (a) $P(f)$ decays much faster than exponentially, and rapidly converges to its asymptotic form with N—larger N corresponds to wider distributions. (b) System size effects are hardly visible for $P(f)$ down to 10^{-6}. (c) $\log_{10} P$ vs f^2 becomes a perfectly straight line for large systems, indicating that the tail of $P(f)$ is well described by a Gaussian decay $\sim \exp(-cf^2)$. (d) A triple-logarithmic plot shows that the asymptotic decay attains a slope close to 2, confirming the Gaussian tail.

2.4   Disordered packings in two dimensions

To investigate the effect of packing disorder and coordination number z, we have
created packings of soft particles with periodic boundary conditions using the com-
pression method, see Section 1.4. The coordination number z is controlled by the
degree of compression. Once a packing is obtained, all particle positions are kept
fixed, and we subsequently explore the ensemble of force networks for that packing.
At this point the interparticle potential is no longer used, so that grain rigidity is not
a parameter in the ensemble.

For all 2D disordered packings, $P(f)$ decays much faster than exponentially, as
shown in Fig. 2.2. Comparing the ordered triangular lattices to a disordered sys-
tem with equal coordination number, $z = 6$, we find nearly indistinguishable $P(f)$
(Fig. 2.2(b)). This suggests that the packing (dis)order and preparation history are
not important for $P(f)$ in the ensemble. However, the contact number influences the
asymptotic decay: a lower z leads to a faster decay, although in the restricted range
$f < 5$, the force distribution appears very close to Gaussian for all z (Fig. 2.2(d)).
For the lowest z in particular, this tendency is cut off at large f, which can be clearly
seen in the triple-logarithmic plot (Fig. 2.2(e)), where all curves tend toward a well-
defined slope $\alpha = 2.0$ for intermediate f, but cross over to a much faster decay for
large f. We suggest that this is a finite-size effect, which is most severe when z
approaches the isostatic point ($z = 4$), where there are fewer and fewer degrees of
freedom available [11, 36, 89]. Indeed, data for $z = 4.5$ and increasing system sizes
suggest that the "kink" in the triple-logarithmic plots becomes less severe for large
systems (Fig. 2.2(f))—our data are not conclusive as to whether this kink will disap-
pear for $N \to \infty$. In conclusion, for two-dimensional, frictionless systems, the ensem-
ble approach yields force distributions $P(f)$ that decay at least as fast as a Gaussian.
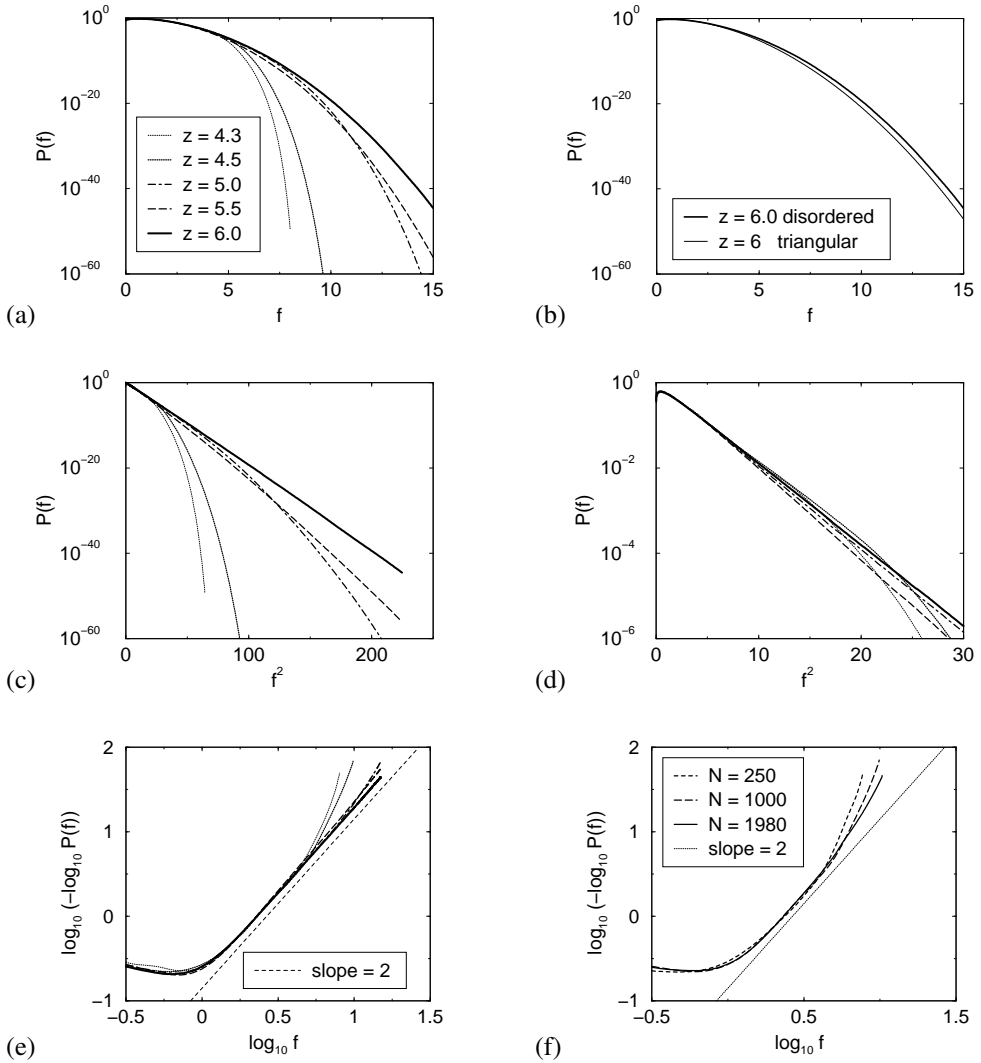
Figure 2.2: Force distribution for two-dimensional systems. (a) $P(f)$ grows in width for disordered systems ($N = 1000$) with increasing values of the contact number z. (b) Comparison of $P(f)$ for a disordered packing with $z = 6$ and $N = 1000$ and the triangular lattice for $N = 2900$. (c) The same data as in (a), now plotted as $\log_{10} P(f)$ vs f^2, tends to a straight curve for large z. (d) The same figure a in (c), but on a smaller range, shows that all curves look Gaussian. (e) Same data as in (a), now on a triple-logarithmic plot. The range in f over which $P(f)$ looks Gaussian grows with contact number z. (f) For fixed small $z = 4.5$, $P(f)$ appears to approach a Gaussian tail for large N.

2.5   Three- and four-dimensional packings

We now turn to three-dimensional systems, which have been generated using molecular dynamics, see section 1.4. Similar to what happens in two dimensions, Fig. 2.3(a) shows that $P(f)$ decays faster than exponentially, and disordered and regular (fcc) packings have very similar force distributions. However, the decay is now *slower* than Gaussian and much more accurately described by $P(f) \sim \exp(-cf^{\alpha})$ with an exponent $\alpha = 1.7 \pm 0.1$ (see Figs. 2.3(c,d)). For comparison we have also included the result for the triangular lattice, which is seen to decrease significantly more rapidly than the $P(f)$'s of the three-dimensional systems. For small systems and small contact number ($N = 250, z = 9.1$), finite-size deviations, similar to those observed in two dimensions, can be seen. The exponent α has also been determined from the triple-logarithmic plots of the contact force distributions (Fig. 2.4(a)) for a range of contact numbers and system sizes, and in all cases the slope is close to $\alpha = 1.7$ over a decade.

Surprisingly, we thus find that the dimensionality of the packing determines the nature of the tail of $P(f)$. Therefore, we have also considered a 4D packing of $N = 256$ with 2681 bonds, leading to $z \approx 20.9$. The topology of this network has been chosen randomly. All bonds vectors were chosen randomly on a 4D unit sphere. Such a packing seems to be a reasonable choice for a typical 4D system, since we have seen earlier that the behavior of large forces does not strongly depend on the packing geometry for 2D and 3D systems. In the simulation, we constrain the system to $\sigma_{\alpha\alpha} = \frac{1}{4}$ and $\sigma_{\alpha\beta(\alpha \neq \beta)} = 0$. Fig. 2.4(b) shows that for this system $\alpha \approx 1.4$.

For very large d, the coordination number becomes large as well, reducing correlations between contact forces acting on the same grain. If these correlations completely vanish, then one would expect $\alpha = 1$ (see also Section 3.4). It would be interesting to validate if this is really the case for $d \to \infty$.
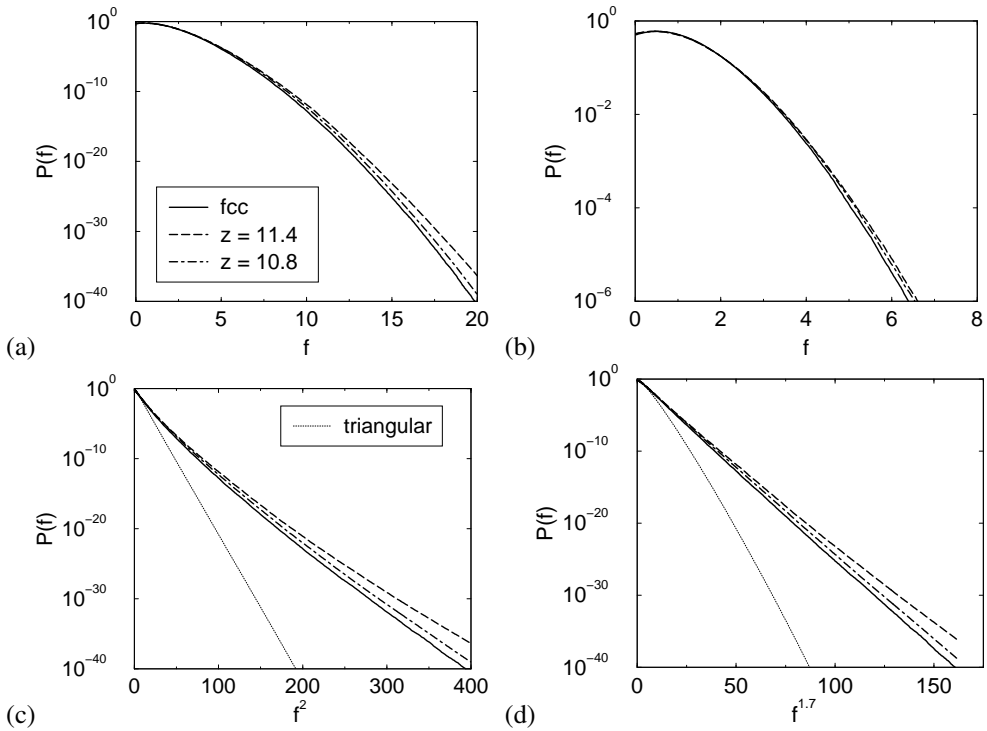
Figure 2.3: Force distribution for 3D systems. (a,b) $P(f)$ for two disordered and a regular fcc packing of $N = 500$ particles—the fcc packing has the smallest width, while for the disordered packs the width grows with contact number. (c) Same, now plotted as function of f^2. The thin dotted line corresponds to a triangular lattice in 2D, which has a Gaussian tail—the tail of $P(f)$ for 3D systems is significantly less steep. (d) Same data, now plotted as function of $f^{1.7}$—the tails for the $P(f)$ of 3D packings are now straight.
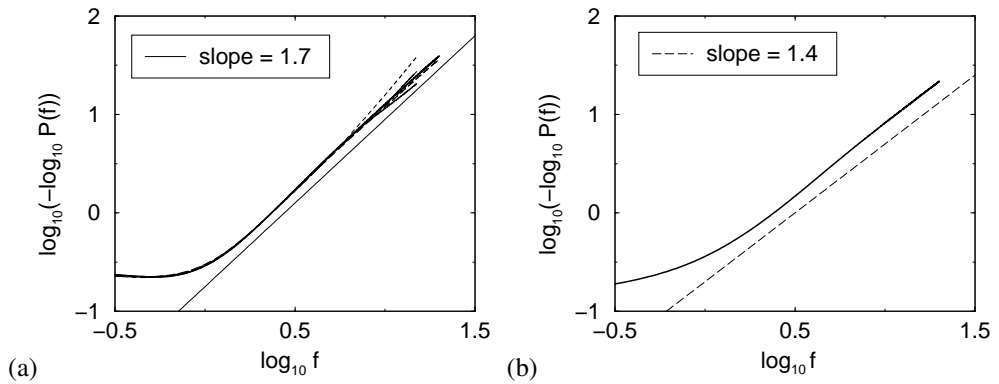
Figure 2.4: (a) Triple-log plot of $P(f)$ for 3D systems: hcp lattice ($N = 180$), fcc lattice ($N = 180$ and $N = 15444$), and four disordered systems ($z = 11.4, 10.8, 8.7$, and 7.8). All curves are plotted as thin and dashed lines, except the curve for largest fcc lattice (bold line). (b) Triple-log plot of $P(f)$ for a 4D system ($N = 256$, $z \approx 20.9$).

2.6   The effect of shear stress

From experiments on (two-dimensional) sheared packs of photoelastic grains, it was found that the distribution broadened significantly, and developed an exponential-like regime in a range up to $f = 4\langle f \rangle$ [25]. The ensemble indeed reproduces this qualitative feature for packs under shear. As can be seen in Fig. 2.5, however, there does not seem to be a simple asymptotic decay. This is because the force anisotropy induced by the shear stress yields a variation in $\langle f \rangle$ depending on the orientation of the contact [11, 80]. The total $P(f)$ becomes a superposition over all orientations, of mixed force statistics, and hence lacks a single characteristic feature. The angle-resolved contact force distribution will be discussed in Chapter 4.
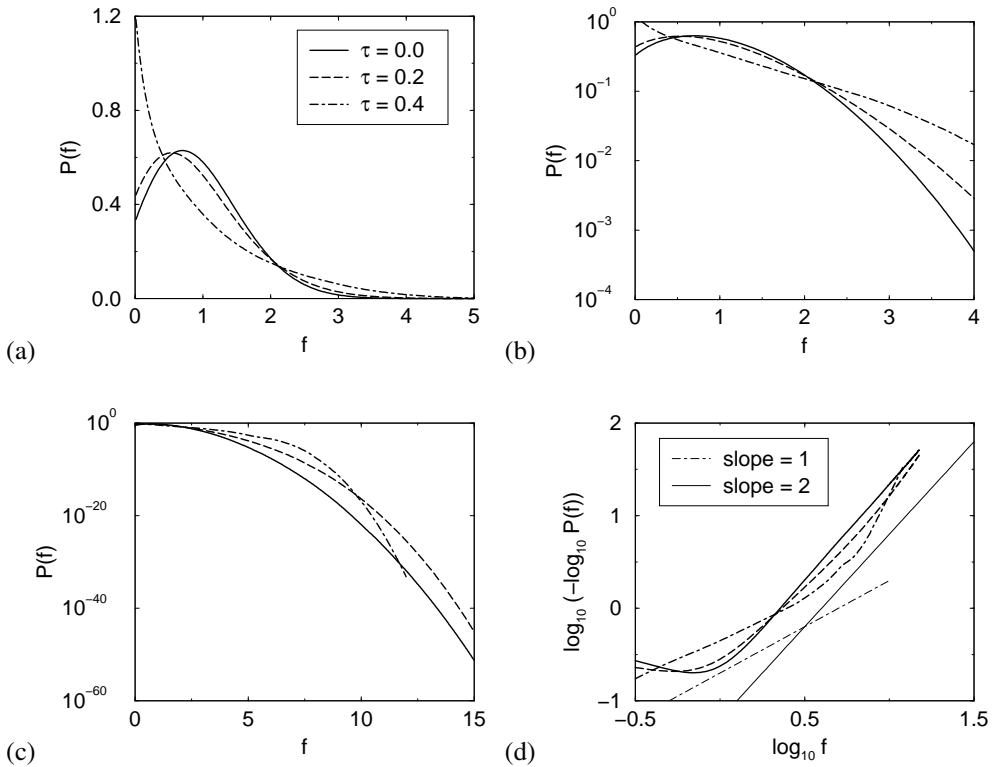
Figure 2.5: (a) 2D disordered system ($z = 5.5$, $N = 2000$) experiencing a shear stress $\tau \equiv \sigma_{xy}/\sigma_{xx}$ [11]. For increasing τ, the characteristic peak of $P(f)$ at $f \approx 1$ disappears and the largest forces in the packing are oriented along the shear direction, see also Figs. 1.1 and 1.2. (b) While, for large τ, the tail of $P(f)$ viewed over a limited range broadens and may appear exponential, (c) the asymptotic decay of $P(f)$ for $f > 10$ in fact increases with τ. (d) The same point is illustrated in the triple-logarithmic plots.

2.7   Discussion

We have shown for the force network ensemble that the tail of $P(f)$ decays faster than exponentially, in agreement with recent experiments [25, 29], but inconsistent with others [15, 20–24]. Our results required extremely accurate statistics, beyond the regime accessible by experiments or conventional simulations. In particular, in experiments it would be difficult to distinguish an exponent $\alpha = 1.7$ from 2.0. Nevertheless the discrepancy between the exponential data sets [15, 20–24] and the faster-than-exponential data sets [25, 29] cannot be explained away by finite error bars, but is convincing and worthwhile of further investigations.

   The experimental and numerical data for $P(f)$ have been obtained from a wide variety of systems and models, and parameters such as dimensionality, friction, hardness of grains vs boundary, and bulk vs boundary measurements may ultimately all play a role in determining the asymptotics of $P(f)$. Note that the glass beads used in the boundary measurements are much harder than the particles used in the bulk measurements of [25, 26, 29], and that realistic particle rigidity is difficult to achieve in molecular dynamics.

   The ensemble can also be extended to include torque balance and to explore boundary measurements. This will be discussed in Chapters 3 and 4 respectively. A crucial untested assumption in the ensemble is the flat measure, i.e., the sampling of all allowed configurations with equal weight. As argued in Ref. [20], different experimental procedures and parameters can lead to a different $P(f)$, so that the effective sampling of force networks may not be universal.

3

Entropy maximization in the force network ensemble for granular solids

A long-standing issue in the area of granular media is the tail of the force distribution, in particular whether this is exponential, Gaussian, or even some other form. We demonstrate that conservation of the total area of a reciprocal tiling, a direct consequence of local force balance, is crucial for predicting the local stress and force distribution. Maximizing entropy while conserving the tiling area and total pressure leads to a distribution of local pressures with a generically Gaussian tail that is in excellent agreement with numerics, both with and without friction and for two different contact networks (triangular lattice and square lattice).

3.1 Introduction

There is as yet no clear consensus on the form of the distribution of local stresses in granular media. Of particular interest is the large-stress tail, which early experiments found to be exponential when measured on the boundary [15, 20–24]. More recent measurements in the bulk [26, 29], along with numerics [12, 28, 37, 90], find distributions that bend downward on a semilogarithmic plot, suggesting faster than exponential decay. A number of proposed theories exploit an analogy to the microcanonical ensemble to arrive at a Boltzmann-like exponential tail [38, 46, 48, 77, 91–93]. These theories should in principle apply to the *force network ensemble* of Snoeijer *et al.* [43]. However, in the previous chapter we have unambiguously shown that this is not the case: the normal force distributions decay much faster than exponentially: $P(f_n) \sim \exp(-c(f_n)^\alpha)$, with $\alpha \approx 2.0$ for 2D systems, $\alpha \approx 1.7$ for 3D systems and $\alpha \approx 1.4$ for 4D systems (see Chapter 2). As the present statistical mechanics approaches fail to describe simple models like the force network ensemble, they must be missing an important ingredient. We argue that *local force balance* is absolutely crucial to describe the correct stress statistics. In particular, we show that the pressure distribution in the force network ensemble directly follows from entropy maximization, but *only* when it respects a conserved quantity overlooked in previous theories. This conserved quantity follows from force balance at the grain scale, and leads to excellent agreement with numerics for both small and large forces.

3.2 Force network ensemble

Snoeijer's ensemble is composed of all "force networks", i.e. sets of noncohesive contact forces on a fixed granular contact network, for which all N grains are in *static force and torque balance*. For packings with more than a critical number of contacts per grain z_c, there exist many balanced force networks. The critical coordination number z_c equals 4 (3) for frictionless (frictional) 2D packings of disks [43]. All force networks on a contact network with the same global stress tensor and local force and torque balance can be sampled uniformly by a series of Monte Carlo moves, termed "wheel moves", see also Section 1.5 and Tighe *et al.* [80]. As by construction the global stress tensor Eq. (1.23) is fixed, the extensive pressure in the system $\mathscr{P}$ is

conserved,

$$\mathscr{P} = \sum_{i=1}^{N} p_i = \text{constant}, \qquad (3.1)$$

where we dropped the usual prefactor. The summation runs over all grains and p_i is the pressure on grain i, which is defined as

$$p_i = \sum_{j} \mathbf{r}_{ij} \cdot \mathbf{f}_{ij}. \qquad (3.2)$$

The summation in Eq. (3.2) is over all neighbors j of particle i. $\mathbf{r}_{ij} = \mathbf{r}_i - \mathbf{r}_j$ is the bond vector between particles i and j and $\mathbf{f}_{ij}$ is the contact force. We restrict ourselves to isotropic states in 2D systems, $\sigma_{xx} = \sigma_{yy}$ and $\sigma_{xy} = \sigma_{yx} = 0$, so that the global stress tensor is fully characterized by $\mathscr{P}$.

Every force network, regardless of its (dis)ordering, coordination number z, or friction coefficient μ, has a corresponding *reciprocal tiling* [94, 95]. Fig. 3.1 shows the real and reciprocal representation of *the same* force network; each grain corresponds to a tile. Each face of the tile corresponds to one of the grain's contact forces. The face is oriented at a $\pi/2$ rotation to the contact force $\mathbf{f}_{ij}$, and its length is proportional to $|\mathbf{f}_{ij}|$. Because the grain is in static force balance, the faces form a loop enclosing the tile. By Newton's third law, the tiles fit together with no gaps. Note that upon rotation by $-\pi/2$, the vertices of the tiling are the loop forces of Ref. [96].
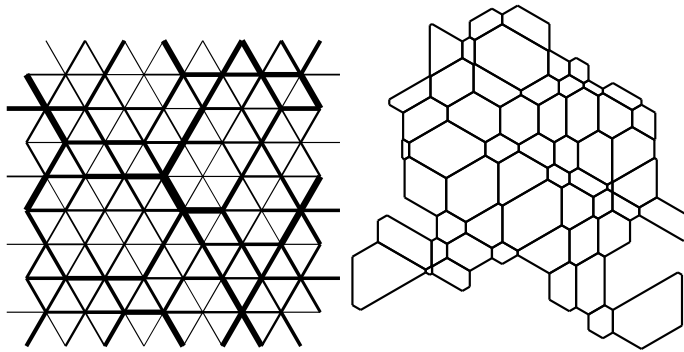

Figure 3.1: Schematic representation of a force network of a frictionless triangular lattice (left) and its corresponding reciprocal tiling (right). The thickness of each line in the left figure represents the magnitude of the force. Larger forces map to longer lines in the reciprocal tiling.

Specifying the boundary forces on a packing establishes the boundaries of its corresponding tiling, and hence the total area of the tiling. Fixing the global stress tensor in a periodic system has the same effect. Rearrangements of bulk forces, i.e. the wheel moves, correspond to local exchanges of area among tiles. It can be shown that the *total* tiling area is unaltered by wheel moves, and therefore the area $\mathscr{A}$ is conserved. That is,

$$\mathscr{A} = \sum_{i=1}^{N} a_i = \text{constant}. \tag{3.3}$$

The sum runs over all tiles and a_i is the area of tile i:

$$a_i = \frac{1}{2}\mathbf{z} \cdot \sum_{j=1}^{z_i-2} \sum_{k=j+1}^{z_i-1} \left[\mathbf{f}_{ij} \times \mathbf{f}_{ik}\right]. \tag{3.4}$$

The indices j and k number the z_i neighbors of grain i in a right-hand fashion. The unit vector $\mathbf{z} = \mathbf{x} \times \mathbf{y}$ points out of the plane. Area conservation is a *global* constraint that results from imposing *local* force balance. It holds for arbitrary force balanced packings in 2D with fixed global stress tensor or boundary forces. Area conservation plays a crucial role in determining the statistics of local stresses.

3.3   Entropy maximization

Armed with the insight that the force network ensemble involves two conserved quantities, $\mathscr{P}$ and $\mathscr{A}$, we explore their implications for the statistics of local stresses. While previous work has incorporated the conservation of $\mathscr{P}$ or its equivalent, the conservation of $\mathscr{A}$ has heretofore been overlooked. We will show that the conservation of $\mathscr{A}$ has a dramatic effect on the force network statistics.

We calculate the probability density $P(p)$ by maximizing entropy while conserving $\mathscr{P}$ and $\mathscr{A}$. Each force network corresponds to a set of pressures $\{p_i\}$, $i=1\ldots N$. We define $X(p)\omega(p)dp$ as the probability of finding a pressure p in the interval $[p, p+\omega(p)dp]$, where $\omega(p)$ is the density of states for pressures. The entropy S is the logarithm of the number of ways of constructing force networks with pressures $\{p_i\}$ consistent with $X(p)$. In the thermodynamic limit [92, 97–99]

$$S = -\int_0^\infty \big(X(p)\ln X(p)\big)\omega(p)dp. \tag{3.5}$$

The experimentally accessible probability density $P(p)$ is related to $X(p)$ by $P(p)dp = X(p)\omega(p)dp$. It is important to note that weighting all force networks equally does

not correspond to a flat measure on the pressures, i.e. $\omega(p) \neq$ constant. B.P. Tighe showed that $\omega(p) \propto p^{\nu}$ [88]. The value of ν depends on the grain's coordination number and the friction coefficient. For the frictionless triangular lattice, $\nu = z - 3$. The entropy is maximized subject to Eqs. (3.1) and (3.3), as well as normalization of $P(p)$. This leads to [88]

$$
\begin{aligned}
\langle p \rangle &= \mathscr{P}/N = \int_0^\infty p\, P(p) dp, \\
\langle a \rangle &= \mathscr{A}/N = \int_0^\infty \langle a(p) \rangle P(p) dp, \\
1 &= \int_0^\infty P(p) dp.
\end{aligned}
\tag{3.6}
$$

$\langle a(p) \rangle = \int a P(a|p)\, da$ is the average area of a tile with perimeter or pressure p; $P(a|p)$ is the conditional probability that a certain tile has area a given its perimeter p. Using the method of Lagrange multipliers, B.P. Tighe $et\ al.$ [88] have shown that the entropy-maximizing density subject to Eqs. (3.6) is

$$
P(p) = Z^{-1} p^{\nu} \exp\left[-\alpha p - \gamma \langle a(p) \rangle\right].
\tag{3.7}
$$

Without the constraint on tiling area we would always have $\gamma = 0$ and thus an exponential tail: *Incorporating local force balance by means of the area constraint has qualitatively changed the form of the distribution*. The Lagrange multipliers Z, α, and γ are determined by substituting Eq. (3.7) in Eqs. (3.6). For frictionless systems a scaling argument shows that $\langle a(p) \rangle$ is quadratic in the thermodynamic limit [88]; we write $\langle a(p) \rangle = c \langle a \rangle (p/\langle p \rangle)^2$ and determine the constant c from numerics. Thus the probability density $P(p)$ has a generically Gaussian tail, as was already shown numerically for the normal contact force distribution $P(f_n)$. As expected, it will turn out that $P(p)$ and $P(f_n)$ have the same asymptotic behavior.

3.4   Results

We employ umbrella sampling on a periodic frictionless triangular lattice with $N = 1840$ to numerically determine $P(p)$, see Sections 1.5 and 1.6. To improve sampling of large pressures, we used the maximum pressure on a single grain ($p_{\max}(\mathbf{f})$) as an order parameter. A typical snapshot of a force network of this system with a large value of $p_{\max}$ is shown in Fig. 3.2. It is important to note that typical force configurations with a large $p_{\max}$ are fundamentally different from those with a large $f_{\max}$, see also Fig. 1.8. Typical force configurations with a large $p_{\max}$ have a single grain on which all contact forces are large, while typical force configurations with a large $f_{\max}$ have at least a single grain on which two forces are very large. Therefore, to accurately compute $P(f)$ and $P(p)$ for large forces and pressures respectively separate umbrella sampling simulations are needed.

In all simulations, forces are normalized in such a way that the average normal force $\langle f_n \rangle = 1$. From the sampled $\langle a(p) \rangle$, shown in Fig. 3.3, we extract $c \approx 0.89$. Fig. 3.4 contains the corresponding probability density of Eq. (3.7) and its numerical counterpart. Theory and numerics are in excellent agreement, even for $P(p)$ as low as 10^{-8}. The slight discrepancies can be attributed to finite size effects and spatial pressure correlations: due to force balance, neighbors of large p grains are more likely to be at high p themselves. Thus large pressures are less entropically favorable than suggested by neglecting correlations.
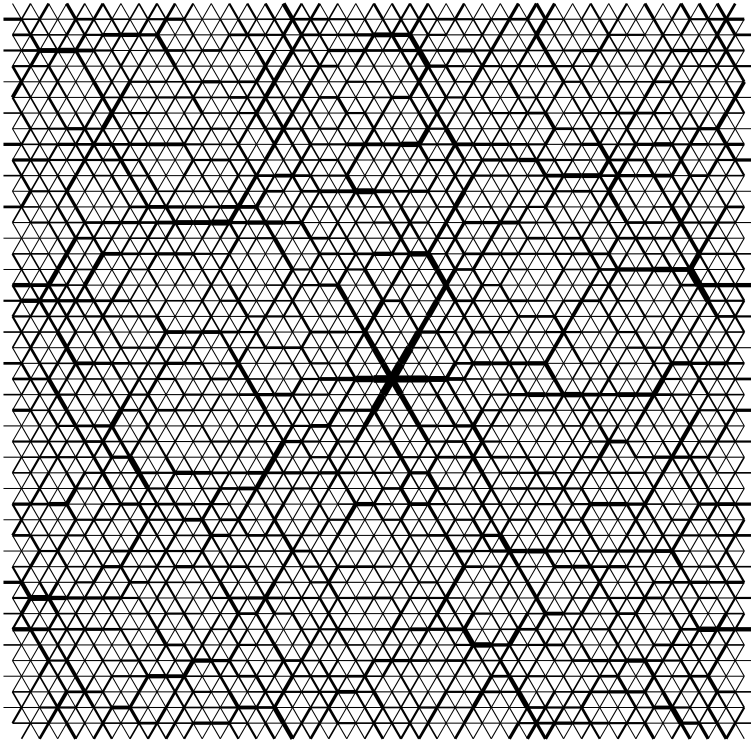
Figure 3.2: Typical snapshot of a force network with a large p_{max}. The picture is centered around the grain with the largest pressure. The thickness of each line represents the magnitude of the force.
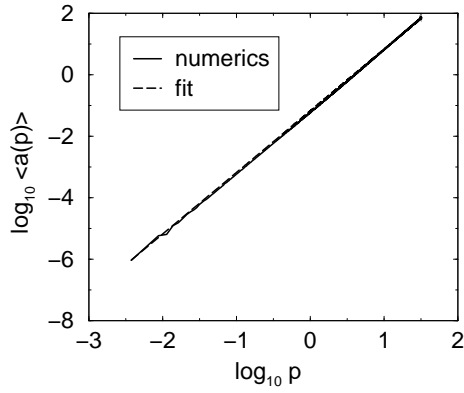
Figure 3.3: Fitted and numerical average area of a tile with perimeter p for a triangular frictionless system.
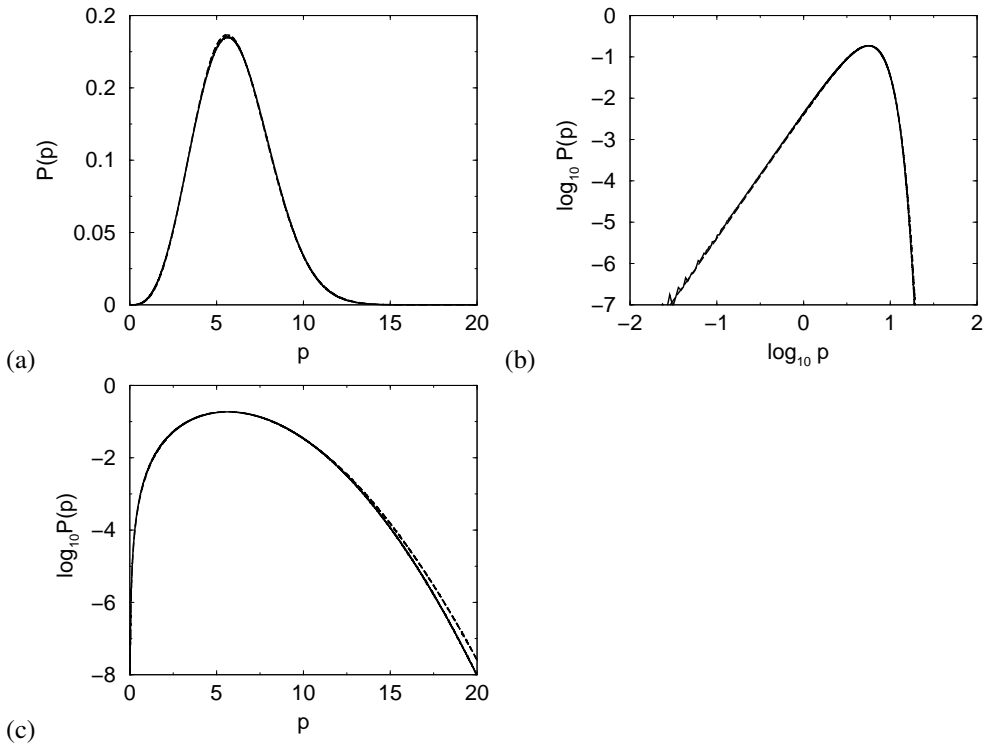

(a)

(b)

(c)

Figure 3.4: Theoretical (dashed) and numerical (solid) pressure probability distributions for the frictionless triangular lattice with $N = 1840$.
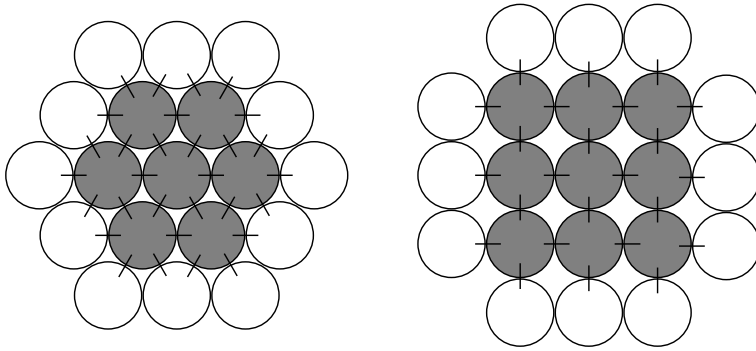
Figure 3.5: Clusters of contact forces. Left: triangular lattice, 7 grains, 30 contact forces. Right: square lattice, 9 grains, 24 contact forces.

We now consider frictional triangular ($z = 6$) and square ($z = 4$) lattices. A system with friction coefficient μ permits contact forces with both normal component f_n and tangential component $|f_t| \leq \mu f_n$. The pressure p remains the sum of normal forces on a grain. Friction has two important consequences. The first is that $\langle a(p) \rangle$ is not strictly quadratic. Friction permits tiles with area $a < 0$, which occurs when tile faces overlap. Nevertheless, on dimensional grounds we expect $\langle a(p) \rangle \sim p^2$ for large p. In numerics, deviations from a quadratic form increase with μ, but for all frictional systems we have studied quadratic scaling holds for $p > \langle p \rangle$. Hence Eq. (3.7) still yields Gaussian tails. Secondly, we find that friction increases spatial correlations [88]. Consequently, as in Ref. [93], we coarse-grain and study clusters of $m = 7$ (9) grains and $k = 30$ (24) contacts on the triangular (square) lattice, see Fig. 3.5. The frictional clusters have exponent $\nu = 2k - 3m - 1$ in their density of states. We find $\langle a(p) \rangle$ for a cluster deviates much less from quadratic behavior than its single-grain counterpart.

Lacking the exact form of $\langle a(p) \rangle$ for frictional systems, we determine the Lagrange multipliers satisfying Eqs. (3.6) using the numerically sampled $\langle a(p) \rangle$. Theory and numerics are again in excellent agreement, as seen in Fig. 3.6. As the Lagrange multiplier γ tends towards zero with increasing μ (Fig. 3.7), we investigate the limit $\mu \to \infty$. For finite friction and circular grains, normal and tangential forces are coupled through the force balance constraints on each grain and the Coulomb constraint on each force. In the infinite friction limit the Coulomb constraint has no effect. For the triangular lattice there are three distinct contacts per grain, and it is

possible to choose a set of tangential forces $\{f_{ti}\}$ to balance force and torque on each grain regardless of the normal forces $\{f_{ni}\}$. The only constraints on the $\{f_{ni}\}$ are positivity, $f_{ni} > 0$, and fixed total pressure $\mathscr{P}$. This leads directly to a Boltzmann distribution

$$P(f_n) = \frac{\exp[-f_n/\langle f_n \rangle]}{\langle f_n \rangle}, \tag{3.8}$$

with $\langle f_n \rangle = \mathscr{P}/zN$. In contrast, for systems with $z - z_c < 3$, such as the square lattice, the normal and tangential forces remain strongly coupled through force balance even for infinite friction. We have confirmed numerically that in the infinite friction limit the Boltzmann distribution holds for $P(f_n)$ in the triangular lattice, and that for finite μ there is a cross-over from a Gaussian (low μ) to an exponential ($\mu \to \infty$) distribution (see Fig. 3.8). The same is observed for $P(p)$, see Fig. 3.9. The normal force and pressure distributions in the square lattice remain close to Gaussian (Figs. 3.8 and 3.9). Indeed, $P(p)$ and $P(f_n)$ have the same asymptotic behavior. Fig. 3.10 shows the distribution of the tangential forces $P(f_t)$, computed using umbrella sampling with the largest tangential force as an order parameter. The distribution of tangential forces shows the same asymptotic behavior as the corresponding distributions $P(p)$ and $P(f_n)$ (for the same value of μ). The reason for this is unclear to us.

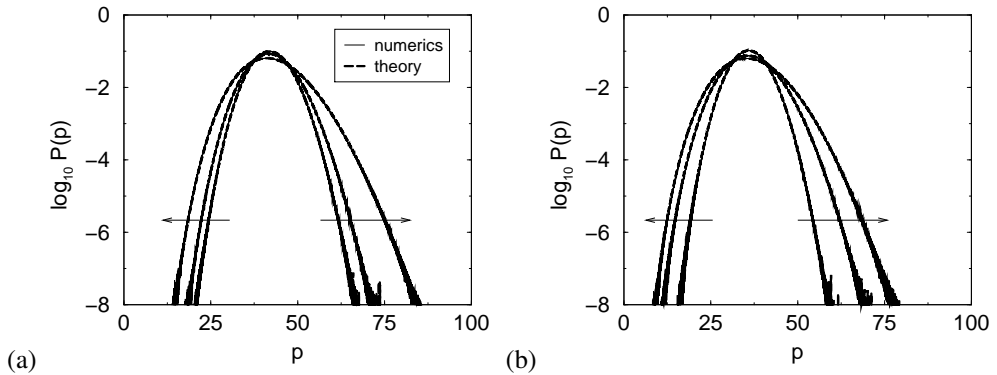(a)   (b)

Figure 3.6: (a) Theoretical and numerical pressure probability distributions for 7-grain clusters in the frictional triangular lattice with $\mu = 0.5$, 1.0, and 3.0 (arrow: increasing μ). (b) Theoretical and numerical pressure probability distributions for 9-grain clusters in the frictional square lattice with $\mu = 0.5$, 1.0, and 2.0 (arrow: increasing μ).
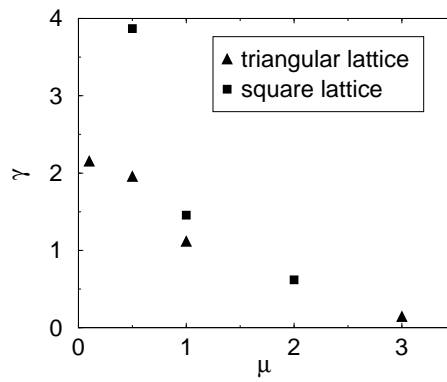
Figure 3.7: Lagrange multiplier γ as a function of the friction coefficient μ for 7-grain clusters in the frictional triangular lattice and for 9-grain clusters in the frictional square lattice.
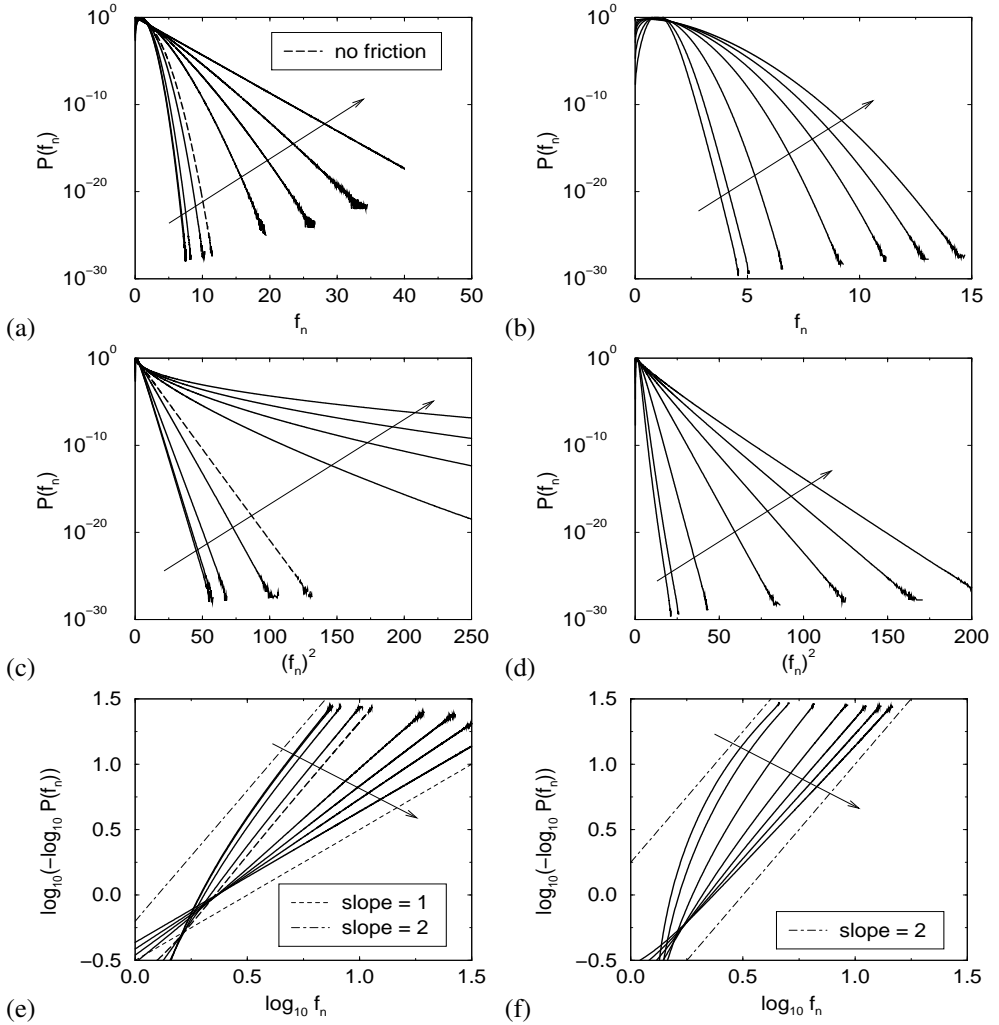
Figure 3.8: Distribution of normal contact forces for various μ computed for the triangular lattice (a,c,e) and square lattice (b,d,f) using the force network ensemble. The direction of the arrow indicates increasing μ. (triangular lattice: $\mu = 0.1$, 0.2, 0.5, 1.0, 3.0, 5.0, 10.0, ∞; square lattice: $\mu = 0.1$, 0.2, 0.5, 1.0, 2.0, 5.0, ∞). For the triangular lattice, the curves for $\mu = 0.1$ and $\mu = 0.2$ are almost identical.

Figure 3.9: Distribution of pressures for various μ computed for the triangular lattice (a,c) and square lattice (b,d) using the force network ensemble. The direction of the arrow indicates increasing μ. (triangular lattice: $\mu = 0.1$, 0.2, 0.5, 1.0, 3.0, 5.0, 10.0, ∞; square lattice: $\mu = 0.1$, 0.2, 0.5, 1.0, 2.0, 5.0, ∞). For the triangular lattice, the curves for $\mu = 0.1$ and $\mu = 0.2$ are almost identical.
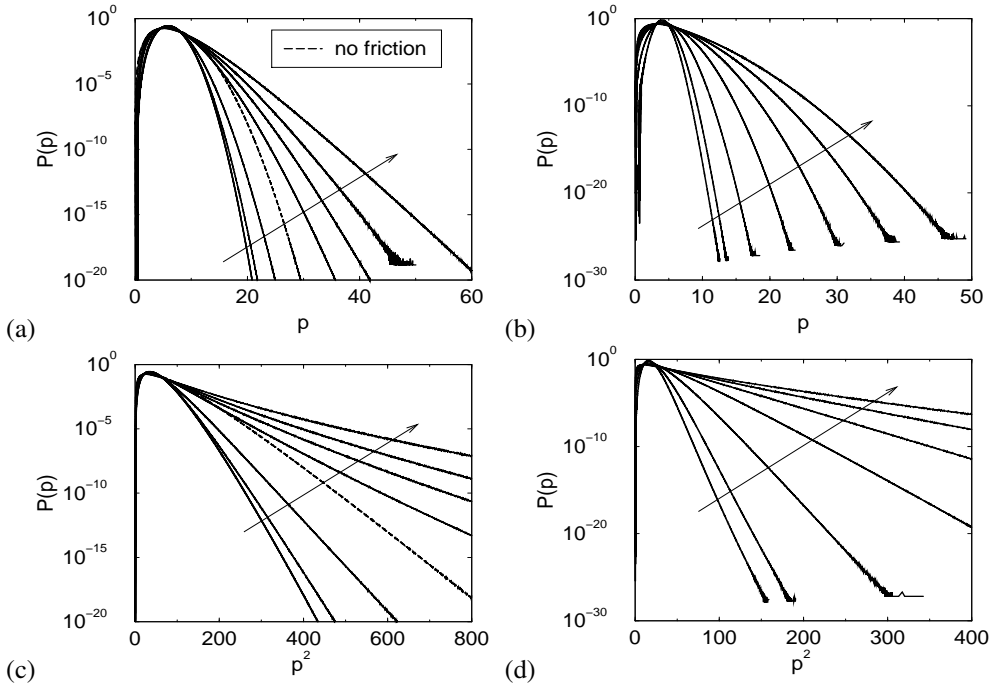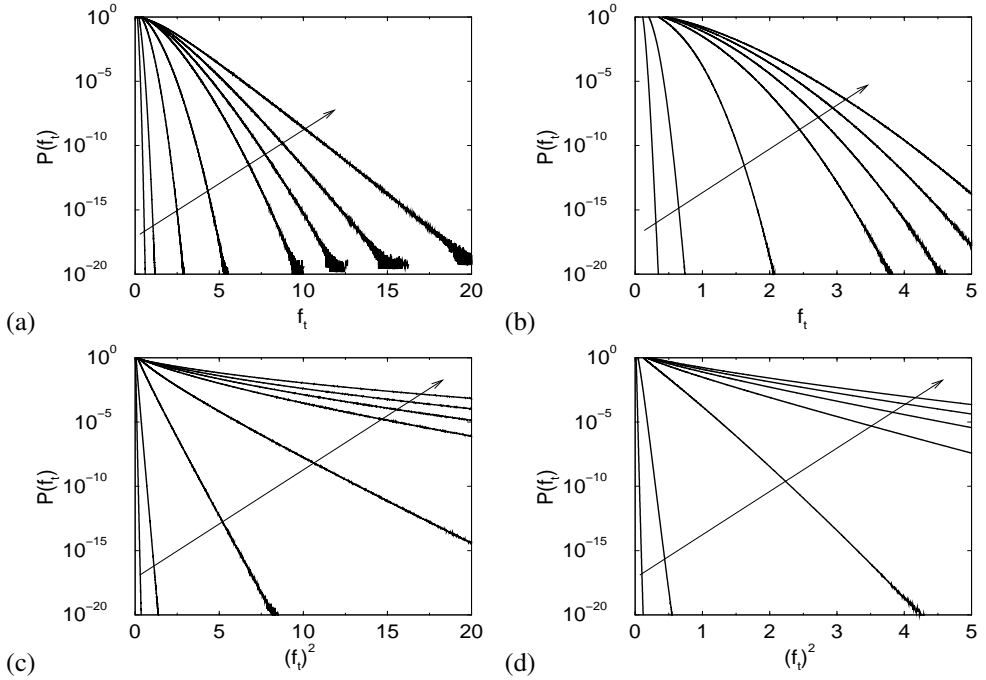
Figure 3.10: Distribution of tangential contact forces for various μ computed for the triangular lattice (a,c) and square lattice (b,d) using the force network ensemble. The direction of the arrow indicates increasing μ. (triangular lattice: $\mu = 0.1, 0.2, 0.5, 1.0, 3.0, 5.0, 10.0, \infty$; square lattice: $\mu = 0.1, 0.2, 0.5, 1.0, 2.0, 5.0, \infty$)

To study the plasticity of the contact forces, we have measured the plasticity index

$$\Sigma = \frac{|f_t|}{\mu f_n} \tag{3.9}$$

and its distribution in the force network ensemble, see Fig. 3.11. In all cases, $P(\Sigma)$ is a monotonously decreasing function which becomes more flat for smaller μ. For $\mu \gg 1$, we have verified that the distribution of the contact force ratio f_t/f_n is independent of μ. The plasticity distribution has been measured in several experiments [100] and simulations [28, 63, 101]. Often, a maximum was observed at nonzero Σ along with a sharp increase close to $\Sigma = 1$. The latter corresponds fully mobilized or "plastic" contacts. In the force network ensemble, the occurrence of these contacts is significantly reduced at all μ.
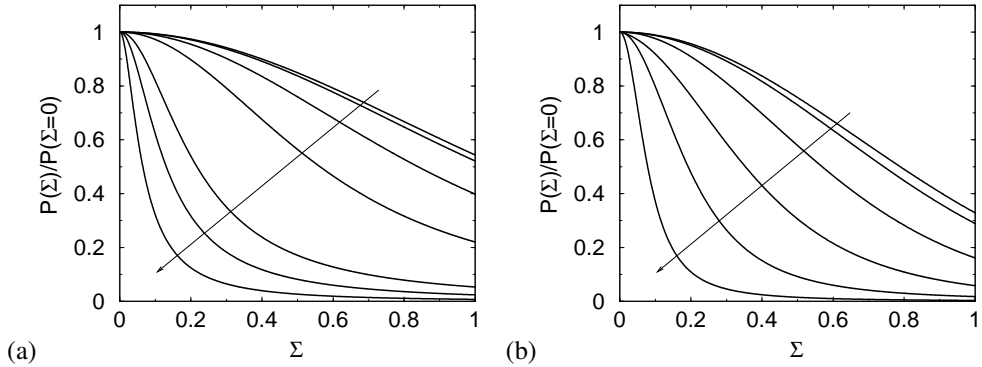

Figure 3.11: Plasticity distribution for the frictional triangular lattice (a) and square lattice (b). The direction of the arrow indicates increasing μ. (triangular lattice: $\mu = 0.1, 0.2, 0.5, 1.0, 3.0, 5.0, 10.0$; square lattice: $\mu = 0.1, 0.2, 0.5, 1.0, 2.0, 5.0$)

3.5   Conclusion

We have derived an analytic expression for the distribution of pressures in the force network ensemble in 2D and found excellent agreement with numerics. Distinct from previous studies, we incorporate *two* conserved quantities, the total pressure and the area of a reciprocal tiling. The latter is a direct consequence of force balance on the grain scale, and we conclude that this is crucial to understand the statistics of local forces in granular media. As a result, large stresses obey Gaussian statistics in 2D. This observation is robust to changes in the contact network, the finite friction coefficient, and the imposed measure.

We have *not* addressed the distribution at the unjamming transition, which could have a signature in the local stress statistics. Marginally rigid packings cannot be studied within the force network ensemble. Similarly, our results are restricted to two dimensions. A naïve extension of the reciprocal tiling to d dimensions suggests an exponent of $d/(d-1)$, so for 3D $P(f_n) \sim \exp[-c(f_n)^{3/2}]$, and $P(p) = Z^{-1}p^{\nu}\exp[-\alpha p - \gamma p^{3/2}]$. For the fcc lattice, $\nu = 12 - 3 - 1 = 8$. However, numerics find $P(f_n) \sim \exp[-c(f_n)^{\alpha}]$ with $\alpha = 1.7 \pm 0.1$ within the force network ensemble, see Chapter 2. Fig. 3.12 shows the numerically obtained $P(p)$ for an fcc lattice. This function is fitted to $P(p) = a_0 \exp[-a_1 p - a_2 p^{a_3}]$ resulting in a best fit with $a_3 \approx 1.7$. However, excellent fits can be obtained as well for a_3 in the range of $1.5 - 1.8$. The discrepancy, if any, may be the result of stronger spatial correlations than in 2D, where coarse-graining suffices, or it may signal new physics.
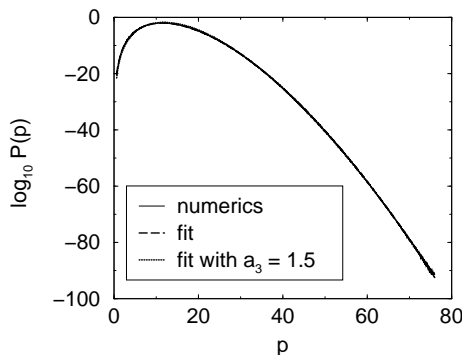

Figure 3.12: Pressure distribution ($P(p)$) for an fcc lattice of $N = 7140$ particles. The dashed curve is a fit of the numerical data to $P(p) = a_0 \exp[-a_1 p - a_2 p^{a_3}]$, resulting in $a_3 \approx 1.7$. Also shown is the same fit with a_3 fixed at 1.5.

It is interesting to speculate further on the role of the torque constraints on the individual particles in frictional systems. It is important to note that for systems that *do* have force balance on each particle, *but no torque balance*, still have a conserved area $\mathscr{A}$ and pressure $\mathscr{P}$ in the force network ensemble. This suggests that torque constrains do not have a large influence on the contact force statistics. To clarify the role of the torque constrains, we have studied the frictional triangular lattice with force balance on each particle, but *without* torque balance. Sampling the force space of these systems requires not only the usual wheel moves for the frictional triangular lattice [80, 87], but also additional wheel moves to sample the extra degrees of freedom introduced by the non-zero torque on each particle. In these wheel moves, a particle is selected at random. The tangential component of the "rim" forces get a (randomly selected) displacement Δf and the tangential component of the "spokes" get a displacement $-\Delta f$ (see also Fig. 1.5). The normal component of the "rim" and "spoke" forces are not affected in this trial move. It is trivial to show that this move conserves local force balance on each grain. The trial move is accepted using the usual acceptance rules (see Section 1.5). Fig. 3.13 shows that the triangular lattice *without* torque balance has almost identical distributions $P(f_n)$ and $P(p)$, while the distribution of tangential forces $P(f_t)$ significantly differs from the system with local torque balance (especially for large μ). Also without torque balance, the numerically sampled distribution $P(p)$ is in good agreement with Eq. (3.7) with the Lagrange multipliers obtained from the numerically sampled $\langle a(p) \rangle$ (note that here $\nu = 12 - 2 - 1 = 9$). The observation that local torque balance strongly influences $P(f_t)$, while $P(f_n)$ and $P(p)$ are hardly changed, along with the results of Fig. 3.11, may suggest that the force network ensemble with friction is a less realistic model for granular systems than the frictionless case. In real granular packings, the plasticity is strongly dependent on the preparation procedure [101] and this is absent in the force network ensemble.

Along with recent experiments [25, 26, 29], our results give serious cause to doubt that exponential statistics are a generic property of jammed granular matter. At the very least, more work is needed to distinguish bulk and boundary phenomena and to clarify why measured boundary forces show exponential statistics. We will come back to the issue of boundary forces in Section 4.6.
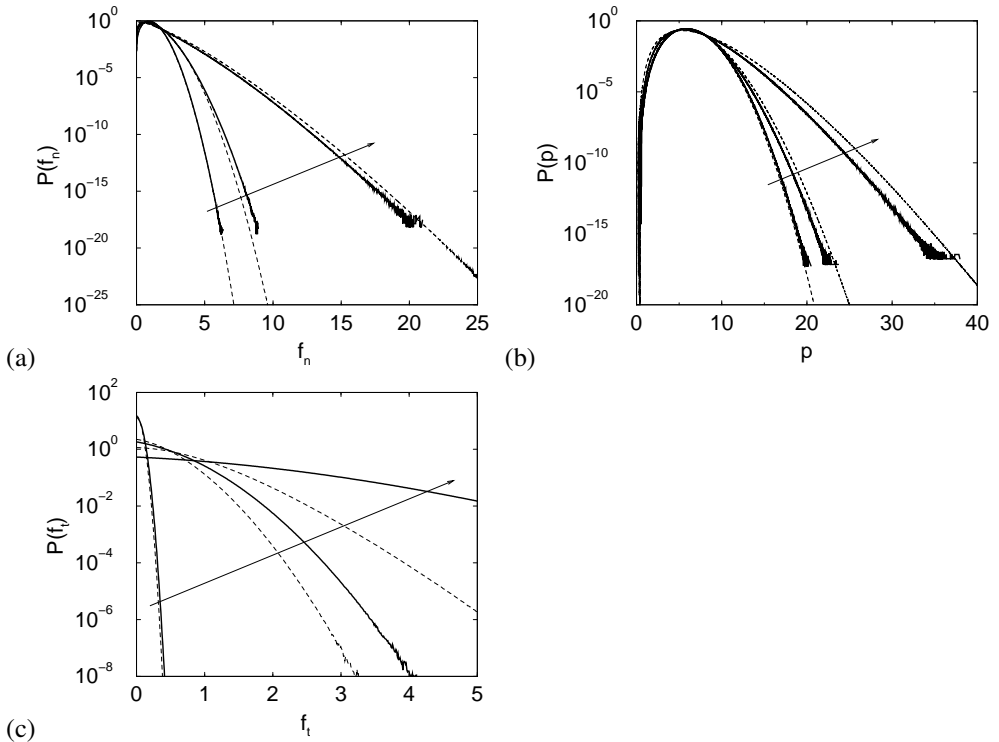
Figure 3.13: Distribution of normal contact forces (a), pressures (b) and tangential forces (c) computed for the triangular lattice of frictional particles using the force network ensemble. The solid lines show the distributions *without torque balance* and the dashed lines show the distributions *with* torque balance. The direction of the arrow indicates increasing μ (0.1, 1.0, 5.0).

4

Extended numerical study of the force network ensemble

4.1   Introduction

In this chapter we will use numerical simulations to study several aspects of the force network ensemble in more detail. In particular, we focus on the details of the stress constraints and finite-size effects for the frictionless triangular lattice (Section 4.2), the angle resolved contact force distribution (Section 4.3), finite-size effects and the maximum possible force of a certain network of contact forces (Section 4.4), the dimensionality of the space spanned by all solutions (Section 4.5) and the effect of boundaries (Section 4.6). In the last part of this chapter (Section 4.7), we will investigate a crucial and longstanding question: how well does the force network ensemble describe systems with "real" interactions?

4.2   Details of the stress constraints and finite-size effects

In Section 1.5 we introduced a force scale by imposing $\langle f \rangle = 1$. In case that $|\mathbf{r}_{ij}| = 1$, this directly results in $\sigma_{xx} + \sigma_{yy}(+\sigma_{zz}) = 1$. For d dimensional systems under isotropic pressure, it is therefore convenient to choose a force scale such that $\sigma_{xx} = \sigma_{yy}(=\sigma_{zz}) = 1/d$. However, in Ref. [102] the rather unphysical constraint $\sigma_{xx} + \sigma_{yy} = 1$ was used instead. With the latter constraint, small anisotropic pressure fluctuations occur.

Monte Carlo simulations in the force network ensemble are used to study the contact force distribution for the triangular lattice for both isotropic and anisotropic pressure. We also unravel the effect of the system size N for both constraints. The results are shown in Fig. 4.1. Contact force distributions calculated with $\sigma_{xx} = \sigma_{yy} = \frac{1}{2}$ show no differences at forces below $f = 5$, but a finite size effect is observed for larger forces, converging to a Gaussian distribution (see also Section 2.3). Contact force distributions calculated with the anisotropic constraint $\sigma_{xx} + \sigma_{yy} = 1$ converge to the same Gaussian distribution, but the finite size effect is much larger. The reason for this is that for small systems, the fluctuations of σ_{xx} and σ_{yy} around $\frac{1}{2}$ are quite large. For larger systems, these fluctuations become smaller so eventually $\sigma_{xx} \approx \frac{1}{2}$ and $\sigma_{yy} \approx \frac{1}{2}$. From now on, for regular packings we use the constraint $\sigma_{xx} = \sigma_{yy}(=\sigma_{zz}) = \frac{1}{d}$, because it is the most physical one.
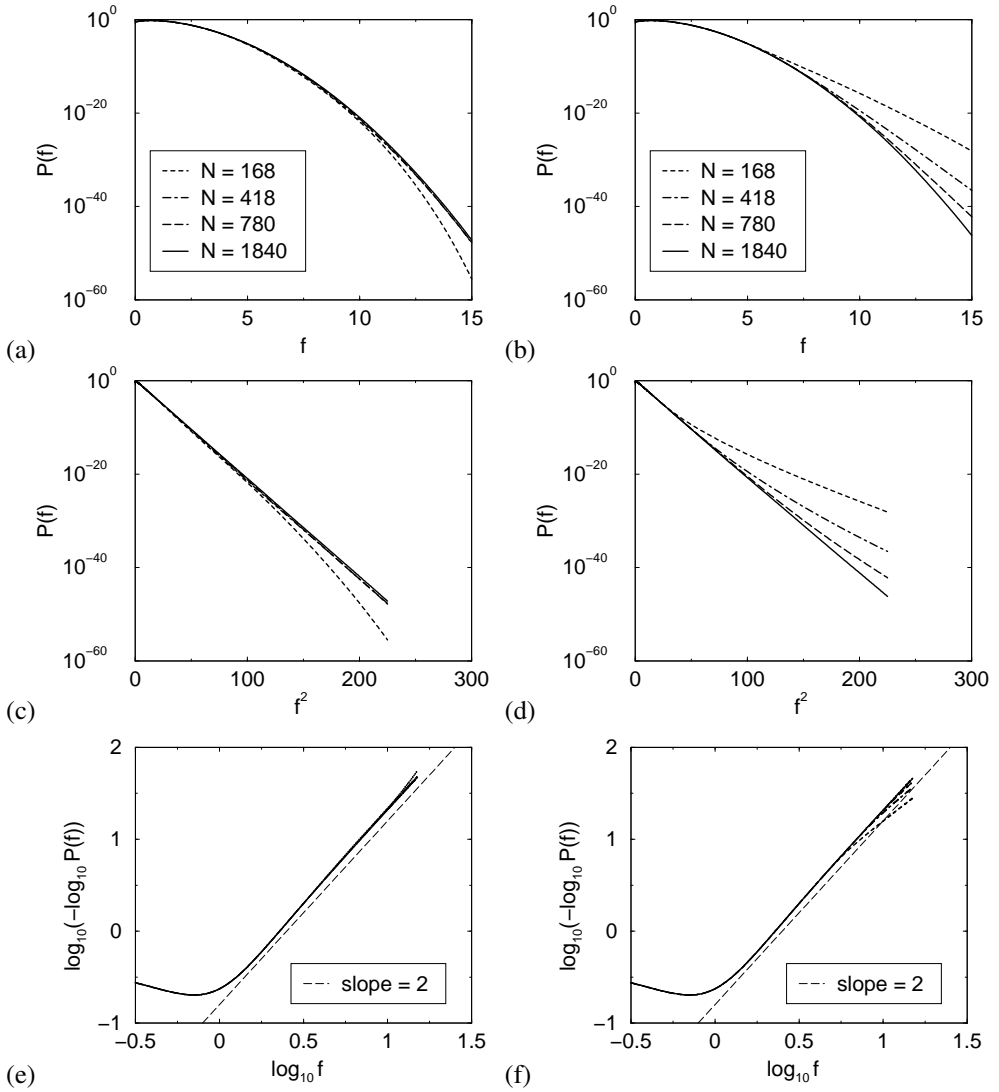
Figure 4.1: Contact force distribution $P(f)$ as a function of the system size (number of particles N) for the triangular lattice. (a,c,e) The constraint $\sigma_{xx} = \sigma_{yy} = \frac{1}{2}$ is used. (b,d,f) The constraint $\sigma_{xx} + \sigma_{yy} = 1$ is used.

4.3   Angle-resolved $P(f)$

In Section 2.6, contact force distributions are shown for a two-dimensional disordered system ($z = 5.5$) experiencing shear stress. These force distributions do not show a single characteristic feature, because shear stress induces force anisotropy that yields a variation in $\langle f \rangle$ depending on the orientation of the contact. In good approximation, the average normal contact force along direction ϕ, see Fig. 4.2, can be described by

$$\bar{f}_n(\phi) = 1 + 2\tau \sin(2\phi) - b_2 \cos(4\phi), \tag{4.1}$$

with $\int d\phi\, \bar{f}_n(\phi) / \int d\phi = 1$ [11, 103]. The parameter b_2 increases with increasing shear stress $\tau = \sigma_{xy}/\sigma_{xx}$ and $b_2 = 0$ for $\tau = 0$. The second term in Eq. (4.1) has the largest contribution to the force anisotropy. The "total" $P(f)$ is a superposition over all orientations ϕ. Here, we study the angle-resolved contact force distribution $P(f, \phi)$ by umbrella sampling. To accurately compute the tail of this distribution, a separate simulation is needed for each ϕ, using the maximum force along the direction ϕ as an order parameter (see also Section 1.6). From Eqs. (1.25), (1.26), and (1.27) it is easy to see that the constraints $\sigma_{xx} = \sigma_{yy}$ and $\sigma_{xy} \neq 0$ imply that $\phi = 45°$ is the shear stress direction. Hence, the following symmetry applies: $P(f, 45° - \phi) = P(f, 45° + \phi)$ and $P(f, 225° - \phi) = P(f, 225° + \phi)$. This has been used to improve sampling statistics.
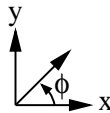

Figure 4.2: The angle ϕ in the used reference frame.

A triangular lattice contains contact forces in three distinct orientations: *(1)* 0° and 180°, *(2)* 60° and 240°, and *(3)* 120° and 300°. In Fig. 4.3 contact force distributions are shown for these three orientations. We see that for $\tau = 0$ all orientations have the same Gaussian decay of $P(f, \phi)$ ($\alpha = 2$ in Eq. (1.37)). The small differences in Fig. 4.3(a) can be attributed to finite-size effects induced by periodic boundary conditions. If the system experiences shear stress ($\tau > 0$), the tails of the force distributions are still Gaussian ($\alpha = 2$), but as expected we observe a different slope in the linear-log plots; the probability of large contact forces oriented close to the direction of the shear stress (60° and 240°) becomes larger, while the probability of

large contact forces oriented almost perpendicular to the direction of the shear stress ($120°$ and $300°$) becomes significantly smaller.
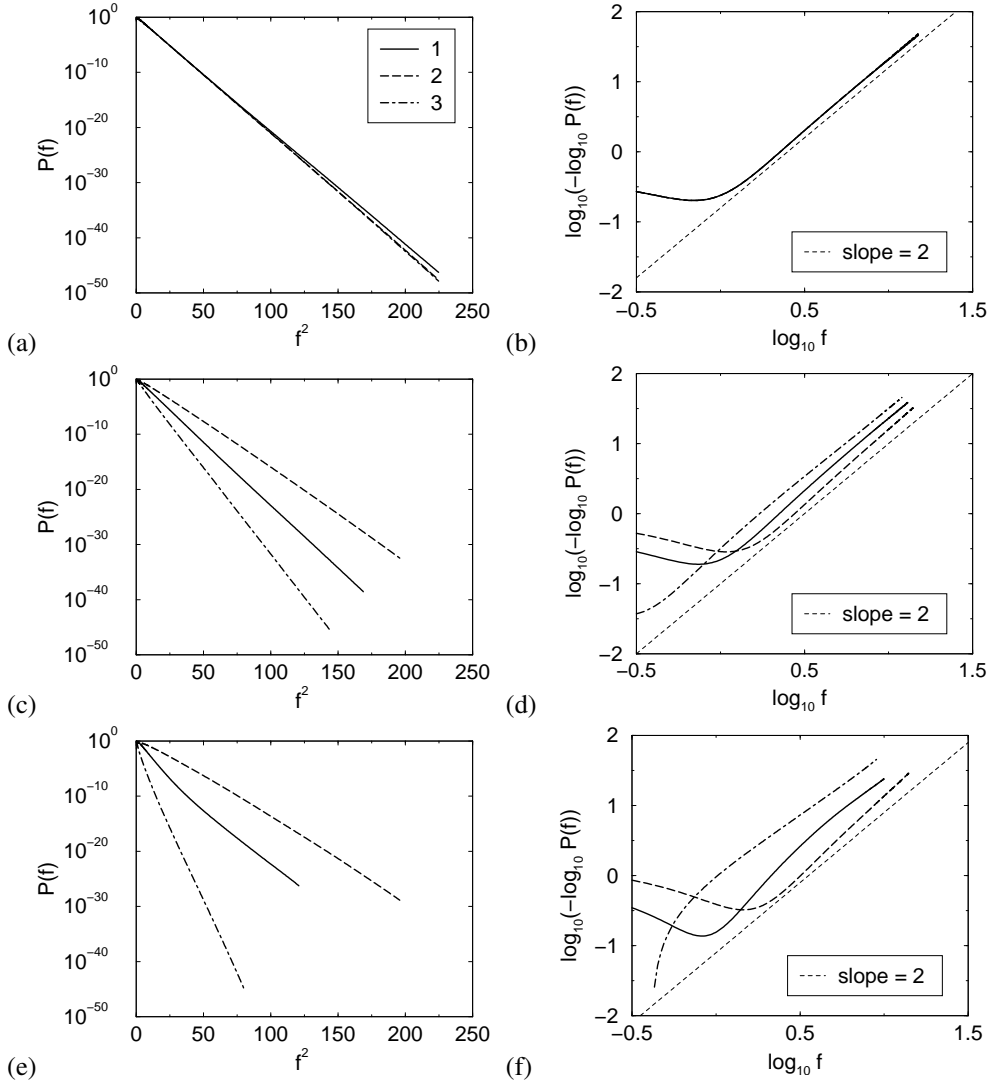
Figure 4.3: Angle-resolved contact force distributions for a triangular lattice ($N = 1840$ particles) with $\tau = 0$ (a,b), $\tau = 0.2$ (c,d) and $\tau = 0.4$ (e,f). The contact forces are oriented in three directions: *(1)* $0°$ and $180°$, *(2)* $60°$ and $240°$, and *(3)* $120°$ and $300°$. If systems experience shear stress, the distribution $P(f, \phi)$ becomes different in the three given directions. However, for a fixed ϕ, $P(\phi)$ shows a Gaussian decay.

To study the angle-resolved $P(f, \phi)$ for 2D disordered systems, we construct a histogram of all contact forces in which the contact forces are grouped according to their orientation ϕ, see Fig. 4.4. In Fig. 4.5 the average normal force for each orientation is plotted in a polar diagram. Without shear stress, the average force equals 1 in all directions. With shear stress ($\tau > 0$), the average force in the direction of the shear stress (label *1* in Fig. 4.4) becomes larger and the average force oriented almost perpendicular to this direction (label *6*) becomes smaller (see Fig. 4.5(a)). The orientation dependence of the average force is given in good approximation by Eq. (4.1). We also show a polar diagram for frictional particles as a function of shear stress (see Fig. 4.5(b)) and as a function of the friction coefficient (see Fig. 4.5(c)). From the latter figure we can conclude that force anisotropy disappears if we allow friction.
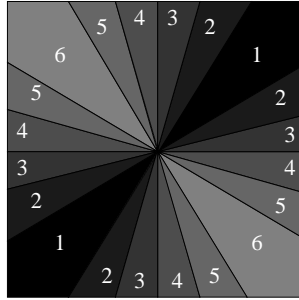
Figure 4.4: Diagram showing the different orientation segments for which the contact forces are evaluated. Note the symmetries $P(f, 45° - \phi) = P(f, 45° + \phi)$ and $P(f, 225° - \phi) = P(f, 225° + \phi)$ are compatible with the symmetry of simple shear.

Fig. 4.6 shows the angle-resolved $P(f, \phi)$ for disordered systems with frictionless particles. We see that the $P(f, \phi)$'s for systems experiencing shear stress decay at least as fast as a Gaussian. Certainly, the decay of the angle-resolved contact force distribution decays significantly faster than an exponential. This means that the (partly) exponential decay of the *total* $P(f)$ as was found in Fig. 2.5 is a direct result of averaging $P(f, \phi)$ over all ϕ, and not a result of exponential statistics of individual contact forces.
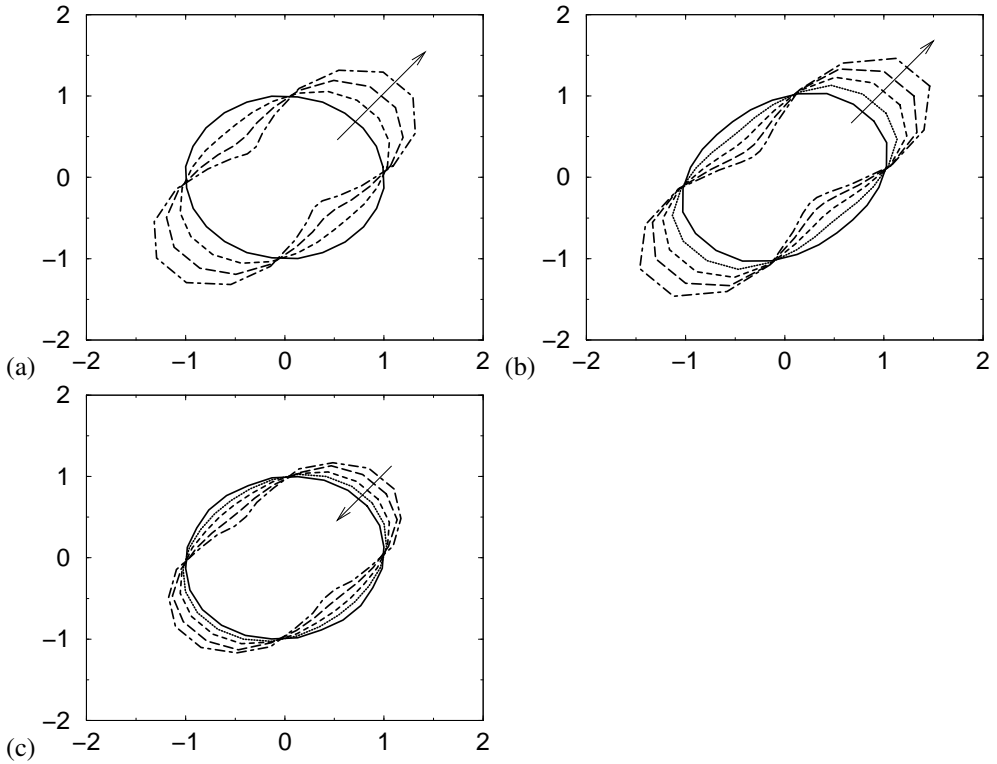
Figure 4.5: Polar diagram of the average normal force per histogram segment for a two-dimensional disordered system with $N = 1024$ and $z = 5.5$. We have used the segments represented in Fig. 4.4. (a) Frictionless particles as a function of the shear stress τ. The direction of the arrow indicates increasing τ: $0, 0.1, 0.2, 0.3$. (b) Frictional particles ($\mu = 0.5$) as a function of the shear stress τ. The direction of the arrow indicates increasing τ: $0.1, 0.2, 0.3, 0.4, 0.49$. (c) Frictional particles experiencing shear stress ($\tau = 0.2$) as a function of the friction coefficient μ. The direction of the arrow indicates increasing μ: $0.1, 0.5, 1.0, 2.0, 10.0$.

Figure 4.6: Angle-resolved contact force distributions of a two-dimensional disordered system with frictionless particles ($N = 1024, z = 5.5$), divided in six directions. The numbers correspond to the segments in Fig. 4.4. (a,b) $\tau = 0.0$, (c,d) $\tau = 0.2$, (e,f) $\tau = 0.3$.
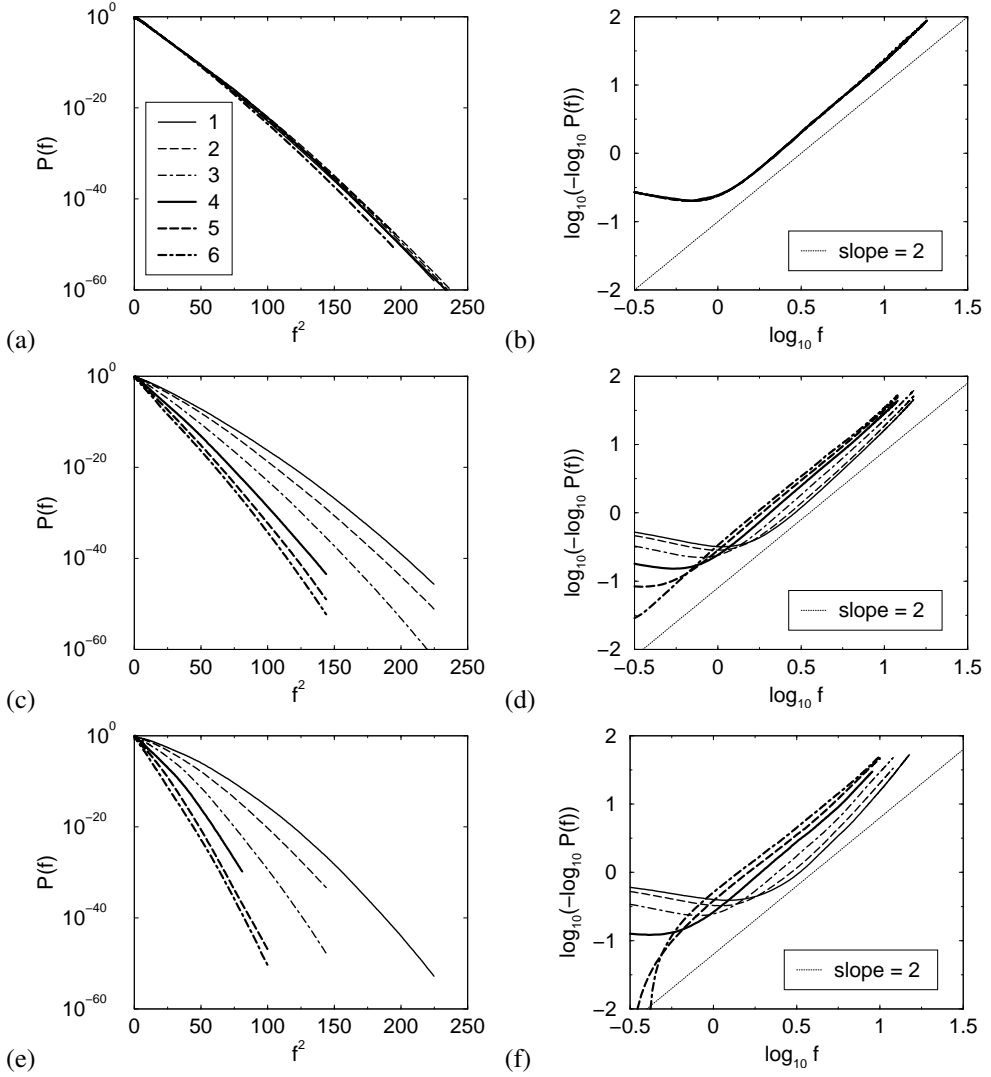
We also studied the angle-resolved contact force distribution for a fcc lattice experiencing shear stress. This lattice is oriented such that the close-packed planes lay in the xy-plane and are stacked along the z-axis. Contact forces in the fcc lattice have six distinct orientations, as shown in Fig. 4.7. Shear stress of the form $\sigma_{xy} \neq 0$ and $\sigma_{yz} = \sigma_{xz} = 0$ is applied and we refer to the parameter $\tau = \sigma_{xy}/\sigma_{xx}$ as the shear stress. The stress direction is in the xy-plane at $45°$ with the x-axis. Fig. 4.8 shows the direction-resolved $P(f)$ for a fcc lattice with frictionless particles. All $P(f)$ decay as $a\exp[-bf^\alpha]$ with $\alpha \approx 1.7$. Similar to the triangular lattice, for different directions we observe a different slope in the linear-log plots. Shear stress has the largest effect on the forces oriented in directions *2* and *3* as both are in the xy plane along the direction of the shear stress. Forces not oriented in this plane (e.g. *5*) are less affected.
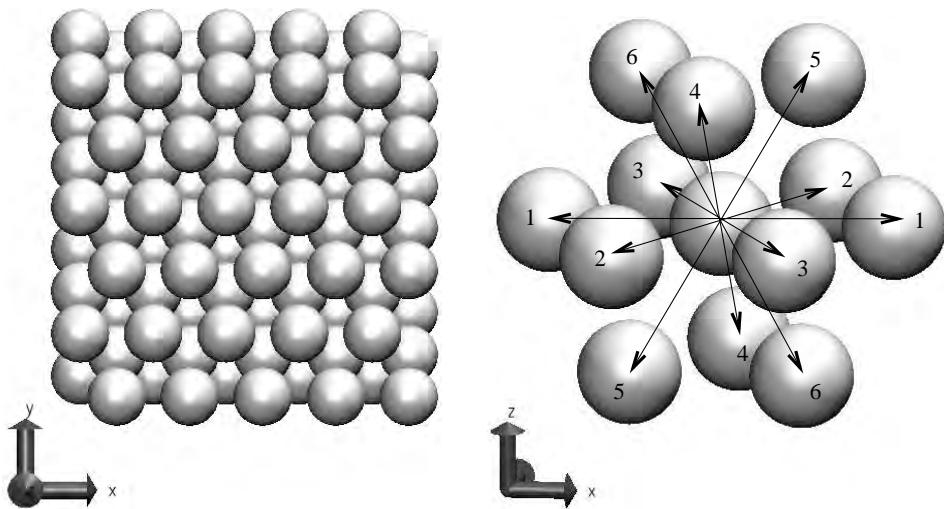
Figure 4.7: (left) Orthografic projection of an fcc lattice along the z-axis. The close-packed planes lay in the xy-plane and are stacked along the z-axis. The orientation becomes important if the system experiences shear stress. (right) Part of the fcc lattice in which the six distinct orientations of contacts between the particles are shown.
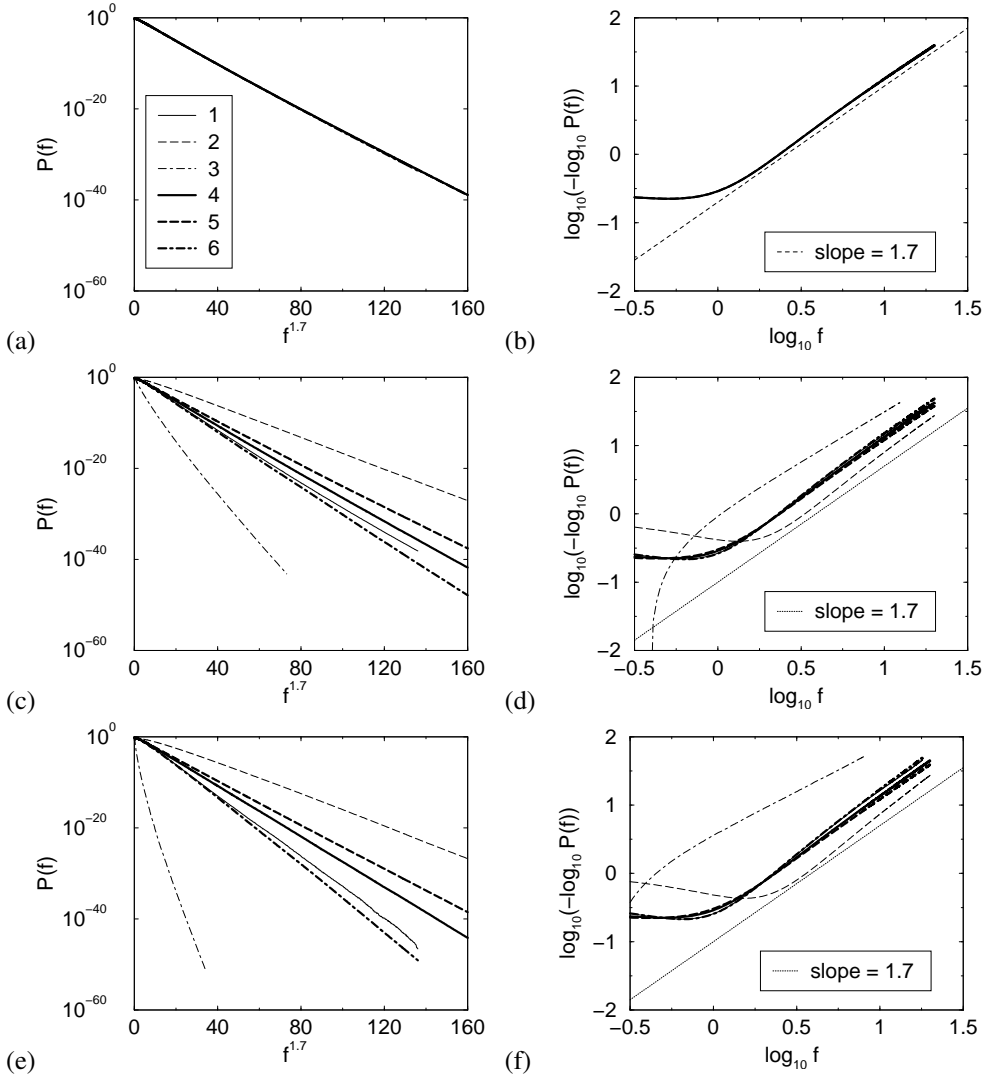
Figure 4.8: Direction-resolved contact force distributions of a three-dimensional crystalline system with frictionless particles (fcc, $N = 7140$), divided in six orientations (see Fig. 4.7). Shear stress τ is defined as $\sigma_{xy}/\sigma_{\alpha\alpha}$ with $\alpha = x, y, z$. (a,b) $\tau = 0$, (c,d) $\tau = 0.3$ and (e,f) $\tau = 0.39$.

4.4   Maximum possible force inside a packing

In Section 2.4 we have seen that for disordered packings in 2D, finite-size effects occur for the contact force distribution $P(f)$, especially for low coordination numbers (z). One would observe such finite-size effects for forces close to the maximum force that a certain packing can sustain. When the maximum force of a packing ($f_{max}(\mathbf{f})$) is close to the maximum force that a certain packing can sustain, $P(f)$ will show a very sharp decrease. Eventually, $P(f)$ will decrease to zero for any packing [85].

In principle, conventional umbrella sampling [52] can be used to determine the maximum possible f_{max}. However, a huge number of iterations will be necessary as $P(f)$ will become extremely small close to the maximum possible f_{max}. To efficiently compute the maximum possible f_{max} for a given packing, we use the central idea of the recently proposed random-walk algorithm of Wang and Landau [104, 105]. In this scheme, a random walk is performed in the space of all possible force networks $\mathbf{f}$. The simulation is started by setting a certain function $\kappa(f_{max}) = 1$ for all f_{max}. Starting from a particular solution $\mathbf{f} = \mathbf{f}_0$, we perform a Monte Carlo scheme to sample all possible force networks (see section 1.5). Trial moves that result in a configuration for which all $f_{n,i} \geq 0$ are accepted with a probability

$$P_{acc}(o \to n) = \min\left(1, \frac{\kappa(f_{max}(o))}{\kappa(f_{max}(n))}\right). \tag{4.2}$$

in which o and n are used to denote the old and new configuration respectively. The crucial difference with conventional Monte Carlo is that each time a force network with a certain f_{max} is visited, $\kappa(f_{max})$ is updated as follows: $\kappa(f_{max}) \to \kappa(f_{max}) \times m$ in which $m > 1$ (typically $m = 2$). This means that this scheme does not obey detailed balance. After many trial moves, eventually all possible values of f_{max} will be visited with (approximately) equal probability. From this, the maximum possible force of a certain contact network can be estimated. In the original version algorithm [104, 105], the parameter m is slowly decreased from 2 to $1 + \delta$ in a controlled way (typically $\delta \approx 10^{-9}$), such that eventually configurations are sampled with a probability inversely proportional to the density of states. In our case, we are only interested in the maximum possible force that a packing can sustain and therefore we can safely set $m = 2$.

Fig. 4.9(a) shows the computed maximum possible force in 2D disordered systems. Indeed, the maximum possible force increases with N and strongly depends on the coordination number z. In Fig. 4.9(b), the corresponding $P(f)$ along with the

maximum possible force is shown for $z = 4.5$. This figure shows strong evidence that the finite-size effects obtained in $P(f)$ are due to the fact that the maximum possible force of a small system with low z is quite small. Fig. 4.10 suggests that finite-size effects in 3D are much smaller. This is in line with the simulations presented in Fig. 2.4(a).

(a)   (b)
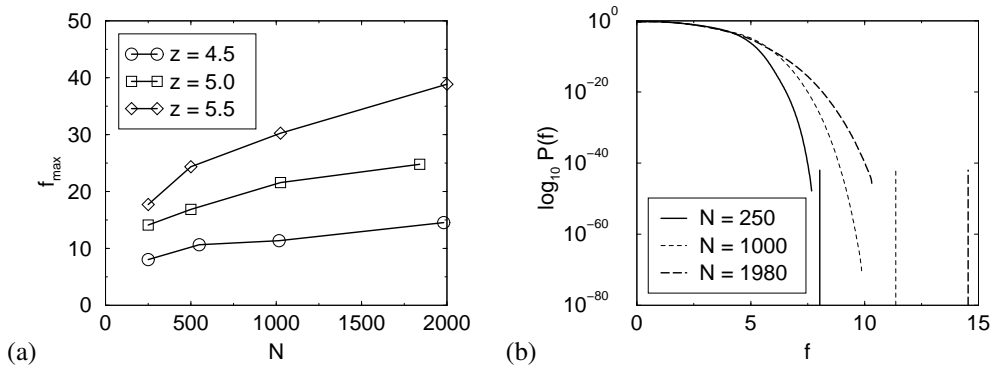
Figure 4.9: (a) The maximum possible force in unsheared networks of two-dimensional disordered systems for different N. (b) $P(f)$ for a 2D disordered systems with $z = 4.5$. The vertical lines show the maximum possible force.
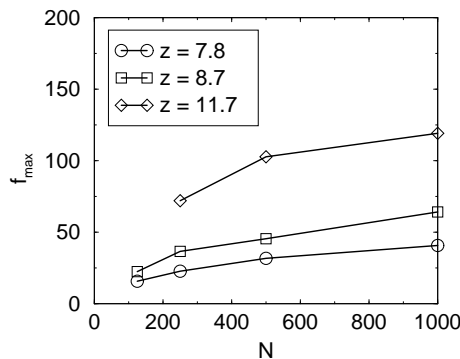

Figure 4.10: The maximum possible force in unsheared networks of three-dimensional disordered systems with a different N.

4.5 Maximum shear stress of a packing

To understand the relation between the maximum shear stress τ_m and the coordination number z of a certain packing, we investigated the volume of the phase space of allowed force networks. J.H. Snoeijer *et al.* showed that for 2D frictionless systems this volume shrinks for increasing τ [11]. The point at which the phase space volume is zero (τ_m) can be considered as a measure for the yield stress of the material. Ellenbroek and Snoeijer predicted that the effect of friction on τ_m is quite small [103]:

$$\tau_m = \frac{1 + \sqrt{1 + 3\mu^2}}{3}. \tag{4.3}$$

This equation is valid for disordered 2D systems in the limit of $z \to 6$. To estimate the accessible volume of the space of all allowed force networks corresponding to a certain shear stress τ, we have used the following approaches:

- An effective linear measure for the size of the force space is the Euclidean distance L:

$$L(\tau) \equiv \sqrt{\left\langle \sum_{ij} (f_{n,ij} - f'_{n,ij})^2 \right\rangle}. \tag{4.4}$$

  The brackets denote an average over independent force networks with normal forces $f_{n,ij}$ and $f'_{n,ij}$. Close to τ_m, $L(\tau)$ will show a sharp decrease.

- Direct calculation of the volume using umbrella sampling. The accessible volume $V(\tau)$ corresponding to a certain τ is proportional to the probability $P(\tau)$ measured in the force network ensemble in which the constraint on σ_{xy} has been removed. The dimension of the null space of this modified ensemble is one higher than given in Table 1.1. Essentially, $P(\tau) = V(\tau)/V_{tot}$ in which $V_{tot} = \int_0^\infty d\tau V(\tau)$. In principle, $P(\tau)$ and $L(\tau)$ will depend on the system size N and the nature of the packing. As L can be considered as a linear measure for the phase space volume, one would expect $P(\tau) \propto V(\tau) \approx cL^\gamma$ in which c is a constant and γ is the dimension of the force space. It describes how the volume of the force space shrinks with increasing τ.

First we will study the Euclidean distance L as a measure for the volume of the phase space. Fig. 4.11 shows the Euclidean distance $L(\tau)/L(\tau = 0)$ for 2D disordered
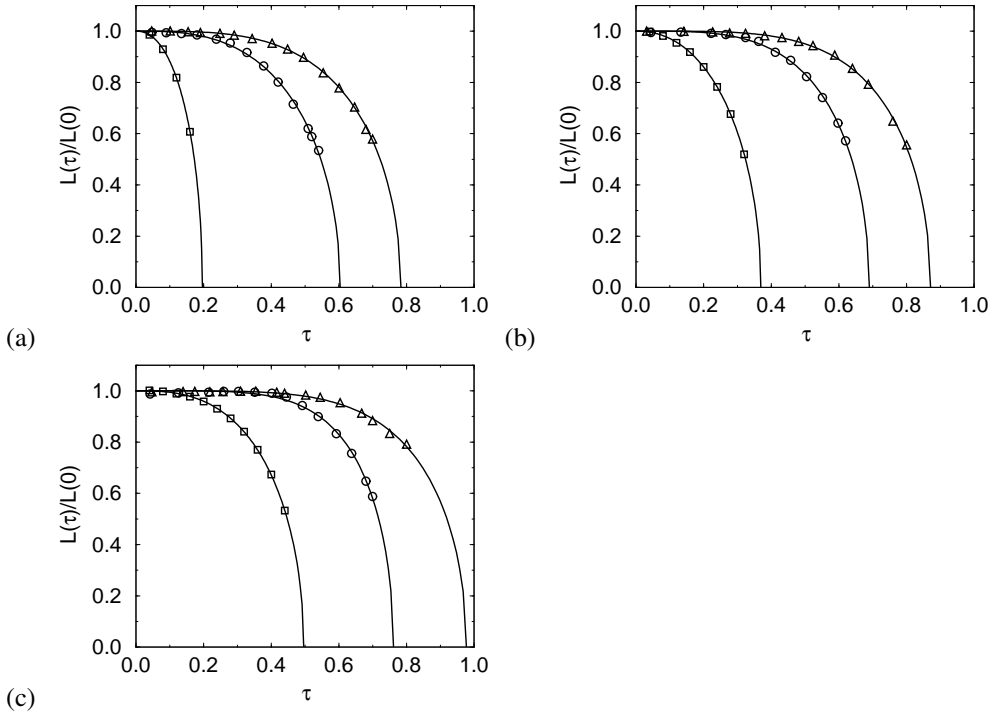
Figure 4.11: Euclidean distance $L/L(\tau = 0)$ as a function of τ for 2D disordered systems with $N = 1024$ and (a) $z = 4.5$, (b) $z = 5.0$ (c) $z = 5.5$. The symbols are simulation data points and the solid lines are fits to Eq. 4.5: no friction (square), $\mu = 0.5$ (circle) and $\mu = 1.0$ (triangle).

systems ($N = 1024$) without and with friction ($\mu = 0.5$ and $\mu = 1.0$). The data is well described by

$$L/L(0) = \sqrt{1 - \left(\frac{\tau}{\tau_m}\right)^\alpha}, \tag{4.5}$$

in which τ_m and α are fitted. For frictionless systems, $\alpha \approx 2$ while frictional systems have a larger value for α. The obtained results for τ_m are summarized in Table 4.1. Our simulation results for frictional and frictionless systems are in excellent agreement with the prediction of Ref. [11], which can be considered as an upper limit and therefore valid for large z. For $\tau < 0.2$, the Euclidean distance of frictional packings is almost constant, suggesting that the shear stress has a negligible influence on the normal contact forces.

Table 4.1: The maximum shear stress τ_m for systems with coordination number z and $N = 1024$ obtained by fitting Eq. 4.5 to the simulation data in Fig. 4.11. Included is also the prediction according to Eq. 4.3.

	$z = 4.5$	$z = 5.0$	$z = 5.5$	Eq. 4.3
no friction	0.20	0.37	0.50	0.67
$\mu = 0.5$	0.60	0.69	0.76	0.77
$\mu = 1.0$	0.78	0.87	0.98	1.00

Table 4.2: Estimated dimension γ of the force space for frictionless 2D disordered systems with $N = 1024$, obtained by plotting $\ln(P(\tau))$ versus $\ln(L(\tau))$. The values between brackets are the dimension of the force space according to Table 1.1.

$z = 4.5$	$z = 5.0$	$z = 5.5$
462 (259)	1120 (523)	2536 (769)

In Fig. 4.12, $P(\tau)/P(\tau = 0)$ is plotted as a function of τ for 2D disordered systems ($N = 1024$) without friction and with friction ($\mu = 0.5$ and $\mu = 1.0$). Already for small τ (i.e. far away from τ_m), $P(\tau)/P(\tau = 0)$ becomes extremely small. This means that within the framework of the force network ensemble, packings do not spontaneously develop a shear stress. Computing $P(\tau)$ beyond $\tau = 0.2$ is very difficult and requires very long simulations, even if more overlapping windows are used in the umbrella sampling simulations. For frictionless systems, $P(\tau)/P(\tau = 0)$ strongly depends on the coordination number z, while this effect is not present for frictional systems. The latter observation is not surprising, as $L(\tau)$ of frictional systems is almost flat for $\tau < 0.2$.

From the slope of $\ln(P(\tau))$ as a function of $\ln(L(\tau))$ we estimated the dimension of the force space γ that describes the shrinking of the force space for increasing τ. The value of γ is related to the dimension of the force space, see Table 1.1.
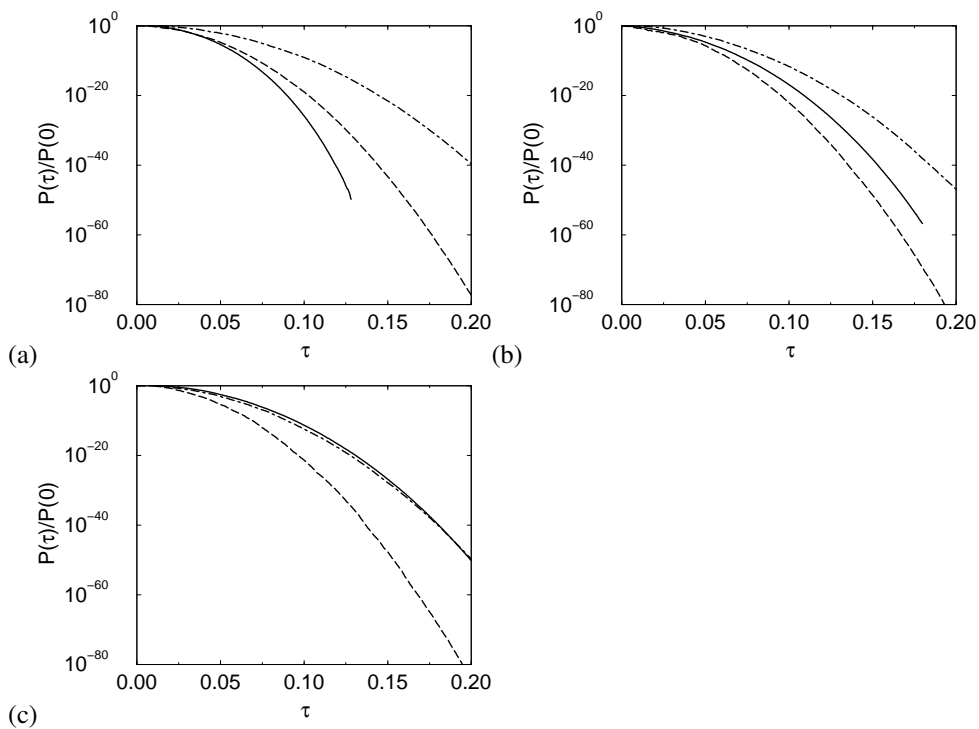
Figure 4.12: $P(\tau)/P(\tau = 0)$ against τ for 2D disordered systems $N = 1024$: no friction (solid), $\mu = 0.5$ (long dashed) and $\mu = 1.0$ (dot-dashed). (a) $z = 4.5$, (b) $z = 5.0$ (c) $z = 5.5$.

4.6   Wall versus bulk forces

In Section 1.2 we have presented a brief overview of experimental, theoretical and computational studies of force network statistics in granular materials. Experimental measurements of contact forces at the boundaries (walls) show convincing exponential contact force distributions, while a stronger than exponential decay is observed in many experimental and computational studies of bulk force statistics. The observed exponential force distributions have often been attributed to "Boltzmann" type arguments, however, in Chapter 3 we have shown that the tail of the force distribution is mainly determined by *local* constraints. This raises the question whether or not contact force statistics at the walls is fundamentally different from the bulk.

A simple model for a system with wall and bulk forces is the so-called Snooker triangle first studied by Snoeijer [42], see Fig. 4.13. The stress on the system is controlled by constraining the sum of the wall forces for each of the three walls. All contact forces are repulsive and we will not consider friction. For $N = 3$ and $N = 6$ balls, it is possible to derive analytical solutions for the bulk and wall force statistics ($P(f_b)$ and $P(f_w)$) in the framework of the force network ensemble. For larger N, $P(f_b)$ and $P(f_w)$ have been computed in Ref. [85]. However, the authors of this study were not able to make conclusive statements about the nature of the tail of these distributions.
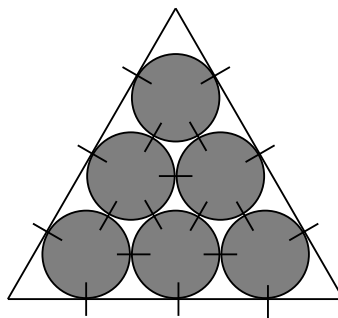

Figure 4.13: Snooker triangle of $N = 6$ balls with 9 forces between the balls (i.e., bulk forces) and 9 forces between a ball and the wall (i.e., wall forces). The stress on the system is controlled by constraining the sum of the wall forces for each of the three walls. Note that particles at the wall have 5 neighbors, while particles in the bulk have 6 neighbors.

We have re-examined the force distribution for snooker packings using umbrella sampling, see Fig. 4.14. The distributions $P(f_b)$ and $P(f_w)$ have been normalized such that $\langle f_b \rangle = 1$ and $\langle f_w \rangle = 1$. The results unambiguously show that for large N both the bulk and wall forces have a Gaussian tail. It is not surprising that for large N, $P(f_b)$ approaches the contact force distribution of a triangular lattice, which is known to have a Gaussian tail, see Chapter 2. Without the presence of local force balance on the balls near the wall, we would have exactly recovered the "Boltzmann" argument resulting in an exponential distribution of wall forces. Apparently, the distribution of wall forces is changed significantly by the presence of bulk forces and local force balance constraints.
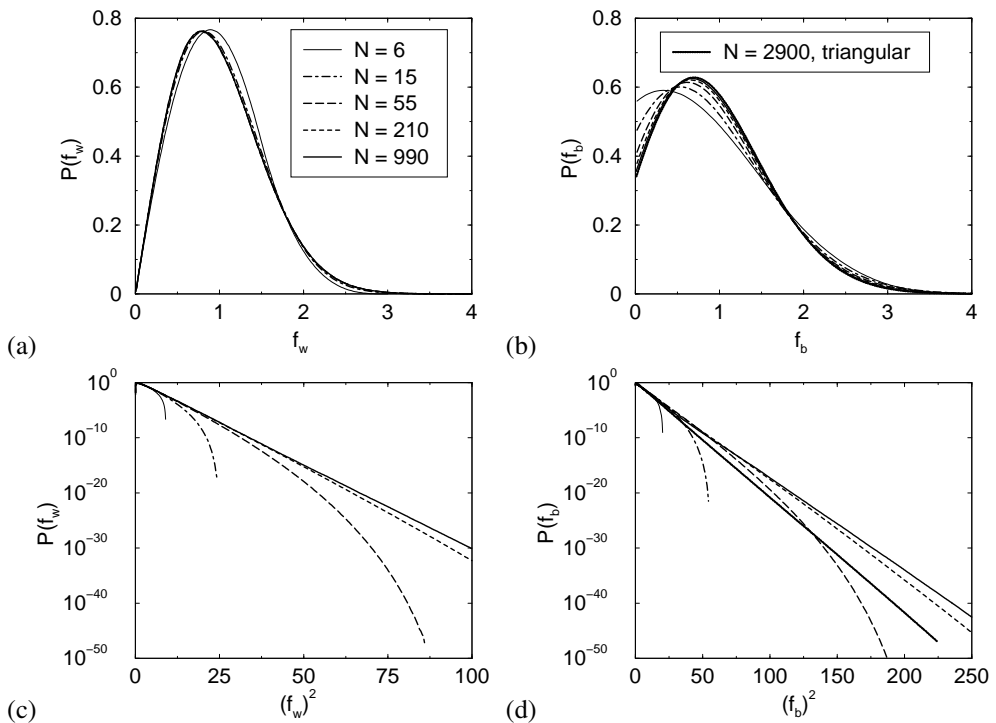

Figure 4.14: Contact force distribution for wall forces (a,c) and bulk forces (b,d) for snooker packings of several sizes. $P(f_w)$ and $P(f_b)$ have been normalized such that $\langle f_b \rangle = 1$ and $\langle f_w \rangle = 1$. For comparison we also show $P(f)$ for a frictionless triangular lattice in (b,d).

In order to further study the effect of wall forces, we have computed contact force distributions for a triangular lattice confined between two walls using the force network ensemble, see Fig. 4.15. The following conditions were studied:

- A flat measure imposed on the whole system, i.e. the sum of the wall forces for each wall is constant. The distribution of bulk and wall forces is shown in Fig. 4.16. Just as for the snooker packing, both the bulk and wall forces show a Gaussian decay because of the local force balance constraints.

- A flat measure imposed on the bulk and wall forces *separately* [106], i.e. all wall forces are constant and drawn from an exponential distribution. Fig. 4.17 shows the distribution of bulk forces as a function of the position in the system for a single realization of the wall forces. Within 10 layers the contact force distribution is identical to the one for the periodic triangular lattice, both having a Gaussian tail. The boundary forces are fixed and drawn from an exponential distribution. As a reference, the contact force distribution of a periodic triangular lattice of $N = 2900$ particles is also shown, see Fig. 2.1.

This simple example demonstrates that the distribution of wall forces may differ considerably from the distribution of bulk forces.
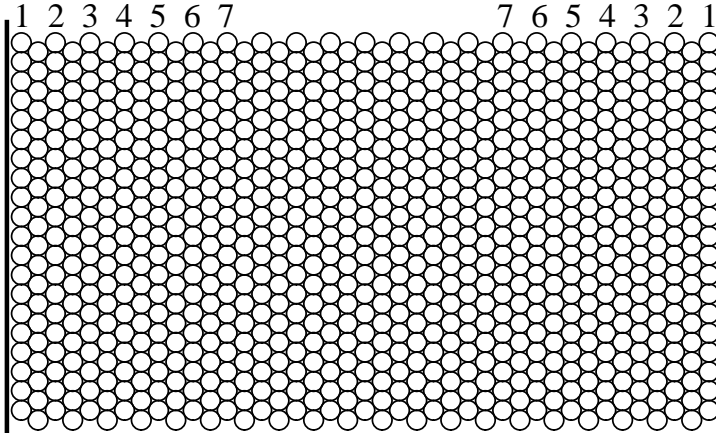
Figure 4.15: Triangular lattice between two walls. Periodic boundary conditions are only used in the vertical direction. The system consists of 820 particles, 2420 interparticle contact forces and $2 \times 20 = 40$ wall forces. All forces are repulsive and we do not consider friction. The numbers indicate the various layers.
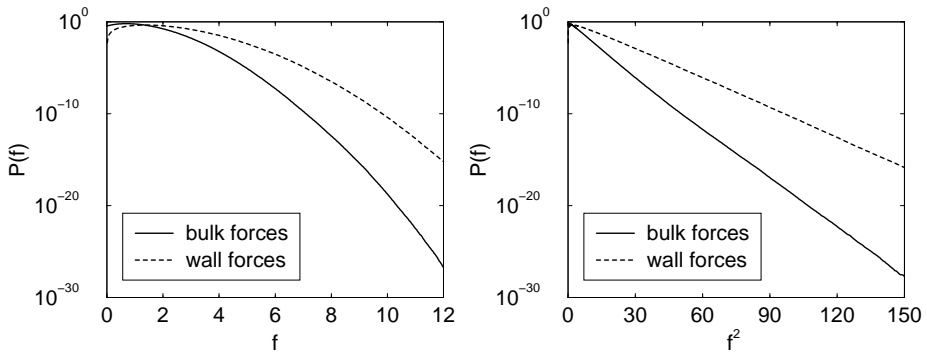
Figure 4.16: Distribution of bulk and wall forces for the system of Fig. 4.15. A flat measure is imposed on the whole system.
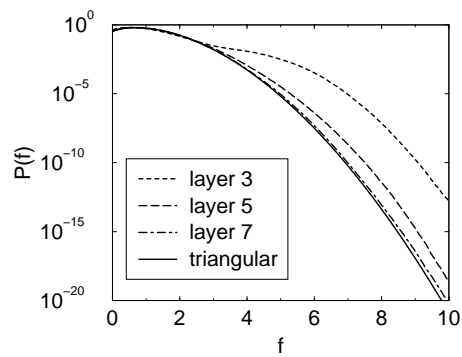
Figure 4.17: Distribution of bulk contact forces as a function of the position, see Fig. 4.15. A flat measure imposed on the bulk and wall forces separately, i.e. all wall forces are constant and drawn from an exponential distribution (see text).

4.7 Contact force distributions for systems with "real" interactions

Until now we studied contact force distributions in the framework of the force network ensemble. In this ensemble, the contact forces between particles are stochastic variables subject to various constraints (i.e. force balance on each grain, only repulsive contact forces, and a prescribed stress tensor) and do not originate from an interaction potential. It is interesting to investigate to which extent the contact force statistics of the force network ensemble is identical to that of forces derived from "real" interactions, i.e. interactions that follow from an interaction (pair) potential.

Two cases are worth studying. First, the force distribution of the unconstrained "real" system and second the force distribution of the "real" system with the constraint of a zero net force on each particle. We shall refer to the latter systems as force balanced packings.

We first discuss force balanced packings of interacting particles. It is natural to expect that the contact force distribution is close to the one obtained in the force network ensemble. Molecular simulations of force balanced packings of interacting particles are non-trivial as one needs to include constraints on the net force on each particle, while one cannot control the contact forces directly. We used the scheme described in Section 1.4 to generate a large number of these packings with equal pressure P. We studied 2D packings of $N = 2000$ bidisperse particles with diameter σ_i (50%/50% mixture, size ratio 1.4) interacting with either a WCA potential (Eq. 1.20) or an harmonic potential

$$u_{\mathrm{HARM}}(r_{ij}) = \begin{cases} \varepsilon \left(\sigma_{ij} - r_{ij} \right)^2, & r_{ij} \leq \sigma_{ij} \\ 0, & r_{ij} > \sigma_{ij}, \end{cases} \tag{4.6}$$

where $\sigma_{ij} = (\sigma_i + \sigma_j)/2$ and ε is the depth of the potential well. The diameter of the smallest particles is used as a unit of length.

Fig. 4.18 shows the contact force distributions and the coordination numbers for forces balanced packings with pressure P consisting of particles that interact with an harmonic potential. In the same figure we also show $P(f)$ for a triangular lattice in the force network ensemble. The graphs for the "real" interactions are obtained from averaging over 4000 force balanced packings for each pressure. The average coordination number z strongly depends on the applied pressure. In the limit of small pressure, the coordination number approaches the isostatic limit $z_c = 4$. For

all simulations, we have verified that the system is sufficiently far from z_c so that the simulations do not suffer from a lack of self-averaging [35, 107]. The contact force distribution for a triangular lattice in the force network ensemble is close to $P(f)$ for the "real" interactions at dimensionless pressure $P \approx 0.03$. Both distributions have a Gaussian tail. For larger pressures (and larger z) the contact force distribution bends down faster than a Gaussian. The observation of a Gaussian tail is in agreement with the simulations of O'Hern *et al*. [12, 35]. These authors also used an argument based on equilibrium systems to predict the decay of the large force tail, resulting in a Gaussian tail for an harmonic potentials and a nearly exponential tail for a WCA potential. It is important to note that the systems of Fig. 4.18 are *not* in thermodynamic equilibrium so the argument may not apply.

To investigate the effect of the interaction potential, we have studied force balanced packings of particles interacting with a WCA potential. We have investigated the effect of the pressure P as well as the (dimensionless) hardness κ of the interaction potential:

$$\kappa = \frac{\langle f \rangle}{\langle r_{ij} \rangle} \left\langle \frac{\partial f}{\partial r_{ij}} \right\rangle^{-1}. \tag{4.7}$$

Particles that are harder have a lower value of κ. The value of κ can be controlled directly by changing the energy parameter ε of the WCA potential. Fig. 4.19(a) shows that systems with the same κ have the same coordination number z, and we have verified that they also have the same contact force distribution. Analogous to what we found for an harmonic interaction, we find that the contact force distribution for a triangular lattice in the force network ensemble is close to $P(f)$ for energy parameter $\varepsilon \approx 16$ and dimensionless pressure $P = 15$. Again, they both have a Gaussian tail. In fact, all distributions of Fig. 4.19(d) have a Gaussian tail.

Next we turn to the case of the force distribution of an unconstrained "real" system. These systems do *not* have force balance. In Chapter 3 we have shown that local force balance determines the decay of the contact force distribution. Fig. 4.20 shows the contact force distribution of particles interacting with a WCA potential simulated at a finite temperature T. The glass transition temperature of this system is $k_B T_g / \varepsilon \approx 1.1$. Clearly, $P(f)$ decays exponentially both for $T > T_g$ and $T < T_g$, in agreement with previous molecular dynamics simulations [12]. This is significantly different from the Gaussian tails of the contact force distribution that we found for the constrained "real" interactions. It would be very interesting to investigate further if the arguments of Chapter 3 are able to explain the differences between the tails of
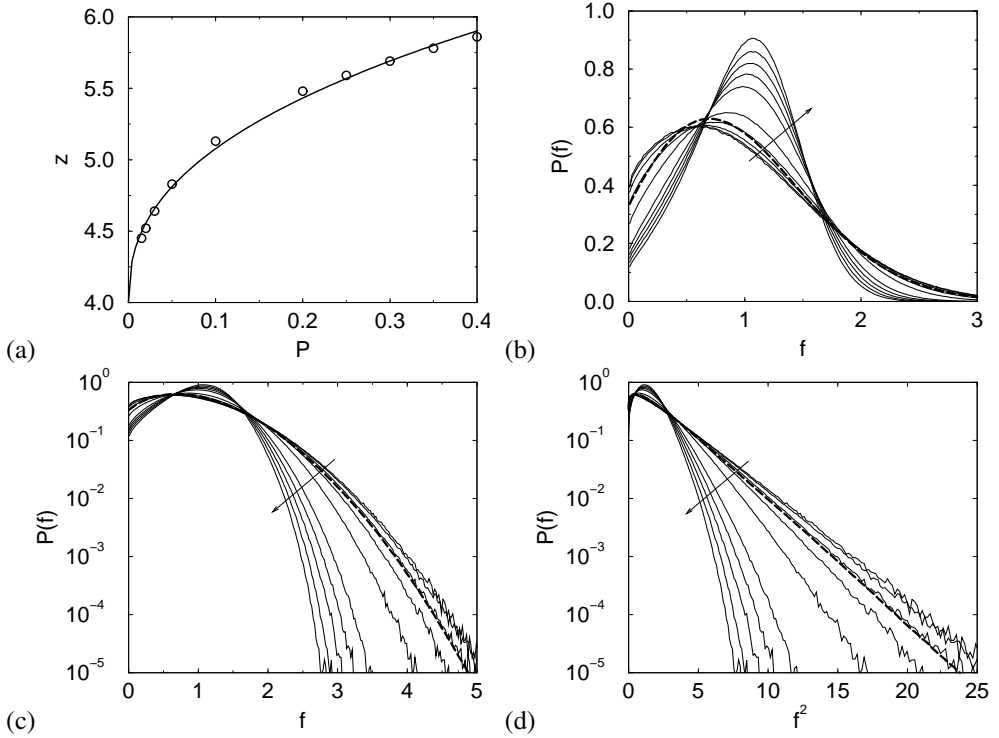
Figure 4.18: (a) The coordination number z as a function of the pressure P resulting from simulations of systems with particles interacting via an harmonic potential ($\varepsilon/k_B T = 1$). The data is well described by $z - z_c \sim P^{0.41}$ (solid line). (b,c,d) Contact force distribution of systems with particles interacting via the harmonic potential ($\varepsilon/k_B T = 1$). The same data are plotted using different axes. The direction of the arrow indicates increasing pressure P (in dimensionless units 0.015, 0.02, 0.03, 0.05, 0.1, 0.2, 0.25, 0.3, 0.35, 0.4). For comparison we also show $P(f)$ for a triangular lattice in the force network ensemble (dashed curve).

$P(f)$ in Fig. 4.19 and 4.20.
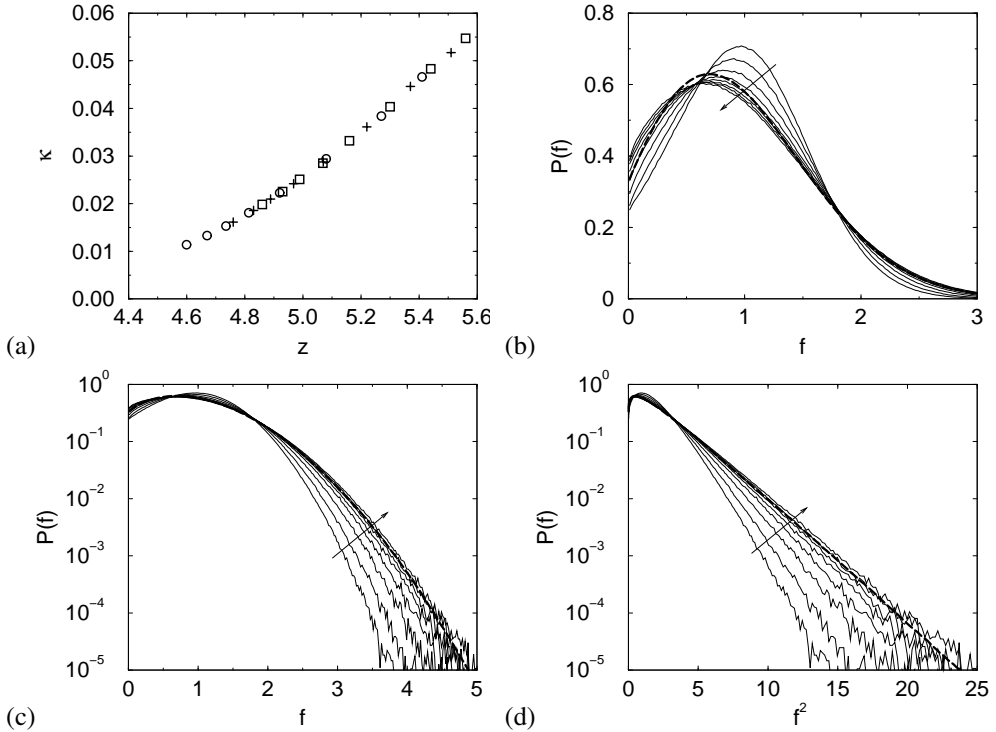
Figure 4.19: (a) The hardness κ as a function of the coordination z. The data points are results from simulations of systems with particles interacting via the WCA potential and dimensionless pressure $P = 15$ (circle), $P = 25$ (plus) and $P = 35$ (square). (b,c,d) Contact force distribution of systems with particles interacting via the WCA potential and dimensionless pressure $P = 15$. The direction of the arrow indicates increasing energy parameter ε/k_BT (1, 2, 4, 7, 10, 13, 16, 20) and decreasing κ (0.0466, 0.0384, 0.0294, 0.02227, 0.01810, 0.01531, 0.01331, 0.01138). For comparison we also show $P(f)$ for a triangular lattice in the force network ensemble (dashed curve).
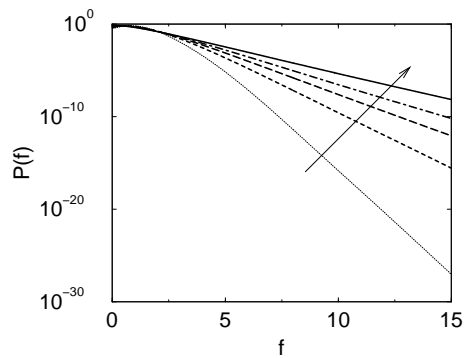
Figure 4.20: Force distributions of a two-dimensional system ($N = 1024$, $\rho = N/V = 0.747$) with a WCA potential without force balance as a function of the temperature. The direction of the arrow indicates increasing $k_B T / \varepsilon$: 0.2, 0.4, 0.6, 0.8, 1.2. These simulations have been obtained using umbrella sampling where we have assumed local equilibrium. We have verified that MD simulations of the same system using a constraint temperature lead to identical results.

References

[1] L. K. A. Dorren, *A review of rockfall mechanics and modelling approaches*, Prog. Phys. Geogr. **27**, 69 (2003).

[2] S. De Toni and P. Scotton, *Two-dimensional mathematical and numerical model for the dynamics of granular avalanches*, Cold Regions Science and Technology **43**, 36 (2005).

[3] W. R. Ketterhagen, J. S. Curtis, C. R. Wassgren, and B. C. Hancock, *Modeling granular segregation in flow from quasi-three-dimensional, wedge-shaped hoppers*, Powder Technol. **179**, 126 (2008).

[4] F. Y. Fraige, P. A. Langston, and G. Z. Chen, *Distinct element modelling of cubic particle packing and flow*, Powder Technol. (in press, doi:10.1016/j.powtec.2007.12.009).

[5] E. DesRosiers Lachiver, N. Abatzoglou, L. Cartilier, and J. S. Simard, *Agglomeration tendency in dry pharmaceutical granular systems*, Eur. J. Pharm. Biopharm. **64**, 193 (2006).

[6] K. Lee, T. Kim, P. Rajniak, and T. Matsoukas, *Compositional distributions in multicomponent aggregation*, Chem. Eng. Sci. **63**, 1293 (2008).

[7] M. van Hecke, *Shape matters*, Science **317**, 49 (2007).

[8] M. van Hecke, *Granular matter: A tale of tails*, Science **435**, 1041 (2005).

[9] H. P. Zhu, Z. Y. Zhou, R. Yang, and A. B. Yu, *Discrete particle simulation of particulate systems: Theoretical developments*, Chem. Eng. Sci. **62**, 3378 (2007).

[10] A. J. Liu and S. R. Nagel, *Jamming is not just cool any more*, Nature **396**, 21 (1998).

[11] J. H. Snoeijer, W. G. Ellenbroek, T. J. H. Vlugt, and M. van Hecke, *Sheared force-networks: anisotropies, yielding and geometry*, Phys. Rev. Lett. **96**, 098001 (2006).

[12] C. S. O'Hern, S. A. Langer, A. J. Liu, and S. R. Nagel, *Force distributions near jamming and glass transitions*, Phys. Rev. Lett. **86**, 111 (2001).

[13] L. E. Silbert, D. Ertas, G. S. Grest, H. T. C., and D. Levine, *Analogies between granular jamming and the liquid-glass transition*, Phys. Rev. E **65**, 051307 (2002).

[14] V. Trappe, V. Prasad, L. Cipelletti, P. N. Segre, and D. A. Weitz, *Jamming phase diagram for attractive particles*, Nature **411**, 772 (2001).

[15] C. h. Liu, A. R. Nagel, D. A. Schecter, S. N. Coppersmith, S. Majumdar, O. Narayan, and T. A. Witten, *Force fluctuations in bead packs*, Science **269**, 513 (1995).

[16] http://www.roymech.co.uk/Useful_Tables/Tribology/co_of_frict.htm.

[17] F. Jones, H. Ryffel, E. Oberg, C. McCauley, and R. Heald, *Machinery's Handbook*, Industrial Press, 27th edition, 2004.

[18] H. M. Jaeger, S. R. Nagel, and R. P. Behringer, *Granular solids, liquids, and gases*, Rev. Mod. Phys. **68**, 1259 (1996).

[19] P. G. de Gennes, *Granular matter: a tentative view*, Rev. Mod. Phys. **71**, s374 (1999).

[20] E. I. Corwin, H. M. Jaeger, and S. R. Nagel, *Structural signature of jamming in granular media*, Nature **435**, 1075 (2005).

[21] D. M. Mueth, H. M. Jaeger, and S. R. Nagel, *Force distribution in a granular medium*, Phys. Rev. E **57**, 3164 (1998).

[22] D. L. Blair, N. W. Mueggenburg, A. H. Marshall, H. M. Jaeger, and S. R. Nagel, *Force distributions in three-dimensional granular assemblies: Effects of packing order and interparticle friction*, Phys. Rev. E **63**, 041304 (2001).

[23] J. M. Erikson, N. W. Mueggenburg, H. M. Jaeger, and S. R. Nagel, *Force distributions in three-dimensional compressible granular packs*, Phys. Rev. E **66**, 040301 (2002).

[24] G. Løvoll, K. J. Måløy, and E. G. Flekkøy, *Force measurements on static granular materials*, Phys. Rev. E **60**, 5872 (1999).

[25] T. S. Majmudar and R. P. Behringer, *Contact force measurements and stress-induced anisotropy in granular materials*, Nature **435**, 1079 (2005).

[26] J. Brujić, S. F. Edwards, I. Hopkinson, and H. A. Makse, *Measuring the distribution of interdroplet forces in a compressed emulsion system*, Physica A **327**, 201 (2003).

[27] H. A. Makse, D. L. Johnson, and L. M. Schwartz, *Packing of compressible granular materials*, Phys. Rev. Lett. **84**, 4160 (2000).

[28] F. Radjai, M. Jean, J. J. Moreau, and S. Roux, *Force distributions in dense two-dimensional granular systems*, Phys. Rev. Lett. **77**, 274 (1996).

[29] J. Zhou, S. Long, Q. Wang, and A. D. Dinsmore, *Measurement of forces inside a three-dimensional pile of frictionless droplets*, Science **312**, 1631 (2006).

[30] P. A. Cundall and O. D. L. Strack, *Discrete numerical model for granular assemblies*, Geotechnique **29**, 47 (1979).

[31] H. A. Makse, *Continuous avalanche segregation of granular mixtures in thin rotating drums*, Phys. Rev. Lett. **83**, 3186 (1999).

[32] T. Unger, L. Brendel, D. E. Wolf, and J. Kertész, *Elastic behavior in contact dynamics of rigid particles*, Phys. Rev. E **65**, 061305 (2002).

[33] M. P. Allen and D. J. Tildesley, *Computer simulations of liquids*, Oxford University Press, Oxford, 1987.

[34] D. N. Perera and P. Harrowell, *Stability and structure of a supercooled liquid mixture in two dimensions*, Phys. Rev. E **59**, 5721 (1999).

[35] C. S. O'Hern, S. A. Langer, A. J. Liu, and S. R. Nagel, *Random packings of frictionless particles*, Phys. Rev. Lett. **88**, 075507 (2002).

[36] A. V. Tkachenko and T. A. Witten, *Stress propagation through frictionless granular material*, Phys. Rev. E **60**, 687 (1999).

[37] L. E. Silbert, G. S. Grest, and J. W. Landry, *Statistics of the contact network in frictional and frictionless granular matter*, Phys. Rev. E **66**, 061303 (2002).

[38] S. N. Coppersmith, C. h. Liu, S. Majumdar, O. Narayan, and T. A. Witten, *Model for force fluctuations in bead packs*, Phys. Rev. E **53**, 4673 (1996).

[39] P. Claudin, J. P. Bouchaud, M. E. Cates, and J. P. Wittmer, *Models of stress fluctuations in granular media*, Phys. Rev. E **57**, 4441 (1998).

[40] A. R. T. van Eerd, W. G. Ellenbroek, M. van Hecke, J. H. Snoeijer, and T. J. H. Vlugt, *The tail of the contact force distribution in static granular materials*, Phys. Rev. E **75**, 060302(R) (2007).

[41] S. F. Edwards and R. B. S. Oakeshott, *Theory of powders*, Physica A **157**, 1080 (1989).

[42] J. H. Snoeijer, *Statistics of force networks in granular media*, PhD thesis, Leiden University (2003).

[43] J. H. Snoeijer, T. J. H. Vlugt, M. van Hecke, and W. van Saarloos, *Force network ensemble: A new approach to static granular matter*, Phys. Rev. Lett. **92**, 054302 (2004).

[44] J. P. Bouchaud, *Slow relaxations and nonequilibrium dynamics in condensed matter, edited by J. L. Barrat, M. Feigelman, J. Kurchan, and J. Dalibard, Proceedings of the Les Houches Summer School of Theoretical Physics, LXXVII*, EDP Sciences, Paris, 2003.

[45] J. Rottler and M. O. Robbins, *Jamming under tension in polymer crazes*, Phys. Rev. Lett. **89**, 195501 (2002).

[46] N. P. Kruyt and L. Rothenburg, *Probability density functions of contact forces for cohesionless frictional granular materials*, Int. J. Solids Struct. **39**, 571 (2002).

[47] P. T. Metzger, *Granular contact force density of states and entropy in a modified Edwards ensemble*, Phys. Rev. E **70**, 051303 (2004).

[48] P. T. Metzger and C. M. Donahue, *Elegance of disordered granular packings: A validation of Edward's hypothesis*, Phys. Rev. Lett. **94**, 148001 (2005).

[49] P. T. Metzger, H *theorem for contact forces in granular materials*, Phys. Rev. E **77**, 011307 (2008).

[50] P. T. Metzger, private communication (2007).

[51] M. Creutz, *Microcanonical Monte Carlo Simulation*, Phys. Rev. Lett. **50**, 1411 (1983).

[52] D. Frenkel and B. Smit, *Understanding molecular simulation: from algorithms to applications*, Academic Press, San Diego, 2nd edition, 2002.

[53] D. P. Landau and K. Binder, *A guide to Monte Carlo simulations in statistical physics*, Cambridge University Press, Cambridge, 2nd edition, 2000.

[54] D. C. Rapaport, *The art of molecular dynamics simulation*, Cambridge University Press, Cambridge, 2nd edition, 2004.

[55] T. J. H. Vlugt, J. P. J. M. van der Eerden, M. Dijkstra, B. Smit, and D. Frenkel, *Introduction to molecular simulation and statistical thermodynamics*, http://www.phys.uu.nl/~vlugt/imsst.

[56] A. R. Leach, *Molecular modelling: Principles and applications*, Prentice Hall, New Jersey, 2nd edition, 2001.

[57] R. J. Sadus, *Molecular simulation of fluids: theory, algorithms and object-orientation*, Elsevier, Amsterdam, 2nd edition, 1999.

[58] J. E. Lennard-Jones, Proc. Camb. Phil. Soc. **22**, 105 (1924).

[59] B. J. Alder and T. E. Wainwright, *Phase transition for a hard sphere system*, J. Chem. Phys. **27**, 1208 (1957).

[60] B. J. Alder and T. E. Wainwright, *Studies in molecular dynamics. I. General method*, J. Chem. Phys. **31**, 459 (1959).

[61] R. W. Hockney and J. W. Eastwood, *Computer simulations using particles*, McGraw-Hill, New York, 1981.

[62] W. C. Swope, H. C. Andersen, P. H. Berens, and K. R. Wilson, *A computer simulation method for the calculation of equilibrium constants for the formation of physical clusters of molecules: Application to small water clusters*, J. Chem. Phys. **76**, 637 (1982).

[63] L. E. Silbert, D. Ertaş, G. S. Grest, T. C. Halsey, and D. Levine, *Geometry of frictionless and frictional sphere packings*, Phys. Rev. E **65**, 031304 (2002).

[64] L. E. Silbert, D. Ertaş, G. S. Grest, T. C. Halsey, D. Levine, and S. J. Plimpton, *Granular flow down an inclined plane: Bagnold scaling and rheology*, Phys. Rev. E **64**, 051302 (2001).

[65] N. Metropolis and S. Ulam, *The Monte Carlo method*, J. Am. Stat. Assoc. **44**, 335 (1949).

[66] V. I. Manousiouthakis and M. W. Deem, *Strict detailed balance is unnecessary in Monte Carlo simulation*, J. Chem. Phys. **110**, 2753 (1999).

[67] D. Frenkel, *Speed-up of Monte Carlo simulations by sampling of rejected states*, Proc. Natl. Acad. Sci. **101**, 17571 (2004).

[68] N. Metropolis, A. W. Rosenbluth, M. N. Rosenbluth, A. H. Teller, and E. Teller, *Equation of state calculations by fast computing machines*, J. Chem. Phys. **21**, 1087 (1953).

[69] G. M. Torrie and J. P. Valleau, *Nonphysical sampling distributions in Monte Carlo free-energy estimation: umbrella sampling*, J. Comp. Phys. **23**, 187 (1977).

[70] J. D. Weeks, D. Chandler, and H. C. Andersen, *Role of repulsive forces in determining the equilibrium structure of simple liquids*, J. Chem. Phys. **54**, 5237 (1971).

[71] W. H. Press, S. A. Teukolsky, W. T. Vertterling, and B. P. Flannery, *Numerical Recipes in Fortran 77: The art of scientific computing*, Cambridge University Press, Cambridge, 2nd edition, 1992.

[72] J. A. Snyman, *A new and dynamic method for unconstrained minimization*, Appl. Math. Modelling **6**, 449 (1982).

[73] J. A. Snyman, *An improved version of the original leapfrog dynamic method for unconstrained minimization: LFOP1(b)*, Appl. Math. Modelling **7**, 216 (1983).

[74] J. A. Snyman, *A convergent dynamic method for large minimization problems*, Comput. Math. Appl. **17**, 1369 (1989).

[75] M. C. Payne, M. P. Teter, D. C. Allan, T. A. Arias, and J. D. Joannopoulos, *Iterative minimization techniques for ab initio total-energy calculations: Molecular dynamics and conjugate gradients*, Rev. Mod. Phys. **64**, 1045 (1992).

[76] J. Baker, *An algorithm for the location of transition states*, J. Comp. Chem. **7**, 385 (1986).

[77] K. Bagi, *Statistical analysis of contact force components in random granular assemblies*, Granular Matter **5**, 45 (2003).

[78] J. P. J. M. van der Eerden, J. Makkinje, and T. J. H. Vlugt, *Local order in interfaces*, J. Cryst. Growth **275**, 83 (2004).

[79] T. Unger, J. Kertész, and D. E. Wolf, *Force Indeterminacy in the Jammed State of Hard Disks*, Phys. Rev. Lett. **94**, 178001 (2005).

[80] B. P. Tighe, J. E. S. Socolar, D. G. Schaeffer, W. G. Mitchener, and M. L. Huber, *Force distributions in a triangular lattice of rigid bars*, Phys. Rev. E **72**, 031306 (2005).

[81] S. Ostojic and D. Panja, *Elasticity from the force network ensemble in granular media*, Phys. Rev. Lett. **97**, 208001 (2006).

[82] S. McNamara and H. Herrmann, *Measurement of indeterminacy in packings of perfectly rigid disks*, Phys. Rev. E **70**, 061303 (2004).

[83] S. Ostojic, E. Somfai, and B. Nienhuis, *Scale invariance and universality of force networks in static granular matter*, Nature **439**, 828 (2006).

[84] S. Ostojic, *Statistical mechanics of static granular matter*, PhD thesis, University of Amsterdam (2006).

[85] J. H. Snoeijer, T. J. H. Vlugt, W. G. Ellenbroek, M. van Hecke, and J. M. J. van Leeuwen, *Ensemble theory for force networks in hyperstatic granular matter*, Phys. Rev. E **70**, 061306 (2004).

[86] S. Ostojic, T. J. H. Vlugt, and B. Nienhuis, *Universal anisotropy in force networks under shear*, Phys. Rev. E **75**, 030301(R) (2007).

[87] B. P. Tighe, private communication (2007).

[88] B. P. Tighe, A. R. T. van Eerd, and T. J. H. Vlugt, *Entropy maximization in the force network ensemble for granular solids*, Phys. Rev. Lett. **100**, 238001 (2008).

[89] C. F. Moukarzel, *Isostatic phase transition and instability in stiff granular materials*, Phys. Rev. Lett. **81**, 1634 (1998).

[90] A. V. Tkachenko and T. A. Witten, *Stress in frictionless granular material: Adaptive network simulations*, Phys. Rev. E **62**, 2510 (2000).

[91] P. Evesque, *A simple incremental modelling of granular-media mechanics*, Poudres et grains **9**, 13 (1999).

[92] J. D. Goddard, *On entropy estimates of contact forces in static granular assemblies*, Int. J. Solids Structures **41**, 5851 (2004).

[93] S. Henkes, C. S. O'Hern, and B. Chakraborty, *Entropy and temperature of a static granular assembly: An ab initio approach*, Phys. Rev. Lett. **99**, 038002 (2007).

[94] J. C. Maxwell, *On reciprocal figures and diagrams of forces*, Philos. Mag. **27**, 250 (1864).

[95] G. de Josselin de Jong and A. Verruijt, *Étude photo-élastique d'un empilement de disques*, Cahiers du group Francais de Rhéologie **2**, 73 (1969).

[96] R. C. Ball and R. Blumenfeld, *Stress field in granular systems: Loop forces and potential formulation*, Phys. Rev. Lett. **88**, 115505 (2002).

[97] S. H. Chan and A. H. W. Ngan, *Statistical distribution of contact forces in packings of deformable spheres*, Mechanics of Materials **37**, 493 (2005).

[98] A. H. W. Ngan, *On the distribution of elastic forces in disordered structures and materials. A statistical mechnics theory*, Proc. R. Soc. A **461**, 1423 (2005).

[99] A. H. W. Ngan, *Erratum: Mechanical analog of temperature for the description of force distribution in static granular packings*, Phys. Rev. E **68**, 069902 (2003).

[100] H. P. Zhang and H. A. Makse, *Jamming transition in emulsions and granular materials*, Phys. Rev. E **72**, 011301 (2005).

[101] K. Shundyak, M. van Hecke, and W. van Saarloos, *Force mobilization and generalized isostaticity in jammed packings of frictional grains*, Phys. Rev. E **75**, 010301(R) (2007).

[102] T. J. H. Vlugt and A. R. T. van Eerd, *Krachtenbalans op zandkorrels*, Vakidioot, Studievereniging A-Eskwadraat , 19 (2005).

[103] W. G. Ellenbroek and J. H. Snoeijer, *Bounds on the yield stress of cohesionless granular matter*, J. Stat. Mech. , P01023 (2007).

[104] F. Wang and D. P. Landau, *Efficient, multiple-range random walk algorithm to calculate the density of states*, Phys. Rev. Lett. **86**, 2050 (2001).

[105] F. Wang and D. P. Landau, *Determining the density of states for classical statistical models; A random walk algorithm to produce a flat histogram*, Phys. Rev. E **64**, 56101 (2001).

[106] R. Blumenfeld, in *Granular and Complex Materials,* Lecture Notes in Complex Systems Vol. 8, edited by T. Aste, A. Tordesillas, and T. D. Matteo, World Scientific, Singapore, (2007).

[107] C. S. O'Hern, L. E. Silbert, A. J. Liu, and S. R. Nagel, *Jamming at zero temperature and zero applied stress: The epitome of disorder*, Phys. Rev. E **68**, 011306 (2003).

Summary

Granular materials such as sand and grains of corn have both liquid-like and solid-like properties similar to both liquids and solids. Dry sand in an hour-glass can flow just like water, while sand in a sand castle closely resembles a solid. Because of these interesting properties granular matter has received much attention from numerous physicists. Part of the research on these materials focuses on the statistics of contact forces between individual particles (grains) and how these statistics can be used to understand and predict material properties. Contact forces in granular materials are organized in so-called *forces networks*. The magnitude of the contact forces may vary considerably. Some particles experience contact forces much larger than the average contact force, see for example Fig. 1.2 and 1.8 of this thesis. The presence of many large contact forces in a sand pile may result in yielding, i.e. breaking down of the sand pile. A common quantity to characterize these force variations is the probability distribution $P(f)$ of the contact force f between two particles. Usually, the contact force distribution of a static system has its maximum near the average force $\langle f \rangle$, see for example Fig. 1.1 of this thesis.

A long-standing issue in the area of granular media is the asymptotic behavior of the contact force distribution $P(f)$ for large forces. In particular, one discusses whether the tail of $P(f)$ is exponential, Gaussian, or has a different form. Furthermore, its relation with material and system properties is under scruteny. In a recent issue of Nature (volume 435, 23 June 2005) three papers pay attention to this subject. Two different experimental methods are often applied to determine contact forces in static granular materials. The first measures *boundary forces* using carbon paper. The force between grains and the wall of the container, that holds the grains, is deduced from imprints on carbon paper. For large boundary forces the measured distribution decays exponentially. This observation is often used to suggest an analogy with the Boltzmann distribution of the microcanonical ensemble. In this ensemble, N random variables x_i satisfy the constraints $\sum_{i=1}^{N} x_i = N \langle x \rangle$ and $x_i \geq 0$. In the thermodynamic

limit, equipartition of N variables x_i results in an exponential distribution (the so-called Boltzmann distribution) for x_i. The second and more recent way to measure *bulk contact forces* in two-dimensional granular materials (grains are disks) uses the photoelastic effect of the disks. Changes in the optical properties of the disks can be translated into contact forces. Distributions of these contact forces show a faster than exponential decay. It should be mentioned that a faster than exponential decay also was found in experiments with three-dimensional emulsions.

In view of the technical difficulty to measure contact forces, especially in the bulk of the material, several research groups use molecular simulations to study contact force statistics. Molecular simulations may be interpreted as computer experiments in which the temporal evolution of a model system consisting of interacting particles can be calculated. From the simulated results statistical properties, like the distribution of the average contact force, can be calculated. Some of these studies claim an exponential tail of $P(f)$. The published graphs however, are less convincing than the graphs obtained from the experiments with carbon paper. The differences in the results give rise to three important questions: *(1)* Which properties are responsible for the behavior of $P(f)$ for large forces? *(2)* What is the fundamental difference (if any) between the statistics of contact forces between particles in the bulk and between particles and the wall? *(3)* Is it possible to explain the shape of $P(f)$ with the Boltzmann-type argument? Answering these questions is seriously hindered by the fact that large contact forces occur *de facto* significantly more rarely than contact forces near the average force $\langle f \rangle$. This applies to experiments as well as to molecular simulations.

In this thesis, we approached these questions using computer simulations in the so-called *force network ensemble* of Snoeijer *et al.* (J.H. Snoeijer, T.J.H. Vlugt, M. van Hecke, W. van Saarloos, Phys. Rev. Lett., 2004, 92, 054302). This ensemble describes the statistics of repulsive contact forces for a particular packing of the particles. The crucial assumption is that the particles are almost undeformable. Hence a small displacement of a particle may result in completely different contact forces on that particle. In the force network ensemble, the particles in the system have fixed positions and the contact forces are chosen in such a manner that all particles are in mechanical equilibrium, i.e. experience a zero net force, and the elements of the stress tensor have a prescribed value. Moreover it is assumed that each realization of repulsive contact forces (a force network) that satisfy the constraints is equally probable. The obtained collection of force networks is called the *force network ensemble*.

Mathematically, the force network ensemble can be considered as the collection of solutions of an underdetermined matrix equation $\mathscr{A}\mathbf{f} = \mathbf{b}$ subject to the constraint that all elements of $\mathbf{f}$ are larger or equal to zero. This constraint expresses that only repulsive contact forces are considered. The solutions of this underdetermined matrix equation can be written as $\mathbf{f} = \mathbf{f}_0 + \sum a_k \mathbf{v}_k$, in which $\mathbf{f}_0$ is a particular solution, the $\mathbf{v}_k$ are the null vectors of matrix $\mathscr{A}$ and the a_k are arbitrary coefficients. The summation is over all null vectors and only $\mathbf{f}$ with exclusively non-negative elements are allowed.

Force networks on arbitrary two- and three-dimensional packings can be generated with Monte Carlo simulations. These simulations are computer calculations in which (pseudo-)random numbers are used to efficiently sample the configuration space. From the simulation results one estimates the average of particular quantities, such as the distribution of the contact forces $P(f)$. The solution space of the force network ensemble can be sampled in a statistically correct way using so-called *wheel moves*. Unfortunately, the standard Monte Carlo procedure for the force network ensemble is inefficient for the estimation of $P(f)$ for large contact forces f. The reason is that by far the largest fraction of generated force networks contains only small forces. For unambiguous conclusions on the asymptotic behavior of $P(f)$, extremely long (of the order of years or even centuries) computer calculations are needed. To obtain better statistics for large contact forces, we developed an *umbrella sampling* method for the force network ensemble. The umbrella sampling method has been introduced in the seventies by Torrie and Valleau (G. M. Torrie, J.P. Valleau, J. Comp. Phys., 1977, 23, 187-199). Since then, the method was "re-invented" by different authors. The central idea is to sample the solution space of the force network ensemble with a biased Monte Carlo simulation in such a way that many forces networks with large contact forces are found. This results in excellent statistics for large contact forces, however, the result can not be used directly because the solution space is incorrectly sampled. Fortunately, the error can be corrected *exactly* afterwards, adding a statistical weight to the sampled force networks. One needs to develop some feeling to sample the solution space of the force network ensemble in an efficient way.

The outline of this thesis is as follows. In Chapter 1, an overview is given of the different methods to study the statistics of force networks. The experimental studies with carbon paper and photoelastic disks and the molecular simulation studies are reviewed. We also explained the umbrella sampling method that we developed to obtain excellent statistics for large forces. In Chapter 2, we applied the umbrella sampling method to study the tail of the force distribution $P(f)$ for different two-,

three- and four-dimensional systems. The average number of contacts z of a particle and the packing configuration are shown not to be important for the asymptotic behavior of $P(f)$. Only the dimensionality of the system has a significant influence: $P(f) \sim \exp[-c f^\alpha]$ with $\alpha \approx 2.0$ for two-dimensional systems, $\alpha \approx 1.7$ for three-dimensional systems and $\alpha \approx 1.4$ for four-dimensional systems. In Chapter 3, a possible explanation is found for the Gaussian decay of large contact forces in two-dimensional systems. It was found that mechanical balance on each particle is essential for the tail of the contact force distribution. Under this constraint maximizing the entropy results in a contact force distribution with a generic Gaussian tail. This distribution is almost in perfect agreement with the umbrella sampling simulations for systems with and without friction, both for triangular and for square lattices. Removing the mechanical equilibrium constraint on each particle, maximization of the entropy results in an exponential tail of $P(f)$. This is consistent with the "Boltzmann" argument. We conclude that the tail of $P(f)$ is determined by local mechanical equilibrium, which throws serious doubts on the statement that exponential statistics are a generic property of static granular materials. In Chapter 4, several aspects are highlighted. We show that in the presence of shear stress $P(f)$ is strongly direction dependent. As a result the tail of the orientation-averaged $P(f)$ may look (partly) exponential even though for each individual direction the tail is Gaussian. We develop methods to find the maximum possible force in a system and to determine the dimension of the force space. We demonstrate that the wall-contact force distribution may differ essentially from the bulk-contact force distribution. This chapter ends with a detailed comparison between $P(f)$ in the force network ensemble and $P(f)$ from molecular simulations of particles with a "real" pair interaction. We show that these distributions are different in general. Nevertheless our preliminary calculations suggest that applying the constraint of local mechanical equilibrium, the force distribution of the "real" system crosses over towards the distribution of the force network ensemble.

Samenvatting

Granulaire materialen zoals zand en graankorrels hebben eigenschappen overeenkomstig met zowel vloeistoffen als vaste stoffen. Zo kan droog zand in een zandloper net als water stromen, terwijl zand in zandkasteel juist meer op een vaste stof lijkt. Door deze bijzondere eigenschappen staan granulaire materialen in de belangstelling bij natuurkundigen. Een deel van het onderzoek naar deze materialen richt zich op de statistiek van contactkrachten tussen individuele deeltjes (zandkorrels) en hoe men deze kan gebruiken om eigenschappen van materialen te begrijpen en te voorspellen. Contactkrachten in granulaire materialen zijn georganiseerd in zogenaamde *krachtennetwerken*. De grootte van deze krachten kan sterk variëren over de ruimte. Sommige korrels ondervinden bijvoorbeeld contactkrachten die veel groter zijn dan de gemiddelde contactkracht, zie bijvoorbeeld Fig. 1.2 en 1.8 van dit proefschrift. De aanwezigheid van veel grote contactkrachten in een zandhoop, al dan niet veroorzaakt door een externe kracht, kan de zandhoop doen instorten. Een veelgebruikte grootheid om krachtennetwerken te karakteriseren is de kansverdeling $P(f)$ van de contactkracht f tussen twee korrels. Voor stilstaande systemen heeft deze verdeling vaak een maximum in de buurt van de gemiddelde kracht $\langle f \rangle$, zie bijvoorbeeld Fig. 1.1 van dit proefschrift.

Het asymptotisch gedrag van de contactkrachtverdeling $P(f)$ voor granulaire materialen staat momenteel ter discussie. Eén van de centrale vragen is of de $P(f)$ voor grote f (de staart) een exponentiële, Gaussische, dan wel een andere vorm heeft. Verder wordt de relatie tussen $P(f)$ en materiaal- en systeemeigenschappen onderzocht. In een recent nummer van het toonaangevende blad Nature (volume 435, 23 juni 2005) besteden maar liefst drie artikelen aandacht aan dit onderwerp. Twee verschillende experimentele methoden worden vaak gebruikt om contactkrachten in statische (in rust zijnde) granulaire materialen te bepalen. Bij de eerste methode gebruikt men carbonpapier om de grootte van de *wandcontactkrachten* te meten tussen korrels en de wand van de container waar het materiaal zich in bevindt. De afdrukken

die ontstaan op de plaatsen van de contacten tussen de korrels en de wand kunnen direct worden vertaald naar contactkrachten. Steeds vindt men dat contactkracht-verdelingen tussen korrels en de wand die op deze manier worden gemeten een exponentiële staart hebben. Deze waarneming wordt vaak gebruikt om een analogie te suggereren met de Boltzmann verdeling in het microcanonieke ensemble. In dit ensemble voldoen de N variabelen x_i aan $\sum_{i=1}^{N} x_i = N \langle x \rangle$ en $x_i \geq 0$. In de thermody-namische limiet levert equipartitie van N variabelen x_i een exponentiële verdeling (de zogenaamde Boltzmann verdeling) op voor x_i. Bij de tweede en meer recente manier om *bulkcontactkrachten* te meten in tweedimensionale systemen maakt men gebruik van het zogenaamde foto-elastisch effect. Veranderingen in de optische eigenschap-pen van plastic schijven kunnen direct worden vertaald naar contactkrachten tussen de schijven. Verdelingen van contactkrachten die op deze manier worden gemeten laten duidelijk een sneller dan exponentieel verval zien. Hetzelfde is waargenomen in experimenten met emulsies (driedimensionale systemen).

Omdat het vaak lastig is om contactkrachten direct in de bulk van het materiaal te meten, hebben verschillende onderzoeksgroepen moleculaire simulaties gebruikt om contactkrachtverdelingen te meten. Moleculaire simulaties kunnen worden gezien als computer-experimenten waarin de evolutie van een modelsysteem bestaande uit wisselwerkende deeltjes wordt berekend. Hieruit kunnen allerlei gemiddelden, zoals de verdeling van de gemiddelde contactkracht worden berekend. Hoewel een aantal van dit soort studies een exponentiële staart van $P(f)$ claimen, is het numerieke be-wijs hiervoor veel minder overtuigend dan bij de experimenten met carbonpapier. De verschillen in de resultaten roepen drie belangrijke vragen op: *(1)* Welke eigenschap-pen bepalen het gedrag van $P(f)$ voor grote krachten? *(2)* Is er een fundamenteel verschil tussen de statistiek van wandcontactkrachten en bulkcontactkrachten? *(3)* Is de Boltzmann-analogie valide om de staart van $P(f)$ te kunnen verklaren? Het beant-woorden van deze vragen wordt sterk gehinderd door het feit dat grote contactkrach-ten *de facto* veel minder vaak voorkomen dan contactkrachten rond de gemiddelde kracht $\langle f \rangle$, zowel in experimenten als in moleculaire simulaties.

In dit proefschrift wordt getracht een antwoord te geven op deze vragen met be-hulp van computersimulaties in het zogenaamde *krachten-ensemble* van Snoeijer *et al.* (J.H. Snoeijer, T.J.H. Vlugt, M. van Hecke, W. van Saarloos, Phys. Rev. Lett., 2004, 92, 054302). Dit ensemble beschrijft de statistiek van repulsieve contact-krachten voor een bepaalde stapeling van de deeltjes. De cruciale aanname hierbij is dat de korrels erg hard (nagenoeg onvervormbaar) zijn, zodat een geringe ver-

plaatsing van een korrels kan leiden tot compleet andere contactkrachten. In het krachten-ensemble wordt uitgegaan van een systeem waarbij de korrels vaste posities hebben en de contactkrachten zodanig gekozen zijn dat alle korrels in mechanisch evenwicht zijn (de nettokracht op iedere korrel is nul) en de elementen van de stress tensor een voorgeschreven waarde hebben. Bovendien wordt aangenomen dat elke realisatie van repulsieve contactkrachten (het krachtennetwerk) die hieraan voldoet, even waarschijnlijk is. De aldus verkregen verzameling van krachtennetwerken wordt het "krachten-ensemble" of "force network ensemble" genoemd. Wiskundig gezien is het krachten-ensemble te schrijven als de verzameling van oplossingen van de ondergedetermineerde matrixvergelijking $\mathscr{A}\mathbf{f} = \mathbf{b}$ met de voorwaarde dat alle elementen van $\mathbf{f}$ groter of gelijk aan nul dienen te zijn. Dit laatste komt door het feit dat we uitsluitend repulsieve contactkrachten beschouwen. De oplossingen van deze ondergedetermineerde matrixvergelijking kunnen worden geschreven als $\mathbf{f} = \mathbf{f}_0 + \sum a_k \mathbf{v}_k$ waarin $\mathbf{f}_0$ een particuliere oplossing is, de $\mathbf{v}_k$ de nulvectoren zijn van matrix $\mathscr{A}$ en de a_k willekeurige coëfficiënten zijn. De sommatie gaat over alle nulvectoren en alleen oplossingen met uitsluitend positieve elementen van $\mathbf{f}$ zijn toegestaan.

Het genereren van krachtennetwerken voor willekeurige korrelposities kan worden uitgevoerd met behulp van Monte Carlo simulaties. Bij deze simulaties worden (pseudo-)willekeurige getallen gebruikt om de configuratieruimte efficiënt te doorlopen. De simulatie-resultaten kunnen worden gebruikt om gemiddelden van bepaalde grootheden af te schatten. Door het gebruik van zogenaamde "wheel moves" kan de oplossingsruimte van het krachten-ensemble op een statistisch correcte manier worden doorlopen en kunnen gemiddelde grootheden zoals de verdeling van contactkrachten $P(f)$ worden berekend. Helaas levert de standaard Monte Carlo procedure voor het krachten-ensemble slechte statistiek op van $P(f)$ voor grote contactkrachten f. De reden is dat verreweg de meeste krachtennetwerken uitsluitend kleine krachten bevatten (i.e. krachten van grootte orde $\langle f \rangle$). Om ondubbelzinnige uitspraken te kunnen doen over het asymptotisch gedrag van $P(f)$ zouden extreem lange computerberekeningen (in de orde van jaren tot eeuwen) nodig zijn. Om een betere statistiek voor grote contactkrachten te verkrijgen hebben we een "umbrella sampling" methode voor het krachten-ensemble ontwikkeld. Het concept *umbrella sampling* is reeds in de jaren '70 van de vorige eeuw bedacht door Torrie en Valleau (G.M. Torrie, J.P. Valleau, J. Comp. Phys., 1977, 23, 187-199), en sindsdien verschillende keren opnieuw "uitgevonden" door verschillende auteurs. Het centrale idee is om in een aangepaste Monte Carlo simulatie zodanig de oplossingsruimte van het krachten-

ensemble te doorlopen dat er veel krachtennetwerken worden gevonden met grote contactkrachten. Dit levert een uitstekende statistiek op voor grote contactkrachten, echter, het resultaat is niet direct te gebruiken omdat de oplossingsruimte van het krachten-ensemble op een statistisch niet-correcte manier is doorlopen. Hiervoor moet achteraf gecorrigeerd worden; het mooie is dat dat ook *exact* kan door aan de gevonden krachtennetwerken een verschillende statistische gewichten toe te kennen. Wel vereist het enig "fingerspitzengefühl" om op precies de gewenste en meest efficiënte manier de oplossingsruimte van het krachten-ensemble te doorlopen.

Dit proefschrift is als volgt opgebouwd. In hoofdstuk 1 wordt allereerst een overzicht gepresenteerd van de verschillende methodes om de statistiek van krachtennetwerken te bestuderen. Met name wordt ingegaan op de eerder genoemde experimentele studies met carbonpapier en foto-elastische schijven, alsmede moleculaire simulatie studies. Vervolgens wordt uitgelegd hoe umbrella sampling kan worden gebruikt om de contactkrachtverdeling $P(f)$ nauwkeurig uit te rekenen voor grote krachten f. In hoofdstuk 2 wordt deze methode verder gebruikt om $P(f)$ te bestuderen voor verschillende twee-, drie- en vierdimensionale systemen, waarbij met name gekeken is naar het effect van het gemiddelde aantal contacten z van een deeltje, de ordening van de korrels en de dimensie. De resultaten laten zien dat alleen de dimensie van het systeem een significante invloed heeft op het asymptotisch gedrag: we vinden dat $P(f) \sim \exp[-c f^{\alpha}]$ met $\alpha \approx 2.0$ voor tweedimensionale systemen, $\alpha \approx 1.7$ voor driedimensionale systemen en $\alpha \approx 1.4$ voor vierdimensionale systemen. In hoofdstuk 3 wordt getracht een antwoord te geven op de vraag *waarom* tweedimensionale systemen een verdeling van contactkrachten hebben die Gaussisch afvalt voor grote f. Het blijkt dat de voorwaarde dat de nettokracht op iedere korrel nul is (mechanisch evenwicht), van essentieel belang is. Maximalisatie van de entropie onder deze voorwaarde resulteert in een contactkrachtenverdeling met een generieke Gaussische staart. Deze gevonden kansverdeling is in vrijwel perfecte overeenstemming met umbrella sampling simulaties voor systemen met en zonder frictie, zowel voor een hexagonaal als vierkant rooster. Wanneer de voorwaarde van mechanisch evenwicht op iedere korrel wordt losgelaten, resulteert maximalisatie van de entropie in een exponentiële verdeling, in overeenstemming met het eerder genoemde "Boltzmann" argument. Hieruit kan worden geconcludeerd dat de staart van $P(f)$ bepaald wordt door lokaal mechanisch evenwicht en dat serieus moet worden getwijfeld aan de veelgehoorde opvatting dat exponentiële statistiek een generieke eigenschap is van statische granulaire materialen. Tenslotte worden in hoofdstuk 4 een aantal as-

pecten nader belicht. We laten zien dat in de aanwezigheid van afschuifspanningen de krachtenverdeling een sterke oriëntatie-afhankelijkheid vertoont. Als gevolg daarvan lijkt de staart van de oriëntatie-gemiddelde krachtenverdeling gedeeltelijk exponentieel hoewel de staart van de verdeling voor iedere oriëntatie afzonderlijk Gaussisch is. We ontwikkelen methodes om de maximaal mogelijke kracht in een systeem te vinden en om de dimensie van de krachtruimte te bepalen. We tonen aan dat de wandcontactkrachtverdeling essentieel kan verschillen van de bulkcontactkrachtverdeling. Dit hoofdstuk besluit met een gedetailleerde vergelijking tussen $P(f)$ berekend in het krachten-ensemble en $P(f)$ berekend uit moleculaire simulaties van deeltjes met een "echte" paarinteractie. We laten zien dat deze krachtverdelingen in het algemeen heel verschillend zijn. Niettemin suggereren onze voorlopige berekeningen dat wanneer we aan het "echte" systeem lokaal mechanisch evenwicht zouden opleggen, dat dan de krachtverdeling van het "echte" systeem zou opschuiven in de richting van de krachtverdeling van het krachten-ensemble.

Curriculum vitae

Naam: Adrianne Rudolfine Titia van Eerd
Geboren: 27 november 1979 te Heesch

Opleiding:

1992 - 1998	VWO, Mondriaan College, Oss	
1998 - 2001	HLO-chemie, Hogeschool van Arnhem en Nijmegen	
	Hoofdvak	Analytische chemie
	Stageplaats	NV Organon, Quality Assurance, Oss
	Onderzoeksonderwerp	Method development for determination of the active component in intact tablets with NIRS and chemometrics
2001 - 2003	Scheikunde, Katholieke Universiteit Nijmegen	
	Hoofdvak	Vaste stof chemie
	Stageplaats	Vakgroep van prof. dr. E. Vlieg
	Onderzoeksonderwerp	Prediction of the morphology of aspartame by computer modelling
2004 - 2008	Promotieonderzoek, Universiteit Utrecht	
	Onderzoeksonderwerp	Statistics of large forces in static granular matter
	Promotor	Prof. dr. J.P.J.M. van der Eerden
	Copromotor	Dr. ir. T.J.H. Vlugt

Per 1 juni 2008 werkzaam als programmacoördinator bij Stichting FOM te Utrecht.

List of publications

B.P. Tighe, A.R.T. van Eerd, and T.J.H. Vlugt
Entropy maximization in the force network ensemble for granular solids
Phys. Rev. Lett. **100**, 238001 (2008)

A.R.T. van Eerd, W.G. Ellenbroek, M. van Hecke, J.H. Snoeijer, and T.J.H. Vlugt
Tail of the contact force distribution in static granular materials
Phys. Rev. E **75**, 060302 (2007)

Other publications:

T.J.H. Vlugt and A.R.T. van Eerd
Krachtenbalans op zandkorrels
Vakidioot, Studievereniging A-Eskwadraat, 19-23 (2005)

H.M. Cuppen, A.R.T. van Eerd, and H. Meekes
Needlelike morphology of aspartame
Cryst. Growth Des. **4**, 989-997 (2004)

Dankwoord

De afgelopen 4 jaar heb ik met veel plezier gewerkt aan simulaties van contactkrachten in granulair materiaal. Het onderzoek was van begin tot eind een grote uitdaging. Gelukkig stond ik er niet alleen voor. Veel mensen hebben op verschillende wijze bijdragen geleverd aan de totstandkoming van dit proefschrift. Bij dezen wil ik dan ook graag een aantal mensen bedanken.

Allereerst gaat mijn dank uit naar Jan van der Eerden en Thijs Vlugt, omdat zij mij de mogelijkheid gaven in hun groep te promoveren. Ook bedank ik hen voor de prettige samenwerking. Thijs, je was altijd even enthousiast en zat vol ideeën. Als ik het even niet meer zag zitten, gaf je mij weer moed. Joachim Gross en zijn groep van de TU Delft bedank ik voor de gastvrijheid en de interesse in mijn onderzoek.

Verder wil ik Shuai, Renée, Philipp, Marjolein Dijkstra, René van Roij en alle mede-'simulanten/theoreten' bedanken voor de waardevolle discussies. Ik heb veel geleerd van de besprekingen tijdens de wekelijkse bijeenkomsten. Voor het verdiepen van het theoretische inzicht in krachtennetwerken bedank ik Jacco Snoeijer, Martin van Hecke, Wouter Ellenbroek, Wim van Saarloos en Brian Tighe. Voor de ondersteuning en het onderhoud van alle computers wil ik Stephan bedanken, want zonder een goed draaiend cluster was ik nu nog aan het rekenen.

Naast het onderzoek is de prettige werksfeer natuurlijk ook belangrijk. Hiervoor bedank ik alle (oud-)groepsgenoten. In het bijzonder bedank ik mijn kamergenoten Arjan, Shuai, Alek en Zhixiang voor hun dagelijkse interesse. Karin, Dennis en Harold bedank ik voor de ontspanningsmomenten, die ook buiten werktijd voortduurden. Verder bedank ik een aantal collega's uit andere groepen van het Debye Instituut: Esther, Yu Ling, Mirjam, Job, Caspar en María. De etentjes waren altijd heel gezellig.

Tenslotte wil ik mijn vrienden en familie bedanken voor de steun en nodige afleiding die ze mij hebben gegeven. Mijn lieve neefjes Lucas en Pascal, jullie vinden op dit moment de zandbak al heel leuk, maar misschien dat ik jullie later ook enthou-

siast kan maken voor het onderzoek naar zand. Chantal bedank ik voor haar nooit aflatende interesse en Michel bedank ik voor het ontwerpen van de omslag van dit proefschrift. Ik vind het erg leuk dat jullie mijn paranimfen willen zijn. Als laatste maar zeker niet minder belangrijk, bedank ik papa en mama voor alle goede zorgen, interesse en steun. Jullie waren er altijd voor mij.

Bedankt,

Rianne